REPUBLIC OF TURKEY
YILDIZ TECHNICAL UNIVERSITY
GRADUATE SCHOOL OF NATURAL AND APPLIED SCIENCES

COMPARISON OF DIFFERENT NITRIDING METHODS ON SURFACE PROPERTIES OF DIN 1.2738 STEEL

ESİL BOZTEPE

MSc. THESIS
DEPARTMENT OF METALLURGICAL AND MATERIALS ENGINEERING
PROGRAM OF MATERIALS

ADVISER
PROF. DR. NURHAN CANSEVER

İSTANBUL, 2015

ACKNOWLEDGEMENTS

I would like to express my sincere appreciation to my supervisor from Yıldız Technical University Prof. Dr. Nurhan Cansever for her valuable guidance and encouragement during the study. I also want to express my deepest gratitude to my thesis co-supervisor from University of Minho Assist. Prof. Dr. Fatih Toptan for his priceless caring, supporting and comments and providing me with an excellent atmosphere all through the study.

My special thanks go to all the members of Centre for Mechanical and Materials Technologies (CT2M) in University of Minho for creating limitless opportunities for my studies. I would like to thank to Prof. Dr. Luís Augusto Rocha for his help and the facilities provided to carry out the research work at the CT2M. Alexandra Alves is gratefully and respectfully acknowledged for her priceless efforts, helps and suggestions. The friendly attitude combined with the knowledge she shared, had a major influence on me. To Edith Ariza, I express my gratefulness for the suggestions and also for providing SEM and X-ray analysis. I also would like to thank Prof. Dr. Amílcar Ramalho for valuable discussions and providing profilometer facilities. I also appreciate valuable efforts of Mr.Sergio Carvalho for the tribological studies.

My sincere thanks ASSAB Çelik ve Isil Islem AS for providing materials for the nitrocarburizing processes and technical assistance. My sincere thanks also go to Istanbul Isil Islem San. ve Tic. AS and Quantum Takim Sanayi Urunleri Çelik ve Tic. AS for their support in applying their treatments.

I am very thankful to all the technical and administrative staff of the Department of Metallurgical and Materials Engineering, of the Faculty of Chemical and Metallurgical Engineering of the Yıldız Technical University in Istanbul.

Finally and most importantly, I would like to thank to my parents who have never lost their belief in me and to my friends for keeping me motivated at all times.

The present research was partially supported by YULAP under Project No. 2012-07-02-YL04 (Turkey), and Centre for Mechanical and Materials Technologies (CT2M) in Portugal.

July, 2015

Esil BOZTEPE

TABLE OF CONTENTS

Page

CHAPTER 5

CHAPTER 6

LIST OF SYMBOLS

α	Alpha – Ferritic Iron
γ	Austenitic Iron
$\overline{D}$	Average Depth
$\overline{W}$	Average Witdh of Each Wear Track
bcc	Body Centered Cubic
a_C	Carbon Activitiy
K_C	Carburizing Potential
cm	Centimeter
i_{corr}	Corrosion Current Density
E_{corr}	Corrosion Potential
d	Diagonal
e^-	Electron
ε	Epsilon – $Fe_{2-3}N$
fcc	Face Centered Cubic
γ'	Gamma Prime – Fe_4N
g	Gram
Hz	Hertz
hcp	Hexagonal Close Packed
h	Hour
F	Load
MPa	Megapascal
m	Meter
µm	Micron
mbar	Millibar
mm	Millimeter
mV	Millivolt
min	Minute
M	Molar
N	Newton
K_N	Nitriding Potential
a_N	Nitrogen Activitiy
Pa	Pascal
P	Pressure

s	Second
S	Total Sliding Distance
l	Total Stroke Length
ΔV	Total Volume Loss
HV	Vickers Hardness
V	Volt
A_w	Wear Loss Area
k	Wear Rate
wt	Weight

LIST OF ABBREVIATIONS

AISI	American Iron and Steel Institute
BSE	Back Scattered Electron
COF	Coefficient of Friction
CE	Counter Electrode
EDS	Energy Dispersive Spectroscopy
FBN	Fluidized Bed Nitriding
GN	Gas Nitriding
NC	Nitrocarburizing
OCP	Open Circuit Potential
OM	Optical Microscope
PN	Plasma (Ion) Nitriding
RE	Reference Electrode
SCE	Saturated Calomel Electrode
SE	Secondary Electron
SEM	Scanning Electron Microscope
UT	Untreated
XRD	X-Ray Diffraction
WE	Working Electrode

LIST OF FIGURES

Page

LIST OF TABLES

ABSTRACT

COMPARISON OF DIFFERENT NITRIDING METHODS ON SURFACE PROPERTIES OF DIN 1.2738 STEEL

Esil BOZTEPE

Department of Metallurgical and Materials Engineering

MSc. Thesis

Adviser: Prof. Dr. Nurhan CANSEVER

Co-adviser: Assit. Prof. Dr. Fatih TOPTAN

A mould which is subjected to continuous impact while in use is the main cause of its short service life. However, a mould with a hardened surface can improve hardness, wear resistance and corrosion resistance, which can effectively extend the service life. Service life of mould steel can be further improved by using proper surface treatments such as nitriding/nitrocarburizing.

In this study gas nitriding (GN), fluidized bed nitriding (FBN), plasma nitriding (PN) and nitrocarburizing (NC) methods were applied in industrial facilities on plastic mould steel, DIN 1.2738 (Impax Supreme), and the results were investigated by comparing the mechanical and chemical properties.

Systematic materials characterization of the nitrided and untreated samples were carried out in terms of microstructural examinations, phase identification, surface and cross-section microhardness measurements, dry sliding wear tests, electrochemical corrosion tests and tribocorrosion tests. After tests, sample surfaces were characterized by field emission gun scanning electron microscope (FEGSEM) equipped with energy dispersive X-ray spectroscopy (EDS).

The reciprocating dry sliding wear tests were performed against AISI 4140 pins under 100 N normal load (contact pressure of 5.1 MPa), the frequency of 1.5 Hz, and the total sliding distance of 400 m. After tests, it was found that all samples presented mainly combination of adhesive and abrasive wear mechanism during the run-in period of sliding (severe wear), and mainly oxidative wear mechanism thereafter (steady-state), i.e. showing mild wear.

Corrosion behaviour of the nitrided and untreated samples was studied using electrochemical techniques namely, open circuit potential (OCP) and potentiodynamic polarization in a 3.5% wt. NaCl solution. After electrochemical measurements, it has found that the nitrided layer had an important effect on the tendency of corrosion of samples.

Additionally, the tribocorrosion behavior of samples was investigated in 3.5% wt. NaCl solution. The tests were carried out against alumina ball using reciprocating ball-on-plate tribometer (under 15 N load and 1 Hz). OCP was measured before, during and after sliding. After electrochemical, tribological and microstructural studies, it was found that nitrided samples presented better tribocorrosion behaviour as compared to the untreated steel.

Experimental results showed that the different nitriding processes considerably improved the wear and corrosion resistances of the material as compared to the untreated sample.

Key words: Nitriding, nitrocarburizing, plastic mould steel, wear, corrosion, tribocorrosion

ÖZET

DIN 1.2738 ÇELİĞİNE UYGULANAN FARKLI NİTRÜRLEME YÖNTEMLERİNİN ÇELİK YÜZEY ÖZELLİKLERİNE ETKİSİ

Esil Boztepe

Metalurji ve Malzeme Mühendisliği Anabilim Dalı

Yüksek Lisans Tezi

Tez Danışmanı : Prof. Dr. Nurhan CANSEVER

Eş Danışman : Yrd. Doç. Dr. Fatih TOPTAN

Kullanım sırasında sürekli darbeye maruz kalan bir kalıp, servis ömrünün kısalmasına neden olur. Oysa yüzeyi sertleştirilmiş bir kalıp, sertlik, aşınma direnci ve korozyon direncini artırarak kalıbın etkili bir şekilde kullanım ömrünü uzatabilir. Nitrürleme/Nitrokarbürleme gibi uygun yüzey işlemleri kullanılarak kalıp çeliklerinin kullanım ömürleri daha da geliştirilebilir.

Bu çalışmada DIN 1.2738 (Impax Supreme) plastik kalıp çeliğine edüstriyel koşullarda gaz nitrürleme (GN), akışkan yatakta nitrürleme (FBN), plazma nitrürleme (PN) ve nitrokarbürleme (NC) işlemleri uygulanmış olup mekanik, kimyasal, tribolojik, elektrokimyasal ve triboelektrokimyasal özellikleri karşılaştırılarak incelenmiştir.

Nitrürlenmiş ve işlem görmemiş numunelerin sistematik malzeme karakterizasyonu, mikroyapı incelemeleri, faz tanımlama, yüzey ve enine kesit mikro sertlik ölçümleri, kuru kayma aşınma testleri, elektrokimyasal korozyon testleri ve tribokorozyon testleri uygulanarak gerçekleştirilmiştir. Deneyler sonrası, numune yüzeyleri SEM ve buna bağlı olarak çalışan EDS ile karakterize edilmiştir.

Kuru kayma aşınma deneyleri ileri geri hareketli aşınma cihazında 100 N normal yük (5.1 MPa temas basıncı) altında, 1.5 Hz kayma frekansında ve 400 m kayma mesafesinde AISI 4140 pinler karşısında uygulanmıştır. Test sonrası tüm numunelerde kayma boyunca esas olarak adhesiv ve abrasiv aşınma mekanizmalarının kombinasyonu ve sonrasında da ağırlıklı olarak oksidatif aşınma mekanizması belirlenmiştir.

Nitrürlenmiş ve işlem görmemiş numunelerin korozyon davranışları % 3.5 NaCl çözeltisi içerisinde açık devre potansiyeli (OCP) ve potansiyodinamik polarizasyon teknikleri ile incelenmiştir. Elektrokimyasal ölçümlerin sonucunda, nitrürleme tabakasının numunelerin korozyon eğilimine önemli bir etkide bulunduğu belirlenmiştir.

Bu çalışmalara ilaveten numunelerin tribokorozyon davranışları yine % 3.5 NaCl çözeltisi içerisinde, alumina bilye karşısında, ileri geri hareketli ball-on-plate aşınma cihazı kullanılarak incelenmiştir (15N yük ve 1 Hz frekans altında). Açık devre potansiyeli (OCP) kayma öncesi, kayma boyunca ve sonrasında ölçülmüştür. En iyi tribokorozyon davranışını nitrürlenmiş numuneler göstermiştir.

Deneysel sonuçlar neticesinde farklı nitrürleme işlemlerine tabi tutulan numuneler işlem görmemiş numune ile kıyaslandığında nitrürleme işleminin malzemelerin sertlik, aşınma, korozyon ve tribokorozyon dirençlerini önemli ölçüde arttırdığı görülmüştür.

Anahtar Kelimeler: Nitrürleme, nitrokarbürleme, plastik kalıp çeliği, aşınma, korozyon, tribokorozyon

CHAPTER 1

INTRODUCTION

Plastic injection moulds are an important economic sector due to the increasing use of injection moulded plastic components [1]. Moulds for plastic injection are normally high cost and quite complicated, consisting of many parts in relative motion with respect to each other and to the plastics material, leading to tribological problems in the moulds. Tribological problems in connection with the moulding of plastics can often be solved by an appropriate surface treatment [2]. Surface treatments of mould steel are of great industrial importance because the mechanical and chemical properties of the surface layers of treated parts can be improved considerably as a result of the chemical and structural changes induced by the thermochemical processes [3].

Nitriding is a surface treatment technique used to introduce nitrogen into metallic materials to improve their surface hardness, mechanical properties, as well as wear and corrosion resistance [4]. In commercial nitriding systems, the uptake of nitrogen can take place in different environments, namely, liquid (salt bath nitriding), controlled gas atmospheres (typically NH_3/H_2 mixtures) and plasma (low pressure N_2/H_2 mixtures) [5].

Gas nitriding (GN) is a case hardening process whereby nitrogen is introduced into the surface of a solid ferrous alloy by holding the metal at a suitable temperature in contact with a nitrogenous gas [6]. As a similar process to GN, in fluidized bed nitriding (FBN) is used a fluidized bed furnace where the ammonia gas usually used as a nitrogen source [7].

Plasma (or ion) nitriding (PN) is an extension of GN process where high-voltage electrical energy is used to form plasma in vacuum. Nitrogen can penetrate and diffuse into the surface after a glow discharge with the steel in a gas of H_2 and N_2 [6], [8]. Nitrocarburizing (NC) involve the diffusional addition of both nitrogen and carbon to the surface of ferrous materials at temperatures within the ferrite phase field temperatures [6].

After nitriding, a compound layer and an underlying diffusion layer are formed at the surface of the steel. The compound layer, also known as the white layer, consists of iron nitrides, the epsilon phase (ε -$Fe_{2-3}N$), the gamma phase (γ'-Fe_4N) or mixed nitride (ε+γ') which are responsible for the good tribological and anticorrosive properties of the surface [9], [10], [11], [12]. In the region beneath the compound layer, known as diffusion layer, consists of very fine nitride particles, where the nitrogen content decreases towards the core [11]. The compound layer is responsible for good physical and chemical properties against wear and corrosion while the diffusion layer improves the fatigue strength of the workpiece [3]. These properties make nitriding one of the most common methods to improve surface hardness, as well as wear and corrosion resistance of materials.

1.1 Literature Review

The nitriding process is one of the most important thermochemical heat treatment processes in metallurgy. The purpose of nitriding is to improve wear, corrosion and fatigue resistance of steel. There are several studies in the literature regarding to the tribological properties of various nitriding process applied on to the steels.

Bermúdez et al. [1] studied the dry sliding wear of a low alloy plastic mould steel (1.2738) heat treated under different conditions. After testing under pin-on-flat reciprocating configuration against AISI 52100 steel pins, the authors reported that under low sliding frequencies, the wear resistance of the low alloy mould steel was not dependent on the hardness or the microstructure, where the main wear mechanism was abrasive and oxidative wear. However, at high frequency, the highest wear resistance was reported for the hard quenched mould steel having a martensitic

microstructure, but the wear mechanism was reported as the same as at low sliding frequencies.

Wen [4] studied the dry sliding wear behaviour of a plasma nitrided precipitation hardenable plastic mould steel (NAK55) using a block-on-ring tribometer against a hardened and tempered AISI-O1 tool steel. Both adhesive and abrasive wear were reported for the untreated sample, whereas abrasive wear was the dominant mechanism for the nitrided samples. The author also investigated the corrosion behavior of the same steel using anodic polarization tests in 3.5% NaCl solution and concluded that the nitriding process improved the corrosion resistance in terms of corrosion potential and corrosion rate. Furthermore the corrosion resistance was dependent on the type of the nitride formed in the compound layer.

Al-Rubaie et al. [13] studied the effect of the nitrocarburizing processes (salt bath, gas, and plasma) on the abrasive wear behaviour of different steel substrates against a flint abrasive. The authors reported that all of the studied nitrocarburizing processes improved the abrasion resistance of the treated steels. Moreover, the abrasion resistance of the treated steels was improved with the increase in the surface hardness of the compound layer.

Basso et al. [14] studied the effects of the treatment parameters on the nitrocarburized layer properties such as thickness, porosity, composition and microstructure and consequently, on the corrosion resistance improvement of the nitrocarburized layer. The authors concluded that the parameters which affect the above properties were very important to the enhancement of the corrosion resistance. Furthermore, the change of the thickness and the porosity of the nitrocarburized layer were the most important factors which control the corrosion resistance of the treated steel.

Fattah et al. [15] studied the corrosion behaviour of the plasma nitrided and nitrocarburized AISI 4140 low alloy steel in 3.5% NaCl solution. The authors stated that better corrosion resistance of nitrocarburized samples was also related to the better corrosion resistance of the ε-phase and higher amount of that in the nitrocarburized compound layer when compared with nitrided samples.

Another study performed by Novak et al. [16] reported that compound layer played an important role on the corrosion and wear behaviour of the steel.

Rosalbino et al. [17] studied the electrochemical corrosion behaviour of precipitation hardening mould steel (1.2738) in 0.1M NaCl solution. The authors concluded that the presence of pearlite has a negative effect on the corrosion behaviour of the steel. A galvanic coupling is formed between the pearlite that acts as a cathode and the bainitic matrix that acts as an anode. Consequently, the bainitic matrix suffers a preferential dissolution.

Even though several studies were performed on the tribological behaviour of the various nitriding surfaces, comparative studies are needed in order to select the suitable nitriding process.

1.2 Objective of the Thesis

The aims of this study;

- Improvement of surface treatments of 1.2738 plastic mould steel with nitriding and nitrocarburizing processes.
- Investigation of effects of nitriding and nitrocarburizing on the development of surface structures and surface mechanical improvements of plastic injection mould steels.
- Comparison of the mechanical and chemical properties of DIN 1.2738 (Impax Supreme) plastic mould steel after NC, GN, FBN, and PN surface treatments
- Extention of plastic mould steel service life.

1.3 Hypothesis

The nitriding/nitrocarburizing process is an important thermochemical surface treatment that is used to increase the steel surface hardness and improve the wear and corrosion resistance of steel parts.

CHAPTER 2

NITRIDING

2.1 Historical Review of Nitriding

Nitriding is one of the processes employed for surface hardening of metals [18]. Nitriding has evolved significantly (Figure 2.1) since the original patent of Adolph Machlet in 1913. Material limitations, such as the lack of low alloy steels, promoted superficial nitriding responses and therefore restricted the wide spread use of this new technology initially. Subsequent to the study of Machlet, Adolph Fry developed steels containing aluminium and in 1921 a patent was approved related to the development and nitriding of these steels. As the design and production of materials improved, nitriding became a viable solution to many engineering problems involving metal to metal wear. Bernhard Berghaus developed the ion nitriding process in 1932. Less than ten years later salt bath nitriding was developed. However, with this new technology leaded to undesirable side effects such as brittle surface layers that required extensive treatment to remove. In a novel way for controlling this brittle surface layer, Carl Floe developed the Floe process which involved a treatment to reduce the surface brittleness. Later, General Electric claimed to have developed what they called, ion nitriding, and wrote about ion nitriding being in full scale production. In 1987 a patent was approved for the development of an innovative process called post discharge nitriding and in 1999 the ASPN system was developed by Georges [19].

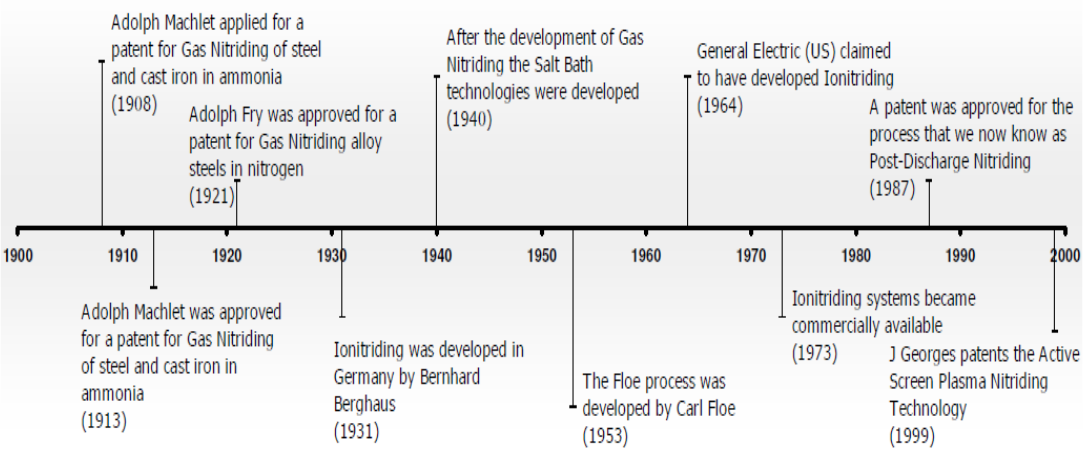

Figure 2.1 Nitriding time-line with significant events [19]

2.2 Nitriding Process

Nitriding is a low-temperature method used to diffuse nitrogen into the surface of steel without changing the phase structure of steel [20]. The steel remains in the ferrite phase during the complete procedure. This means that the molecular structure of the ferrite (body-centered cubic, bcc, lattice) does not change its configuration or grow into the face centered cubic (fcc) lattice characteristic of austenite [7]. The process does not involve heating into the austenite phase, thereby quenching is not required. The low process temperature and the absence of phase transformations, nitriding process produces less distortion and deformation [3]. Another benefit of nitriding is that it acts as a stabilizing process by providing an additional temper to the processed steel (Figure 2.2).

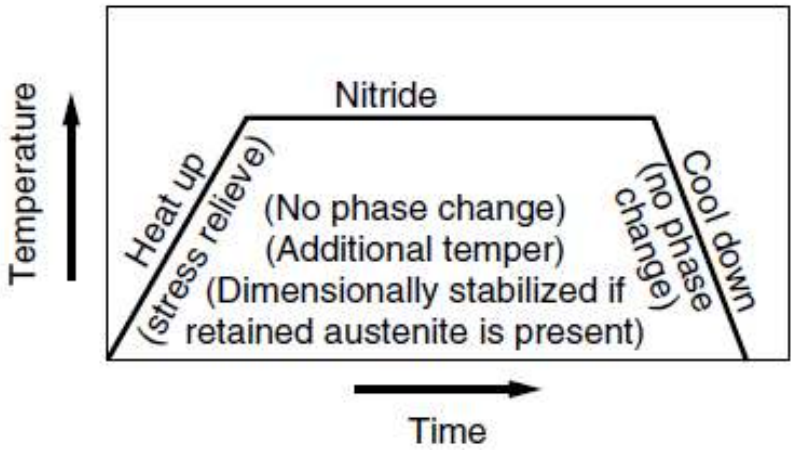

Figure 2.2 Benefits of the nitriding process [7]

The nitriding process has been successfully applied to carbon steels, alloy steels, tool steels, stainless steels and cast irons [7]. Nitriding is widely used in automotive, mechanical and aeronautical engineering. Typical components are gears, crankshafts, camshafts, cam followers, valve parts, extruder screws, die-casting tools, forging dies, aluminium-extrusion dies, injectors and plastic mould tools [3].

Traditional methods such as gas nitriding (box furnace or fluidized bed), salt bath nitriding, and plasma nitriding have been used by engineers to improve the tribomechanical properties of parts and components in a number of different industries for many years [7].

2.2.1 Thermodynamics of Nitriding

The iron-nitrogen phase diagram, shown in Figure 2.3, provides information essential for the practice of nitriding iron and low carbon steels [21]. This diagram is the base to understand the phase evolution during the nitriding process [9]. Phase transformations during nitriding are dependent on the nitrogen content diffused into the ferritic matrix during the thermochemical treatment [22]. Depending on the nitrogen content, iron nitride phases with different structure and properties can be formed. All iron nitrides are metallic conductors and metastable with respect to decomposition into Fe and N_2.

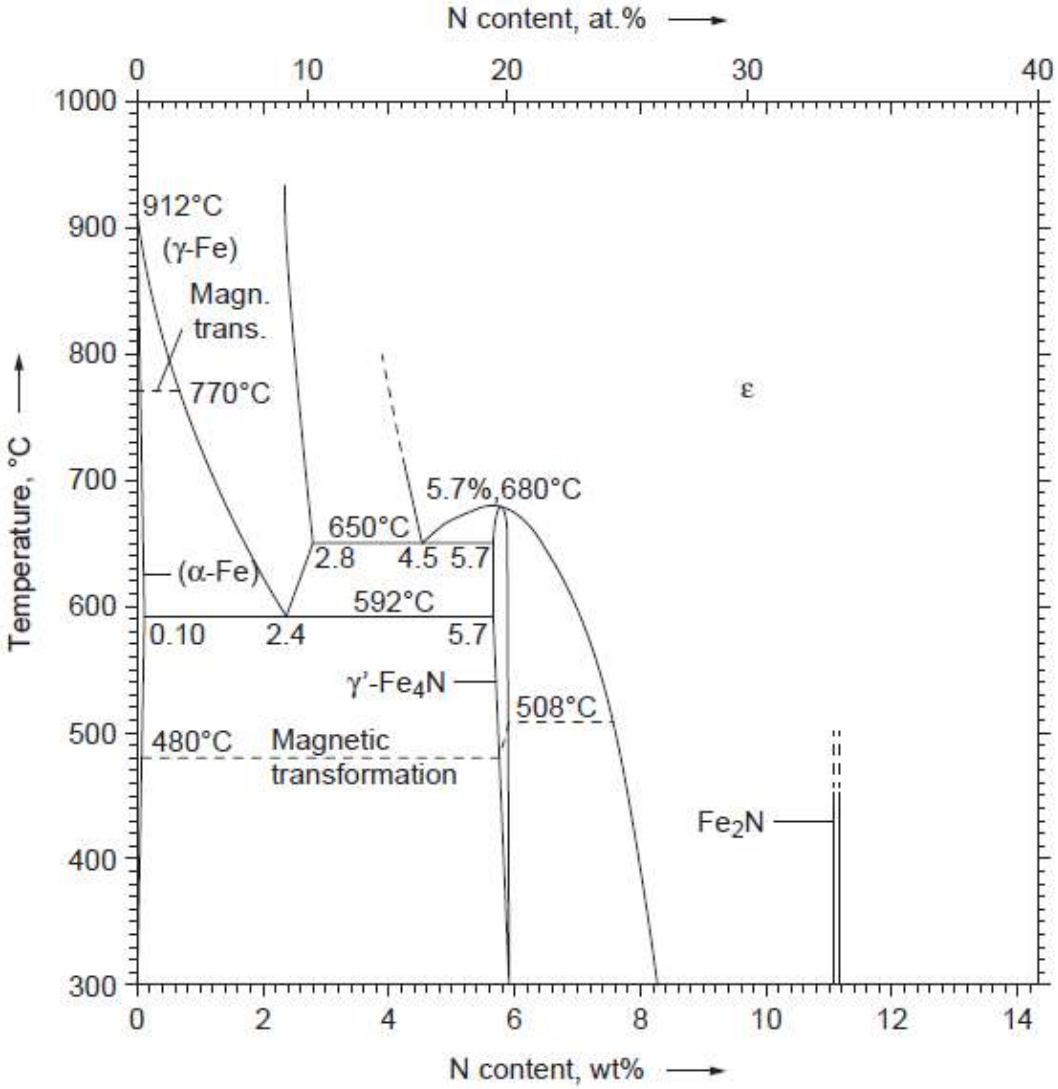

Figure 2.3 Iron – Nitrogen equilibrium phase diagram [23]

Iron (Fe) exists in three basic crystallographic forms; up to 912 °C bcc (α-Fe), between 912 °C – 1394 °C fcc (γ-Fe) and 1394 °C – 1538 °C bcc (δ-Fe). The effects of introducing nitrogen into the α-Fe lattice are shown in the Fe-N equilibrium phase diagram (Figure 2.3). It is evident that there is a limited interstitial solid solubility of N in α-Fe, with a maximum of 0.1 wt% N at 585 °C. A new phase is precipitated, namely γ'- Fe_4N (fcc) (Figure 2.4 a) as the concentration of interstitial N in the α-Fe matrix increases beyond 0.1 wt% N and at a temperature below 585 °C.

In the composition range of 5.7 – 5.9 wt% N, γ'- Fe_4N forms as a single phase field. Increasing the N concentration higher than 5.9 wt% N, results in the precipitation of another iron nitride phase namely ε-$Fe_{2-3}N$ (hexagonal) (Figure 2.4 b) [19].

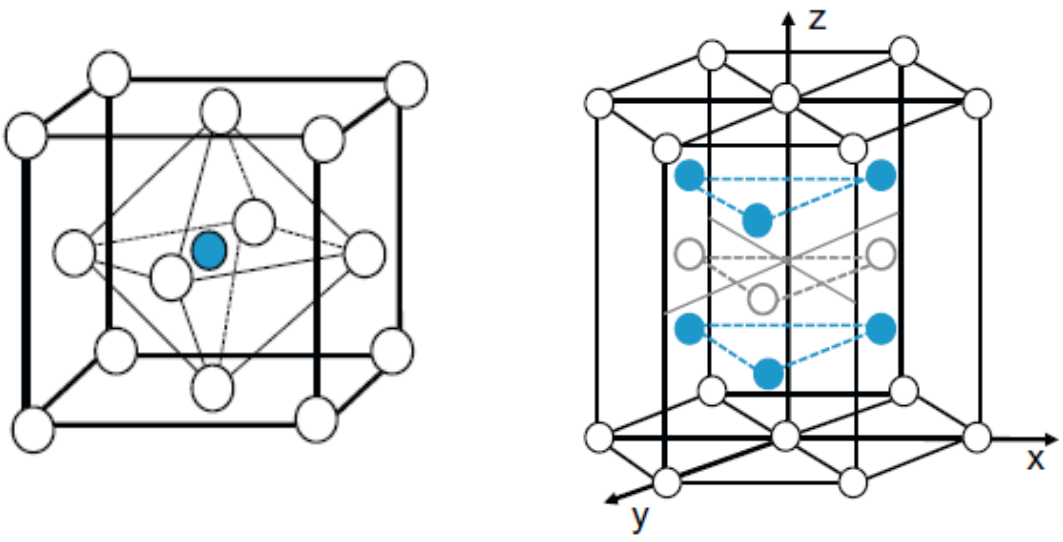

(a) (b)

Figure 2.4 Crystal lattice structures of (a) γ' and (b) ε components [24]

2.2.2 Diffusion Kinetics of Nitriding

Nitriding involves the diffusion of atomic nitrogen on the surface of a steel workpiece. Nitrogen enters the ferrite phase during the nitriding process [3]. The process of the smaller nitrogen atoms passing between the iron-base crystals as heat is applied up to a suitable process temperature is known as "interstitial diffusion" [7].

The diffusion of nitrogen into steel leads to the formation of a compound layer at the surface which may consist of the iron nitrides ε-$Fe_{2-3}N$ and γ'-Fe_4N. Beneath the compound layer, there is a diffusion layer which is composed of interstitial solid solution of nitrogen dissolved in the ferrite lattice [3]. Both of these layers make up "the nitrided layer". The nitrides begin their formation by the nucleation of γ' at the immediate steel surface interface with the nitriding atmosphere.

This nucleation process progresses and continues until the subsequent nucleation of ε at the steel surface interface (Figure 2.5). The nitrogen diffusion is much slower in the compound layer than in the steel substrate [7].

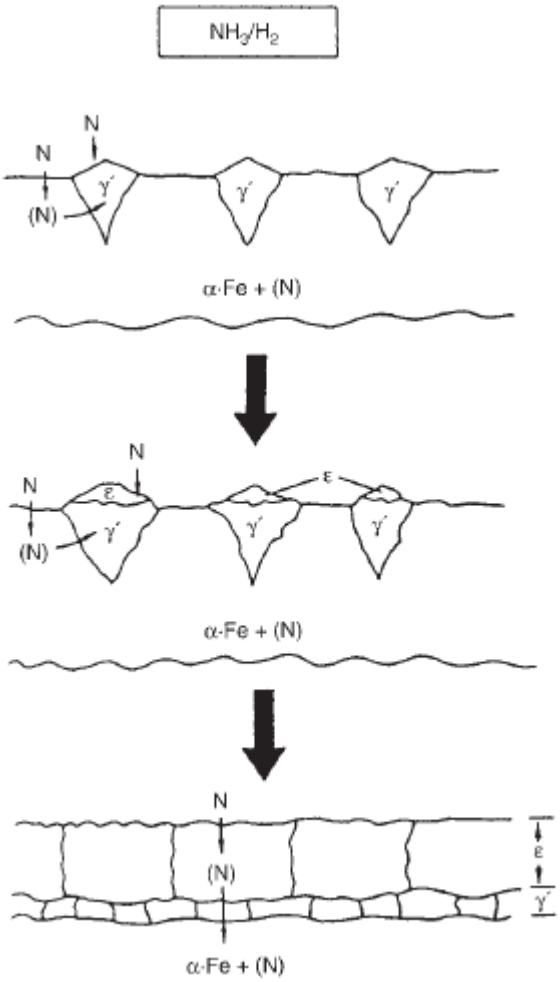

Figure 2.5 Schematic showing the nucleation of γ ’ and ε-nitrides on iron [7]

The heat effect of slow cooling after nitriding or the separate heating cycle leads to formation of the γ'- Fe_4N nitride which, in turn, increases the nitrogen content in the ε-Fe_2N nitride. Morphologically that process can change a ratio between sublayer thicknesses within the compound layer at the expense of ε-Fe_2N or cause a precipitation of γ'- Fe_4N phase within the ε-Fe_2N layer, as shown in Figure 2.6 [25].

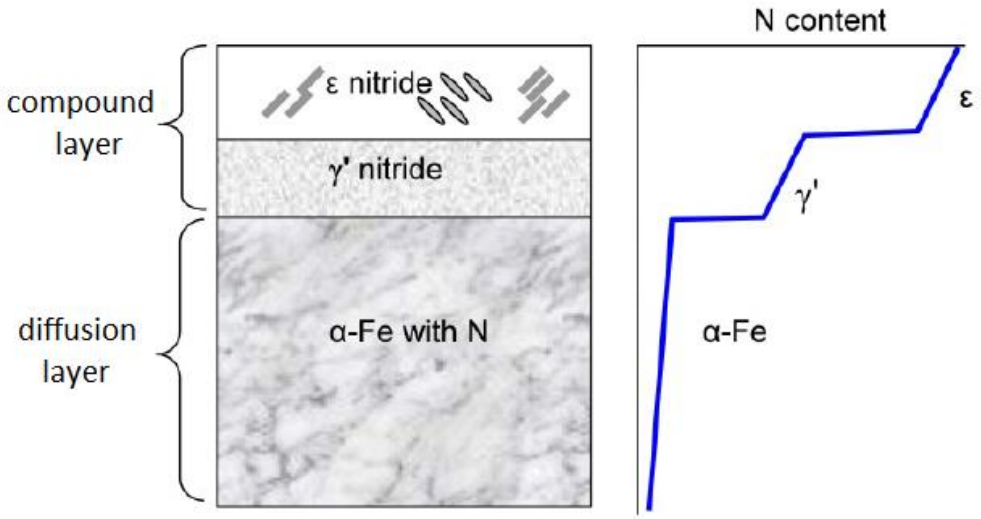

Figure 2.6 Phase distribution within a nitrided layer on steel and accompanied nitrogen depth concentration [25]

2.3 Structure of Nitrided Layer

The microstructure of the nitrided layer which develops upon nitriding pure iron (or iron-based alloy), below the eutectoid temperature (592°C for pure iron-nitrogen) using a nitriding potential which stabilizes the ε-$Fe_{2-3}N$ at the iron surface [26].

Formation of the nitrided layer begins through a series of nucleated growth areas on the surface of the steel, a "compound layer", with the diffused and reacted nitrides forming beneath the surface called the "diffusion layer" [12], as is shown in Figure 2.7.

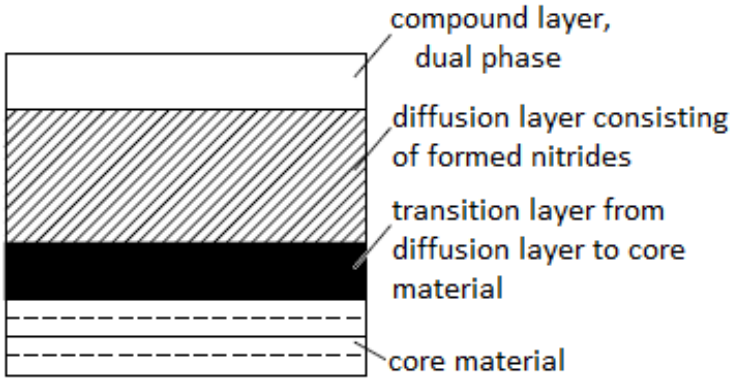

Figure 2.7 Typical nitrided layer [7]

Outer part is called the compound layer (white layer) which is very hard, brittle and does not diffuse into the steel but remains on the immediate surface. Process variables that such as gas composition, duration and process temperature are the main parameters to control the depth of the compound layer [7]. During nitriding, a compound layer, composed of iron nitrides ε and/or γ', is formed at the steel surface. Below the compound layer a diffusion layer extends in the ferrite matrix in which nitrogen is dissolved interstitially. The particular depth structure of diffusion layer depends on the substrate chemistry and nitriding process [25]. The compound layer can have greatly improved wear and corrosion resistance. The hardened diffusion layer is responsible for a considerable enhancement of the fatigue endurance and also increases the wear resistance [9].

The area below the diffusion layer is the core of the steel and is unaffected by the surface nitriding activity [27].

All three regions, namely the compound layer, diffusion layer, and core are shown in Figure 2.8.

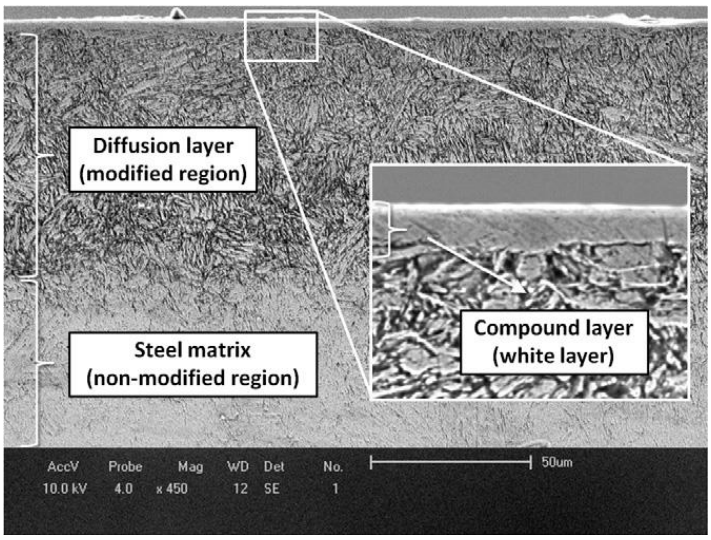

Figure 2.8 Microstructure of the nitrided layer [28]

2.4 Properties of the Nitrided Surface

Nitriding enhances the surface hardness of the material and, depending on the parameters used, it also improves its fatigue properties, besides providing wear and corrosion resistance [7], [29].

2.4.1 Surface Roughness

Surface roughness increases in most materials after nitriding due to nitrogen absorption into the surface. The increase in surface roughness depends on the processing gas compositions, the treatment time and temperature in addition to substrate material [25], [30].

Surface roughness is also increased by porosity formed in the outer zone of the compound layer by trapped molecules of nitrogen that recombine to N_2. The tendency to form porosity by this mechanism grows with the temperature of the nitriding process, as well as with the nitriding potential.

Surface roughness prior to the nitriding process has a significant influence on final roughness, as can be seen in Figure 2.9 [31].

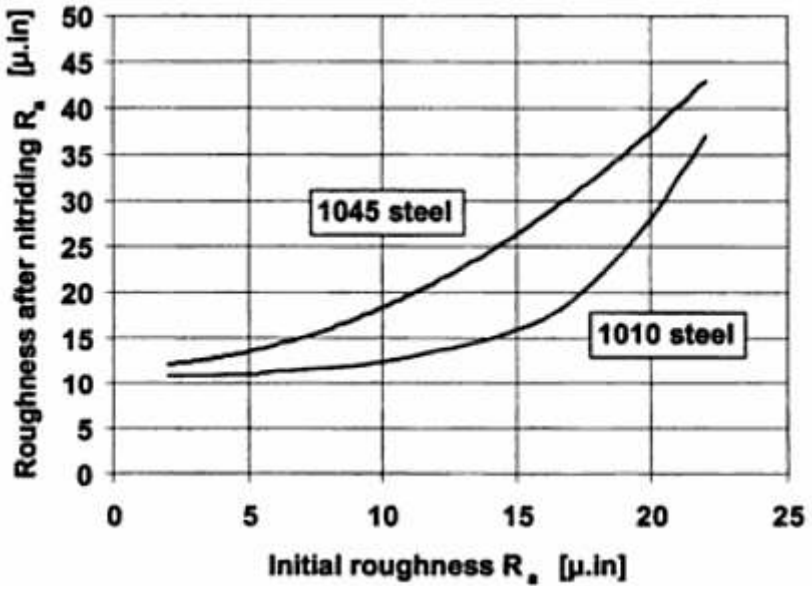

Figure 2.9 Effect of prior roughness on final roughness after nitriding for 1010 and 1045 steel [31]

2.4.2 Hardness

As the nitrogen concentration increases toward the surface, very fine, coherent precipitates are formed when the solubility limit of nitrogen is exceeded. The precipitates can exist both in the grain boundaries and within the lattice structure of the grains themselves. These precipitates, nitrides of iron or other metals, distort the lattice and pin crystal dislocations and thereby substantially increase the hardness of the material.

The hardness of the diffusion layer depends on precipitation hardening, while that of the compound layer depends on the type and thickness of the compound formed. Because the compound layer is compounds of only iron and nitrogen, the hardness of this layer is essentially independent of alloy content [6]. The hardness of the compound layer is about constant through its thickness with the exception of the outer porous zone, where hardness is reduced due to porosity. It is higher than the diffusion layer hardness, which continuously decreases from the surface into the steel interior [32]. Typical hardness after nitriding as shown in Figure 2.10.

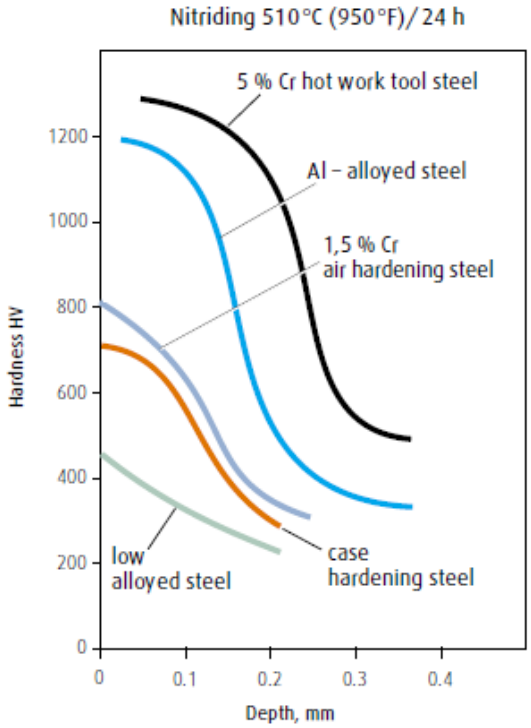

Figure 2.10 Typical hardness after nitriding [32]

2.4.3 Fatigue Strength

Fatigue strength can be significantly improved by nitriding, and this improvement attributes to increasing the surface hardness and residual stress distribution or increasing the case depth (Figure 2.11) [33], [34].

Both increased residual stress and surface hardness result in improvements in the fatigue life because the thin, hard layer prevents plastic flow. Therefore, the slip bands can only be activated by very high stresses in this region. This means that plastic deformation, which is the source of crack initiation, probably appears in the subsurface. The suppression of slip band formation at the surface delays crack initiation and propagation, thus being responsible for the improvement of fatigue life. The effect of increasing the case depth on the fatigue limit can be viewed as effectively moving the fatigue crack initiation site further into the core. This means that a greater applied bending stress will be required at the surface to create a sufficiently high level of stress at the case–core interface to initiate failure [33].

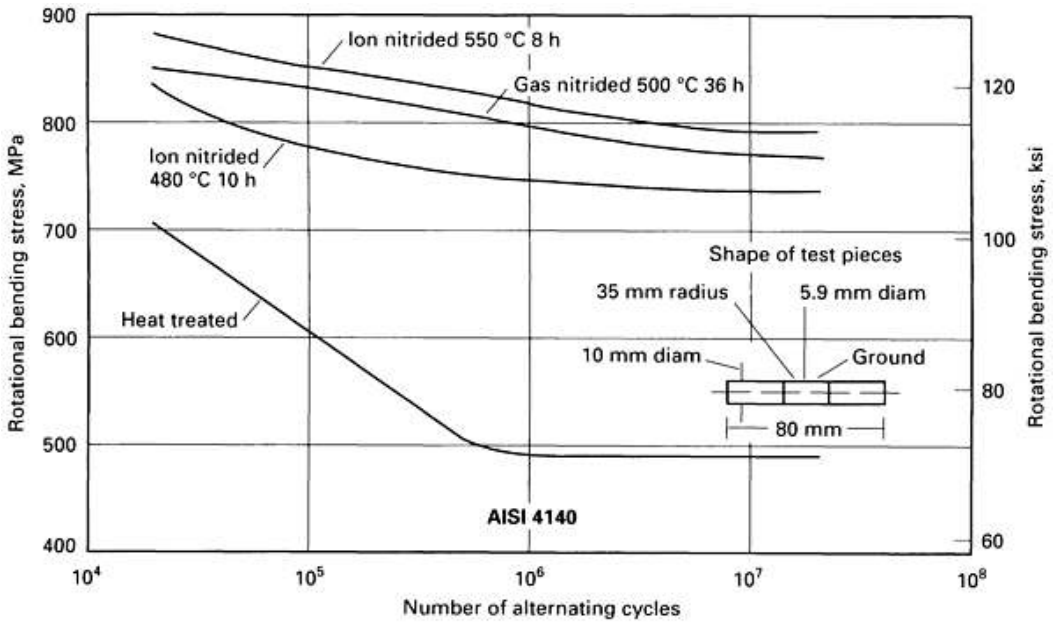

Figure 2.11 Effect of nitriding on fatigue strength [6]

2.4.4 Wear Resistance

Nitriding is widely applied in the mechanical engineering industry to improve the wear of steel and cast-iron parts [35].

The wear resistance of a nitride layer changes with distance from the surface (Figure 2.12). Wear resistance is reduced in the porous zone of the compound layer because of the lower fatigue strength and reduced density. The wear resistance of the poreless zone of the compound layer is significantly higher than that of the diffusion layer and the core material. If the compound layer has a homogeneous structure, wear resistance is constant throughout. In the diffusion layer, wear resistance decreases to the value of the core material with increasing distance from the surface this is because of the reduction of the density of the nitride precipitates and the supersaturation of the matrix with nitrogen.

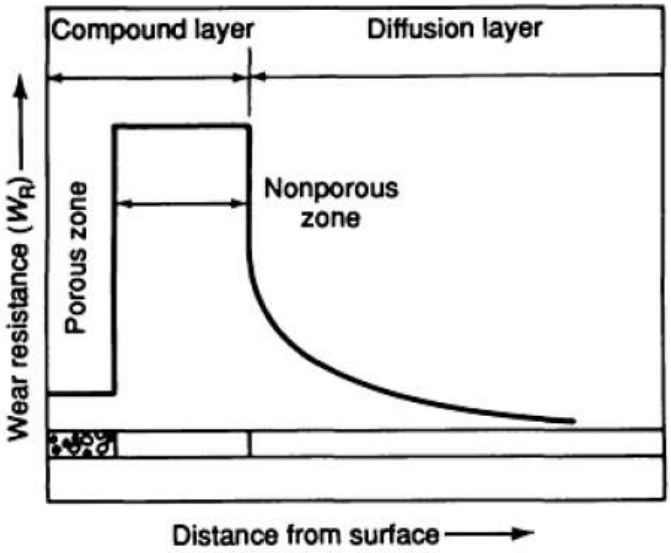

Figure 2.12 Plot of adhesive and abrasive wear resistance versus distance from the surface for a nitride layer [36]

The wear behavior of a nitride layer is often assumed to be an integral reaction of the nitriding layer to wear loading. This view does not explain wear mechanisms and their interaction during loading. Therefore, wear resistance and mechanisms must be discussed in conjunction with the structure of the nitriding layer [36].

2.4.5 Corrosion Resistance

The nitrided surface of an alloy steel or tool exhibits increased resistance to saltwater corrosion, moisture and water [37].

Corrosion resistance of nitride layers depends primarily on factors related to their structure, i.e., its special features, morphology, and phase composition.

Compound layer thickness increaes by increasing the nitriding potential and nitriding time. Meaning that, corrosion resistance increases by these parameters. The corrosion protective properties of the compound layer relies more on porosity than thickness. The compound layer is usually porous and this tends to decrease the corrosion resistance [38].

The compound layers with iron nitrides have good corrosion resistances [2]. The corrosion resistance increases due to the formation of a compound layer constituted by highly dense γ'-Fe_4N and ε-$Fe_{2-3}N$ nitrides [39].

2.5 Types of Nitriding

In commercial nitriding systems, the uptake of nitrogen can take place in different environments, namely, liquid (salt bath nitriding), controlled gas atmospheres (typically NH_3/H_2 mixtures) and plasma (low pressure N_2/H_2 mixtures). Each technology has associated advantages and disadvantages [5].

2.5.1 Gas Nitriding

Gas nitriding is a case-hardening process whereby nitrogen is introduced into a steel surface in a controlled atmosphere by holding the metal at a suitable temperature in contact with a nitrogenous gas [3]. During the gas nitriding, ammonia, NH_3 is used as nitrogen providing medium due to the relatively higher chemical potential of nitrogen compared to nitrogen gas, N_2. The chemical potential of nitrogen in N_2 is extremely low and an equilibrium N_2 pressure up to several thousand atmospheres would be necessary to incorporate a considerable amount of nitrogen into the steel surface.

As illustrated in Figure 2.13 the dissolution of nitrogen in steel occurs via the dissociation of ammonia at the surface, by the chemical reaction indicated in Equation (2.1).

$$NH_3 \longrightarrow N_{ad} + 3/2\ H_2 \quad (2.1)$$

Followed by the dissolution of nitrogen in steel

$$N_{ad} \longrightarrow [N] \quad (2.2)$$

and/or the formation of nitrogen gas

$$N_{ad} + N_{ad} \longrightarrow N_2 \quad (2.3)$$

where N_{ad} denotes N adsorbed at the steel surface and [N] represents nitrogen which is dissolved in the steel surface [9].

The nascent nitrogen diffuses into steel forming a solid solution which is the diffusion layer. If the process is continued, as soon as the equilibrium concentration of nitrogen in α-Fe is reached, the compound layer is formed.

Depending on the nitriding condition, the compound layer may contain only γ'-Fe_4N as shown by the chemical reaction in Equation (2.4):

$$4Fe + [N] \longrightarrow Fe_4N \quad (2.4)$$

If the nitriding process is continued, an additional formation of ε-Fe_2N or ε-Fe_3N, shown by chemical reactions in Equation (2.5) and Equation (2.6), is possible depending on the surface kinetics which determines the amount of nascent nitrogen available for compound layer formation.

$$Fe_4N + [N] \longrightarrow 2Fe_2N \quad (2.5)$$

$$3Fe_4N + [N] \longrightarrow 4Fe_3N \quad (2.6)$$

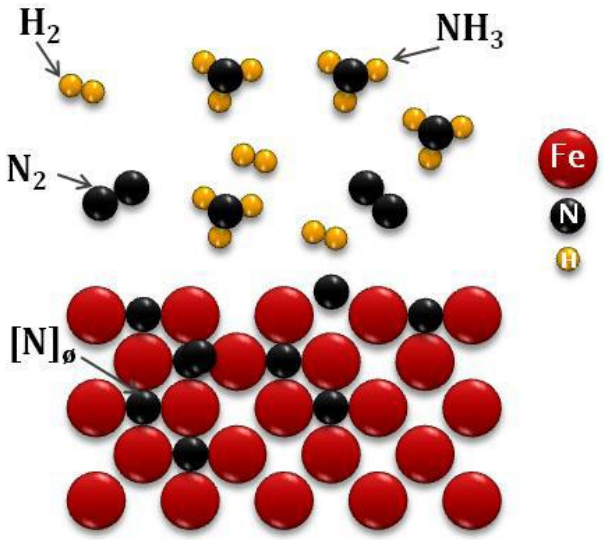

Figure 2.13 Schematic illustration of gas nitriding [9]

The transfer of nitrogen atoms from the gas phase to the solid phase is by transport of ammonia in the gas phase and adsorption of molecules at the solid surface through a diffusion boundary layer. It is followed by a chemical reaction at the surface, which depends on the partial pressures. Subsequently, there is the desorption of N_2 and H_2 which depends on the total gas flow rate. Finally the nascent nitrogen is transferred through the surface and diffused into the steel material. Another way of obtaining nitrogen for gas nitriding is by using ammonia and hydrogen gases. This approach gives more control over the nitrogen activity of the furnace atmosphere [3].

The nitrogen activity, which is the driving force in the mass transfer, can be calculated according to the following formula;

$$a_N = K_N \frac{P_{NH_3}}{P_H^{3/2}} \qquad (2.7)$$

where K_N is the equilibrium constant of nitrogen, and P_{NH3} and $P^{3/2}H$ are the partial pressures of ammonia and hydrogen, respectively [7].

K_N is the quotient of the partial pressure of the ammonia still present in the furnace (the amount of ammonia that has not yet dissociated) and the partial pressure of the hydrogen that has already formed by ammonia dissociation. K_N is calculated as follows:

$$K_N = \frac{P_{NH_3}}{P_{H_2}^{3/2}} \tag{2.8}$$

If K_N is known as a value for nitride forming, it can be obtained from the diagram developed by Lehrer [40]. Lehrer's equilibrium diagram (Figure 2.14) shows the areas of existence of nitride phases and lines of equal nitrogen concentrations. To each combination of nitriding potential and temperature, a concentration of nitrogen in iron, in equilibrium with the atmosphere, can be ascribed [31].

The dissociation rate of ammonia or the nitriding potential are the most critical parameters to understand and control the nitriding process [9].

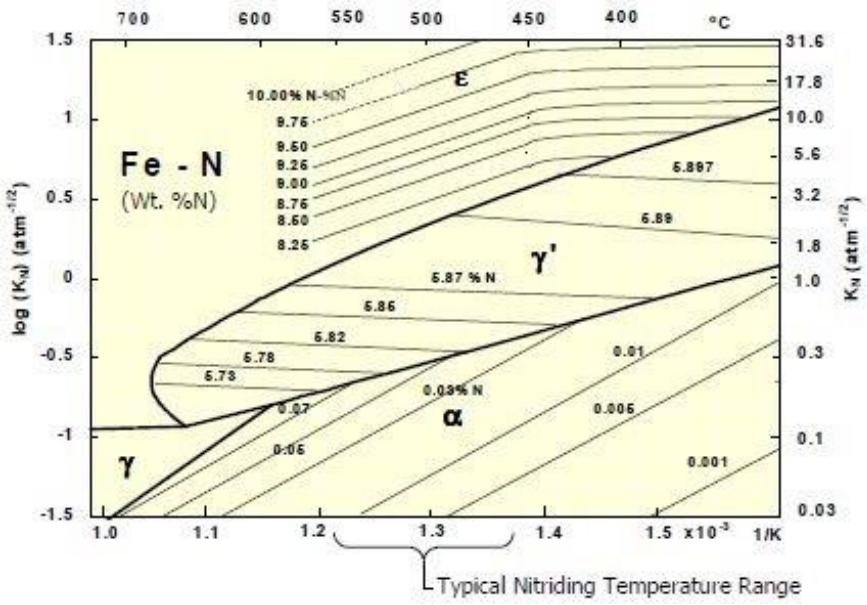

Figure 2.14 Lehrer diagram [41]

Gas nitriding has been conducted as either a single stage or a double stage process. Temperatures in the single stage process range from about 495 °C to 525 °C, and dissociation from 15% to 30%. The first stage normally lasts for a period of 4 to 10 hours [42]. The temperature is selected to maintain the required core hardness, but at the same time the highest possible to enhance the diffusion rate and shorten the process cycle [31]. The process creates an intense layer at the work surface, which is known as the compound layer [42].

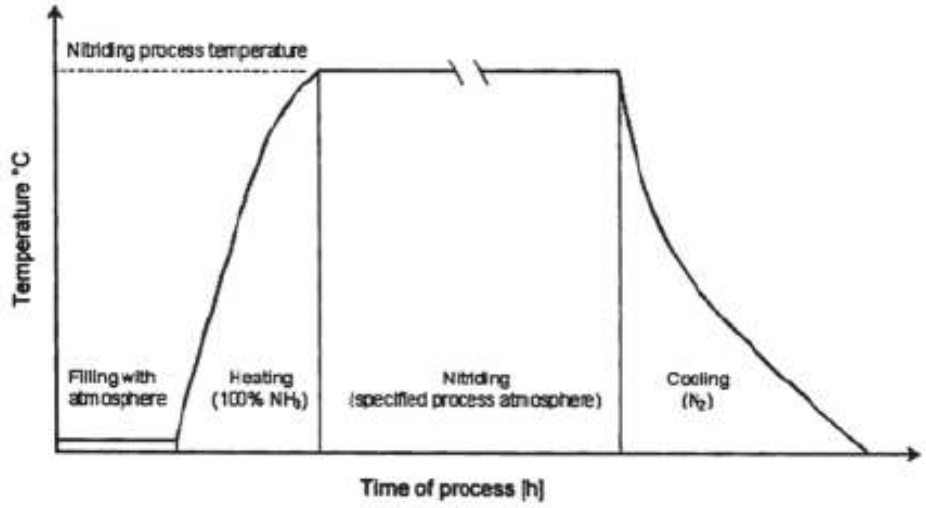

Figure 2.15 Schematic representation of a single stage nitriding process [31]

When the double stage process, known also as the Floe process is used, it has the advantage of reducing the thickness of the compound layer. The first stage of the two-stage process is, except for time, a duplication of the single-stage process. The second stage may proceed at the nitriding temperature employed for the first stage or the temperature may be increased from 550 °C to 565 °C. However, at either temperature, dissociated ammonia in the second stage is increased to 65-80%. Generally, an external ammonia dissociate is necessary for obtaining the required higher second-stage dissociation [7], [42], [43].

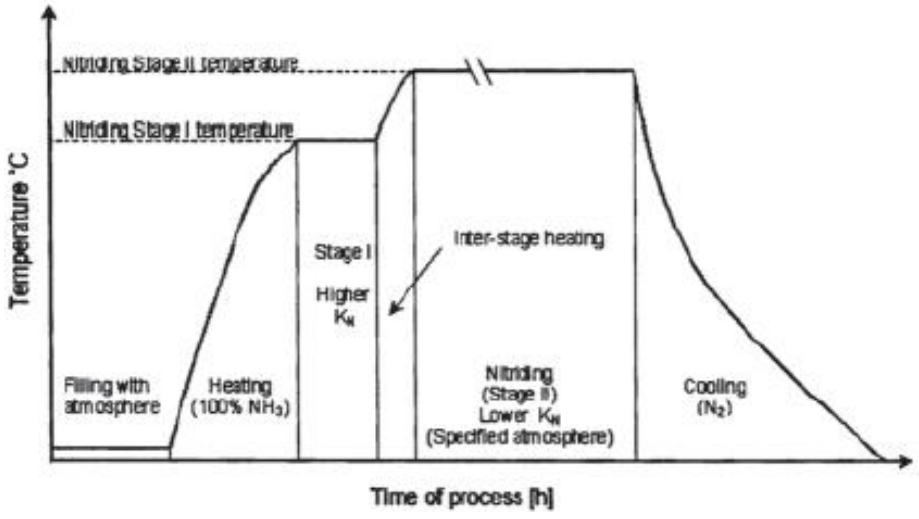

Figure 2.16 Schematic representation of a double stage nitriding process [31]

Gas nitriding is typically performed in convection furnaces, either of pit type vertical furnace as shown in Figure 2.17 or a box furnace. The parts to be nitrided are placed on fixtures or in “baskets”, which are transferred to and loaded into the furnace. The furnace cover or door is then closed. To ensure precision with regard to compound layer and diffusion layer thickness, it is important with enough good furnace temperature uniformity, typically ± 5 °C.

Figure 2.17 Pit-type furnace installation used for gas nitriding [32]

A nitriding cycle consists of the steps illustrated in Figure 2.18. Nitrogen purging of the furnace is conducted to remove the air before ammonia is let into the furnace. This purge is carried out to eliminate the risk of explosion, as ammonia and oxygen form an explosive mixture within a certain concentration range. For this reason it is also advantageous to perform heating to nitriding temperature in nitrogen. When the nitriding temperature is reached, ammonia is let into the furnace. In the beginning a high flow rate is used to increase the efficiency of nitrogen transfer to the steel surface.

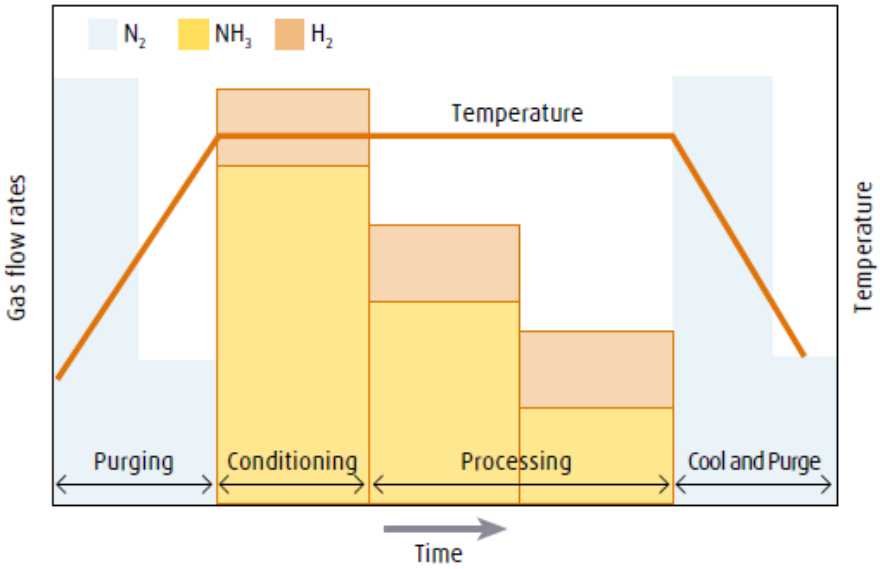

Figure 2.18 Nitriding steps and connected gas consumption [32]

After finishing the nitriding step, the furnace interior is purged with nitrogen to remove the ammonia gas in order to ensure safety. In furnaces without a retort, cooling takes place in the furnace [32].

2.5.2 Fluidized Bed Nitriding

For heat treatment of metal parts wide variety of furnaces are employed. Protective atmosphere furnaces like sealed quench furnace, vacuum furnaces, pit type retort and salt bath furnaces are used for heat treatment processes [44]. The fluidized bed furnace is a unique metallurgical processing tool that enables the user to complete most heat treatment processes [7].

Fluidization is the method of making a bed of small particles behaves like a liquid [6]. This is achieved by passing a stream of air or gas upward through the particle bed. As the velocity of the air or gas stream is raised, it meets with resistance due to the mass of the particles. However, at a critical point (where the frictional resistance equals the particle mass) the bed suddenly expands.

Particles that were touching each other move apart and float on a cushion of air. The particles are now said to be "fluidized" [44].

The particles in this instance are aluminum oxide. Several gases can be used to fluidize the aluminum oxide particles: nitrogen, ammonia, methane, endothermic gas or gas mixtures. Good heat transfer takes place from the heating medium to the aluminum oxide particles, which in turn transfer the heat to the workpiece. When the bed is in operation, its surface of finely divided aluminum oxide particles bubbles just like water bubbles when air passes through it (Figure 2.19) [7].

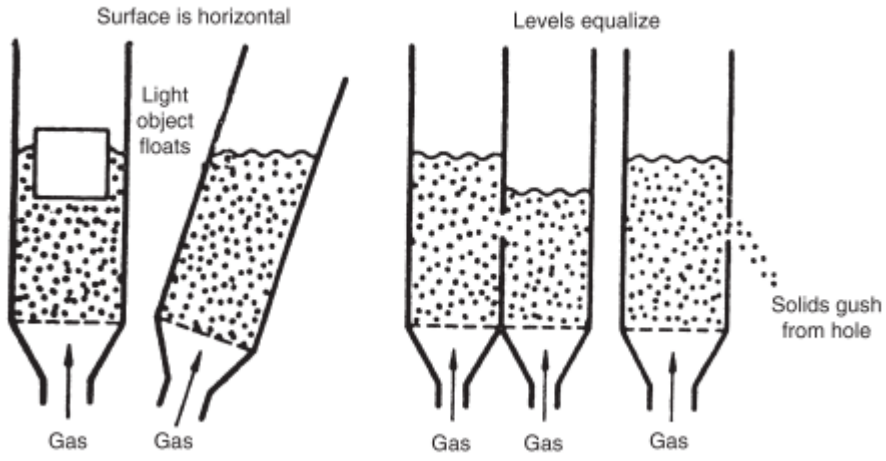

Figure 2.19 Liquid like behavior of gas fluidized beds [7]

The construction of the fluidized bed is shown in the Figure 2.20. The fluidized bed furnaces house a bed (a retort) containing very dry, uniformly sized particles of inert aluminium oxide. Air or blends of gases for specific treatment processes are introduced through a diffusion plate beneath the retort, separating and mobilizing the minute particles to give them fluid like characteristics. Silicon carbide elements, between the retort wall and furnace's outer insulated wall, heat the flowing particles. Into the fluidized bed, which resembles a vat of boiling liquid, are introduced metal parts or tools for heat treatment. The mobilized particles engulf the object and begin radiating a uniform heat.

The ability to alter temperature and atmosphere quickly gives the furnaces their superior flexibility. The fluidized particle medium conducts heat rapidly and uniformly to achieve quick heat-ups, reduced cycle times, and to provide efficient energy utilization [45].

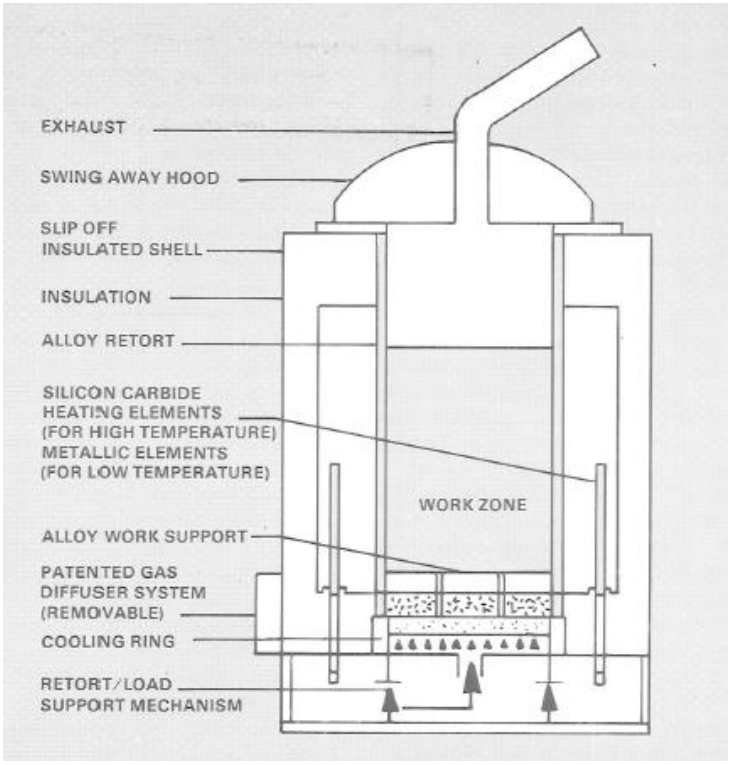

Figure 2.20 Cross section of a typical fluidized bed furnace [45]

The ability of the fluidized bed to recover to the process temperature after the workload has been removed from the furnace and a new load introduced makes it an attractive choice for nitriding. The bed does not require conditioning or purging when changing from one atmosphere system to another, making it productive and economical in terms of operating costs and throughput [7]. And the other advantage of the fluidized bed is that process cycle times are reduced simply because of faster temperature recovery and the ability to rapidly change the atmosphere composition when necessary. With the advantages, there are also disadvantages. The principal disadvantage is the volume of the reactive gas required to fluidize the bed is considerably higher than the gas flow that would be required for say, an integral quench furnace [46].

2.5.3 Salt Bath Nitriding

Salt bath nitriding has been used for a long time in metallurgical processes. Other technologies have been developed, such as the fluidized bed nitriding and plasma nitriding, which have undergone improvements with respect to heating and cooling. However, notwithstanding the performance of the new techniques, the molten salt bath is used the most in industry [24].

Salt bath nitriding is conducted in the fused salt bath containing either cyanides or cyanates [25]. Typically, the salt mixture consists of 60-70% sodium salts (96.5% NaCN, 2.5% Na_2CO_3, 0.5% NaCNO) and 30-40% potassium salts (96% KCN, 0.6% K_2CO_3, 0.75% KCNO, 0.5% KCl) [6]. The bath composition has a decisive effect on formation of the case layers [7], [24].

The salt-bath process is carried out in a pot, in which powdered salt is melted by gas or electrical heating (Figure 2.21) [31]. When heat is applied from either an internal or external source, the salt melts and liberates nitrogen to the steel for diffusion. When a steel workpiece is introduced into the salt and heated up to a temperature in the molten salt, similar reactions begin to occur as in gas nitriding; that is, controlled amounts of nitrogen are released to diffuse into the steel surface [7].

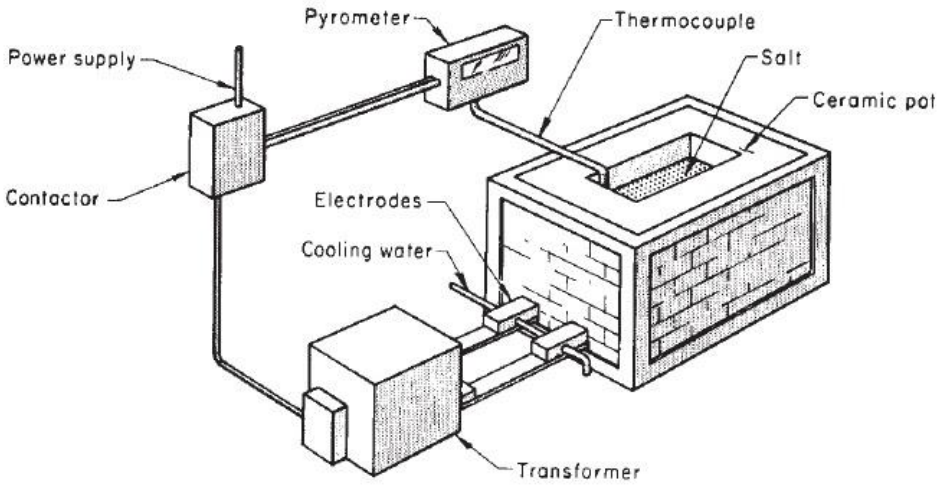

Figure 2.21 Internally heated salt bath furnace [7]

The salt bath nitriding process has several proprietary modifications and is applied to a wide variety of carbon, low alloy steels, tool steels, stainless steels, and cast irons [6].

Workpieces of iron and steel with usual carbon contents can be nitrided in salt melts low in cyanide or even without cyanide, with cyanate being used as the nitrogen-supplying component [24]. Salt bath nitriding process includes various techniques such as, liquid pressure nitriding, aerated bath nitriding and aerated low cyanide nitriding [6].

The major advantage is the short cycle times, due in part to rapid heating of the load immersed in the salt bath [31]. An added benefit was that operating costs were considerably lower, making it a cost effective method of nitriding steel [7]. A disadvantage of the salts used are highly toxic (disposal of salts are controlled by stringent environmental laws in western countries) and only one process possible with a particular salt type [47].

2.5.4 Plasma Nitriding

Plasma nitriding is a plasma assisted thermochemical surface treatment that involves diffusion of nitrogen in the target-surface leading to formation of nitrogen rich solid solution and nitrides [48]. Plasma nitriding uses plasma discharge technology at lower temperature to introduce nascent nitrogen on the steel surface [9]. Plasma is formed in a vacuum using a high voltage electrical energy to accelerate nitrogen ions which bombard the alloy surface (Figure 2.22) [25].

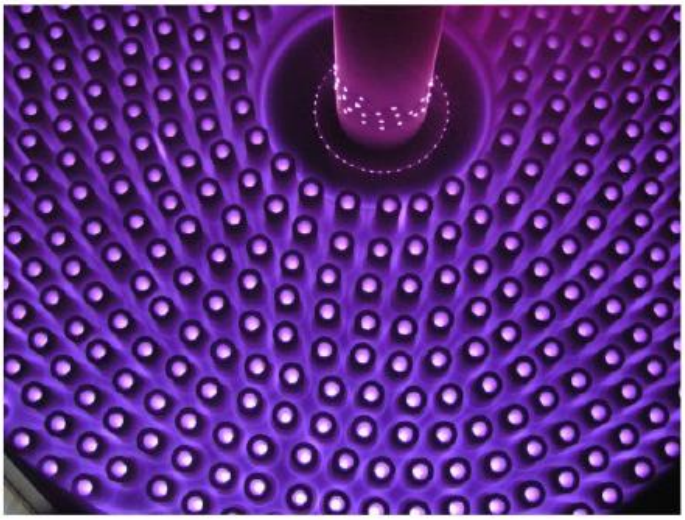

Figure 2.22 Plasma state [25]

The plasma nitriding process is accomplished in a vacuum chamber where the sample is connected to a cathode. A high voltage (about 300–1000 V) is applied between the cathode and the vessel, which works as an anode, and the gas pressure varies from about 100 to 1300 Pa (1–13 mbar). Under these conditions, an abnormal glow discharge that covers the sample is obtained. The plasma nitriding process normally is preceded by a cleaning and pre-heating stage that is carried out under an atmosphere of hydrogen. Then, the addition of the nitrogen initiates and sustains the nitriding action [11]. The principle of operation of the plasma nitriding furnace is shown in Figure 2.23.

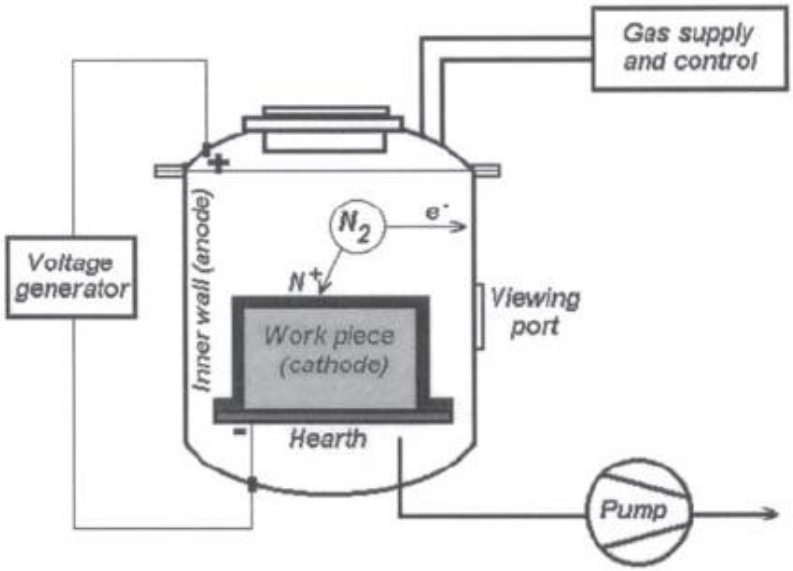

Figure 2.23 Principle of operation of a plasma nitriding furnace [32]

During plasma nitriding, four reactions occur at the surface of the material being treated [7].

Reaction I. Ionized and neutral nitrogen atoms are produced by energized electrons:

$$e^- \longrightarrow N_2 = N^+ + N + 2e^- \quad (2.9)$$

Reaction II. Iron and other contaminants are removed from the surface of the work by an action known as sputtering. The impact of the nitrogen ions bombarding the work surface dislodges the contaminants, which are removed by the vacuum pumping system. Contaminant removal can be loosely described as atomic cleaning and allows nitrogen to diffuse into the work surface:

$$N^+ \longrightarrow \text{Work surface} = \text{Sputtered Fe and Sputtered Contamination} \quad (2.10)$$

Reaction III. As a result of the impact of the sputtered iron atoms, case formation begins at the work surface of iron nitrides:

$$\text{Sputtered Fe} + N = FeN \quad (2.11)$$

At this point, intensive surface cleaning of the workpiece occurs due to the sputtering action on the surface.

Reaction IV. At the work surface the breakdown of FeN begins under the influence of continual plasma bombardment. The plasma causes instability of the FeN, which begins to break down into the ε-phase, followed by the γ'-phase and an iron/nitrogen compound layer (Figure 2.24) [8]:

$FeN \longrightarrow Fe_2N + N$ (ε-phase) (2.12)

$Fe_2N \longrightarrow Fe_3N + N$ (ε-phase) (2.13)

$Fe_3N \longrightarrow Fe_4N + N$ (γ'-phase) (2.14)

$Fe_4N \longrightarrow Fe + N$ (iron/nitrogen compound layer) (2.15)

The formation of a compound layer and a diffusion layer depends on the concentration of nitrogen (Figure 2.25) [6].

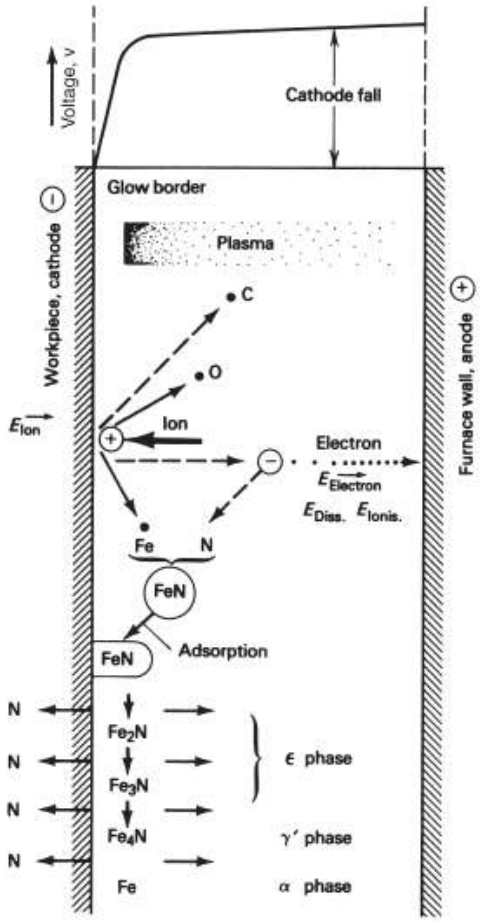

Figure 2.24 Glow discharge plasma nitriding mechanisms (Koelbel's models) [8]

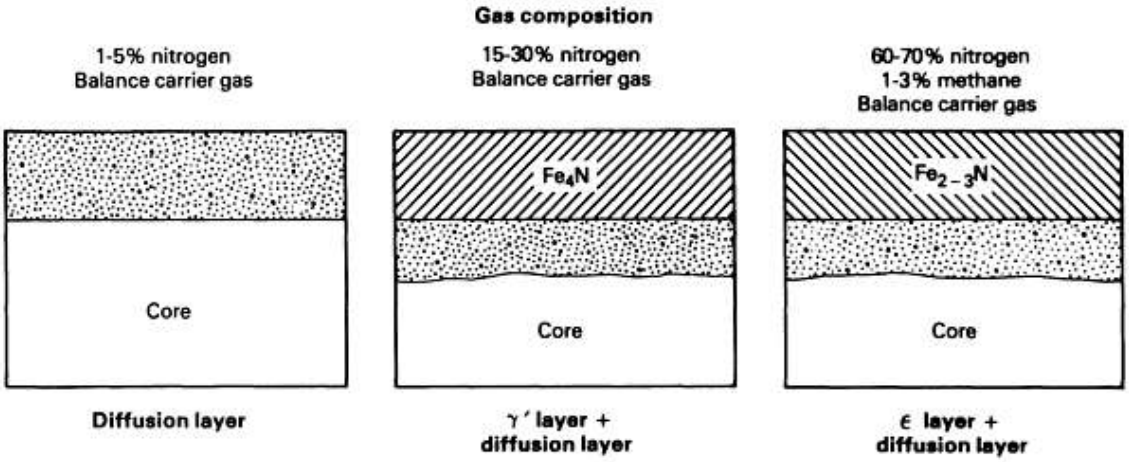

Figure 2.25 Typical gas compositions and the resulting metallurgical configurations of plasma nitrided steel [6]

The advantages of plasma nitriding include the low temperature, short saturation time and simple mechanical masking. The unique advantage is surface activation sputtering. Due to the sputtering effect of positive ions in the glow discharge, the protective oxide, inherent for surfaces of stainless steels, aluminum or titanium alloys, is removed. In the conventional direct current system the nitrided component is subjected to the high cathode potential and plasma forms directly on the component surface. This may create disadvantages such as the temperature non-uniformity with a possibility of overheating, sensitivity to the part geometry, causing edge effect and a possibility of surface damage due to arcing [25].

2.6 Advantages and Disadvantages of Nitriding Processes

Advantages and disadvantages of nitriding processes are compared in Table 2.1.

Table 2.1 Advantages and disadvantages of nitriding processes [31]

Process	Advantages	Disadvantages
Salt Bath Nitriding	➢Rapid heating and processing ➢Ease of obtaining good nitrided layers on low carbon and low alloy steels ➢Possibility of quenching parts immediately after process	➢No in-process control ➢Limited to those applications that can be heated to higher temperatures, without losing core hardness. ➢Short processes only ➢Requires thorough washing to remove salt residues which may cause corrosion ➢Health hazard and waste disposal problems
Plasma (Ion) Nitriding	➢Selective nitriding by simple masking techniques ➢Ease of surface activation through cathodic sputtering ➢Low temperature processes possible	➢Problems with temperature measurement and uniformity ➢Risk of overheating if not closely monitored ➢Results critically sensitive to part geometry and arrangement in furnace
Gas Nitriding	➢Simple control techniques	➢ Controlling parameter: (ammonia dissociation rate) inadequate for precise process control ➢Ammonia, as a nitriding medium is toxic and environmentally unsound ➢Masking requires copper plating or painting with protective paste

Table 2.1 Advantages and disadvantages of nitriding processes [31] (cont'd)

Process	Advantages	Disadvantages
Fluidized Bed Nitriding	➢Fast heating end cooling possible without the problems connected with salt bath nitrding	➢High gas consumption due to necessity of running high flow rates to overcome sand bed resistance ➢Difficult process control

2.7 Nitridable Steels

Aluminum, chromium, vanadium, tungsten, and molybdenum, as the commonly used alloying elements in commercial steels, are beneficial in nitriding because they form nitrides that are stable at nitriding temperatures. Other alloying elements, such as nickel, copper, silicon, and manganese, have little, effect on nitriding characteristics [6].

By measuring the hardness of various alloy steels so treated it is possible to investigate the tendency of the different alloying elements to form hard nitrides or to increase the hardness of the steel by a mechanism known as precipitation hardening. The results obtained by such investigations are shown in Figure 2.26, from which it can be seen that very high hardnesses result from alloying a steel with Al or Ti in amounts of about 1.5%. On nitriding the base material in Figure 2.26 a hardness of about 400 HV is obtained and according to the diagram the hardness is unchanged if the steel is alloyed with Ni since this element is not a nitride former and hence does not contribute to any hardness increase [49].

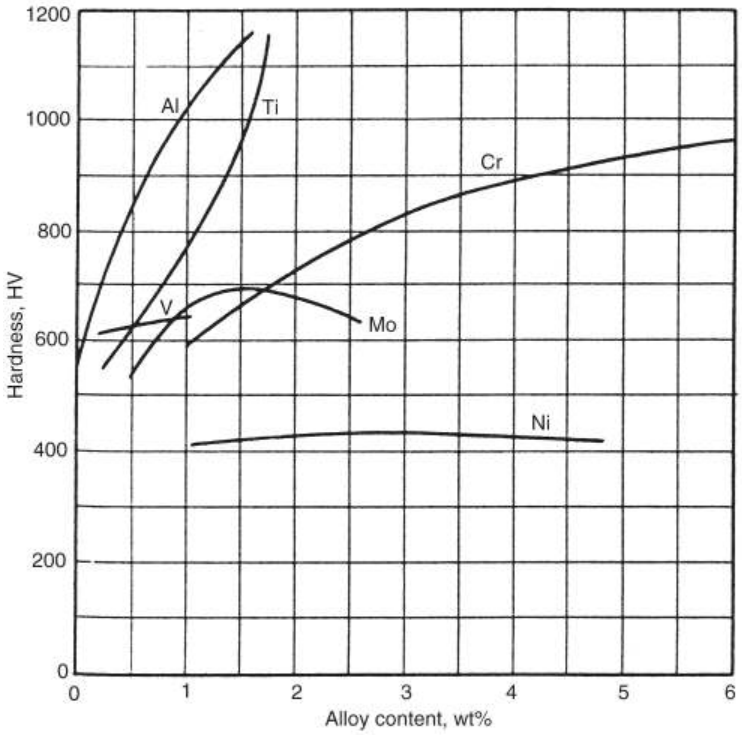

Figure 2.26 Effect of alloying element additions on hardness after nitriding [7]

Aluminum forms very hard nitrides in the surface of the steel when nitrided. Generally the maximum amount of aluminum permitted in the steel is in the region of 1.5%.

Molybdenum forms stable nitrides at the nitriding temperature and reduces the risk of surface embrittlement at the nitriding temperature.

Chromium also forms stable nitrides at the nitriding temperature; however, the high chromium contents found in some stainless steels make them more difficult to nitride. The reason for this is that chromium reacts with oxygen and forms a chrome oxide barrier on the surface of the material to be nitrided. It is necessary to break down the barrier of chromium oxide on the surface. Once the barrier has been broken down, then the nitriding is effective. The higher the percentage of available chromium at he surface of the steel, the more difficult the steel is to nitride. The positive side of this is usually high surface hardness values.

Vanadium in nitriding steel also is conducive to the formation of stable nitrides. In addition, fine grain toughness is exhibited within the formed case.

Tungsten enables the steel to retain its hardness at high operating temperatures without any loss of surface hardness. Depending on the tungsten content and the general composition of the steel, the nitrided steel is able to operate at temperatures up to 590 °C without any appreciable loss of surface hardness and has enhanced wear characteristics [7], [50].

Various classes of nitridable steels are given below:

- Aluminum-containing low alloy steels
- Medium-carbon, chromium-containing low alloy steels of the 4100, 4300, 5100, 6100, 8600, 8700, and 9800 series
- Hot-work die steels containing 5% chromium such as H11, H12, and H13
- Low-carbon, chromium-containing low alloy steels of the 3300, 8600, and 9300 series
- Air-hardening tool steels such as A-2, A-6, D-2, D-3, and S-7
- High-speed tool steels such as M-2 and M-4
- Nitronic stainless steels such as 30, 40, 50, and 60
- Ferritic and martensitic stainless steels of the 400 and 500 series
- Austenitic stainless steels of the 200 and 300 series
- Precipitation-hardening stainless steels such as 13-8 PH, 15-5 PH, 17-4 PH, 17-7 PH, A-286, AM350, and AM355
- Nitriding steels DIN series [6].

CHAPTER 3

NITROCARBURIZING

3.1 Historical Review of Nitrocarburizing

The first ferritic nitrocarburizing methods were done at low temperatures, around 550 °C, in a liquid salt bath. The first company to successfully commercialize was the Imperial Chemical Industries in England. They called their process a "Sulfinuz" treatment because it had sulfur in the salt bath. While the process was very successful with high speed spindles and cutting tools, there were issues with cleaning the solution off because it was not very water soluble.

Because of the cleaning issues the Joseph Lucas Limited company began experimenting with gaseous forms of ferritic nitrocarburizing in the late 1950s. The company applied for a patent by 1961. It produced a similar surface finish as the Sulfinuz process with the exception of the formation of sulfides. The atmosphere consisted of ammonia, hydrocarbon gases, and a small amount of other carbon-containing gases.

This spurred the development of a more environmentally friendly salt bath process by the German company Degussa. Their process is the widely known Tufftride process. Following this the plasma nitriding process was invented in the early 1980s. This process had faster cycle times, required less cleaning and preparation, formed deeper cases, and allowed for better control of the process [6], [7].

Today, “ferritic nitrocarburizing” is commonly called simply “nitrocarburizing”.

3.2 Nitrocarburizing Process

Nitrocarburizing is a thermochemical surface treatment during which nitrogen and carbon are supplied simultaneously to a steel surface at temperatures usually between 550 °C and 580 °C [51].

Nitrocarburizing accomplishes surface treatment of a part in the ferrite region of the iron-carbon equilibrium diagram (Figure 3.1) [7]. Nitrogen is soluble in iron at the temperature range of 315 °C and upward. Carbon is also soluble in iron at the temperature higher than 370 °C. These elements are soluble in a solid solution of iron [46]. As the process takes place in the ferrite region, both nitrogen and carbon diffuse into the steel surface [7].

In comparison to other surface engineering technologies, nitrocarburizing is distinguished by its low treatment temperature and short treatment time, and high degree of shape and dimensional stability. As nitrocarburizing is applied in gas, liquid and plasma forms [52].

Nitrocarburizing improves the surface characteristics of plain carbon steels, low alloy steels, cast irons, and sintered ferrous alloys: resistance to wear, fatigue, and corrosion are improved with the introduction of nitrogen and carbon [7], [27].

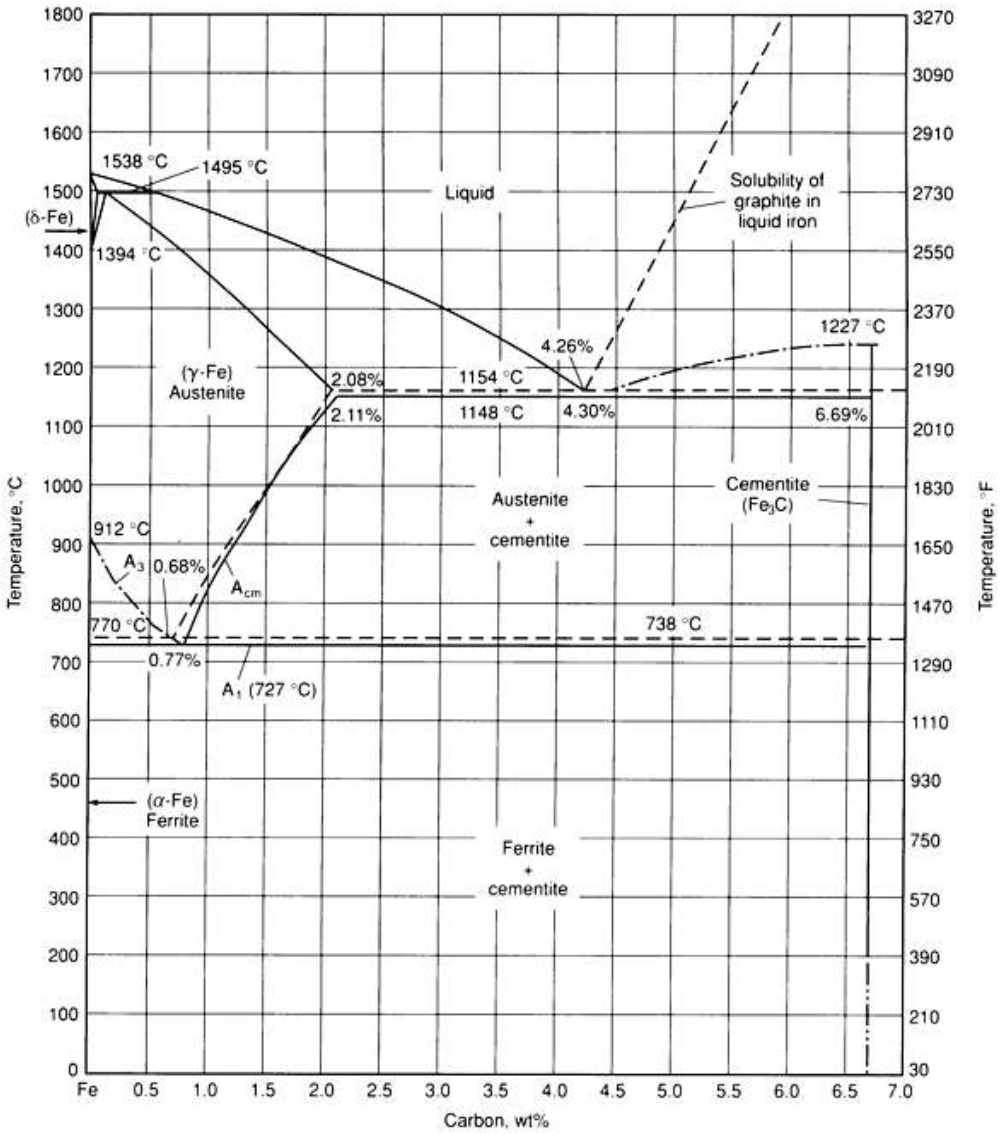

Figure 3.1 Iron-Carbon equilibrium diagram [6]

3.3 Nitrocarburized Layer

During nitrocarburizing, a two part surface layer is formed, initially an outer compound layer, followed by a diffusion layer below it [53]. A schematic view is shown in Figure 3.2. The compound layer and diffusion layer dimensions vary according to the composition of the substrate, nitrogen and carbon activity and treatment temperature and time [52].

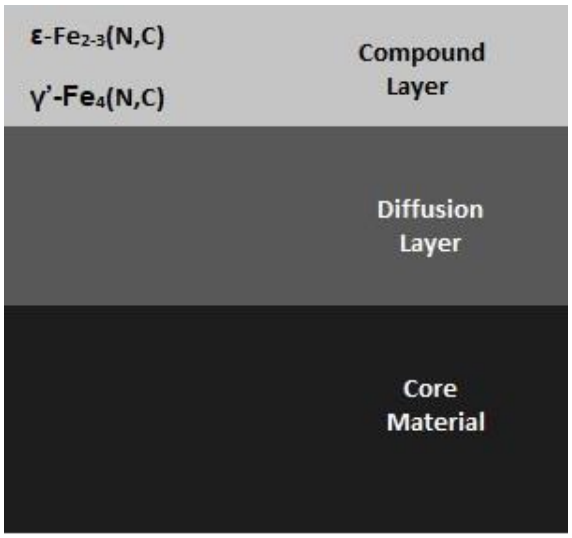

Figure 3.2. Typical nitrocarburized layer

The compound layer provides the materials with good physical and chemical properties against wear and atmospheric corrosion [54]. The compound layer is typically composed of carbonitrides of iron ε-Fe_{2-3}(N,C) and/or iron nitride γ'-Fe_4(N,C) and occasionally cementite θ-Fe_3C (Table 3.1) [25], [55].

Table 3.1 Characteristics of phases in Fe-N-C system at 580-590 ^{o}C [25]

Phase	**N (at. %)**	**C (at. %)**	**Crystallography**	**Atom arrangement**
α-Fe	0-37	0-0.02	Fe bcc,	N, C in octahedral sites
θ-Fe_3C	0	25	Fe complicated orthorhombic	C in bicapped trigonal prisms
γ'-Fe_4N_{1-z}	19.4-20	<0.7	Fe fcc,	N ordered in central octahedral sites
ε-$Fe_3(N,C)_{1+x}$	15-33	0-8	Fe hcp,	N ordered in octahedral sites

The development of the composition and morphology of the compound layer is schematically shown in Figure 3.3. On nitrocarburizing pure iron the first phase appearing at the surface is cementite (θ-Fe_3C). After the initial development of cementite, the ε-phase becomes dominant in the compound layer on prolonged treatment. The appearance of the ε-phase in the compound layer is promoted by a high nitrogen potential and is retarded by a high carburizing activity. [56]. The amount of ε-phase in the compound layer then increases strongly by growth of ε into the substrate by conversion of θ into ε. The next step in the formation of the compound layer is the formation of γ' between ε and the substrate [57].

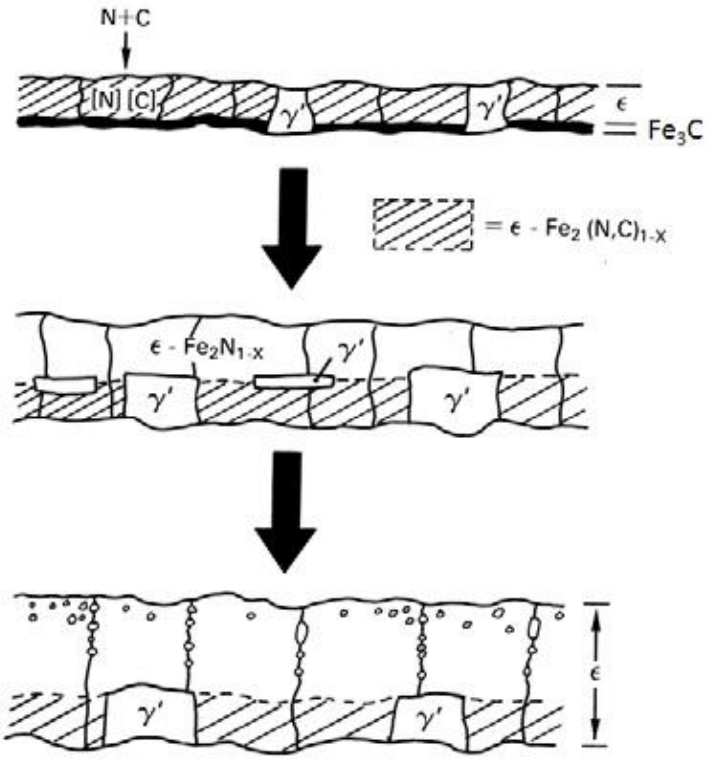

Figure 3.3 Stages of compound layer development during nitrocarburizing of iron at a temperature below 592 °C [56]

The growth rate of the compound layer is governed by which phases it contains. Figure 3.4 shows an isothermal section of the Fe-N-C phase diagram at 580 °C. The γ'-phase is an almost stoichiometric compound with a narrow solubility range for carbon and nitrogen. This makes the growth rate of γ' relatively slow.

The ε-phase has a higher solubility range for both nitrogen and carbon and a high nitrogen mobility, which lets it grow quicker. Since the ε-phase is favored by high nitriding potential and by high alloy content, increasing these parameters makes the compound layer grow faster [52].

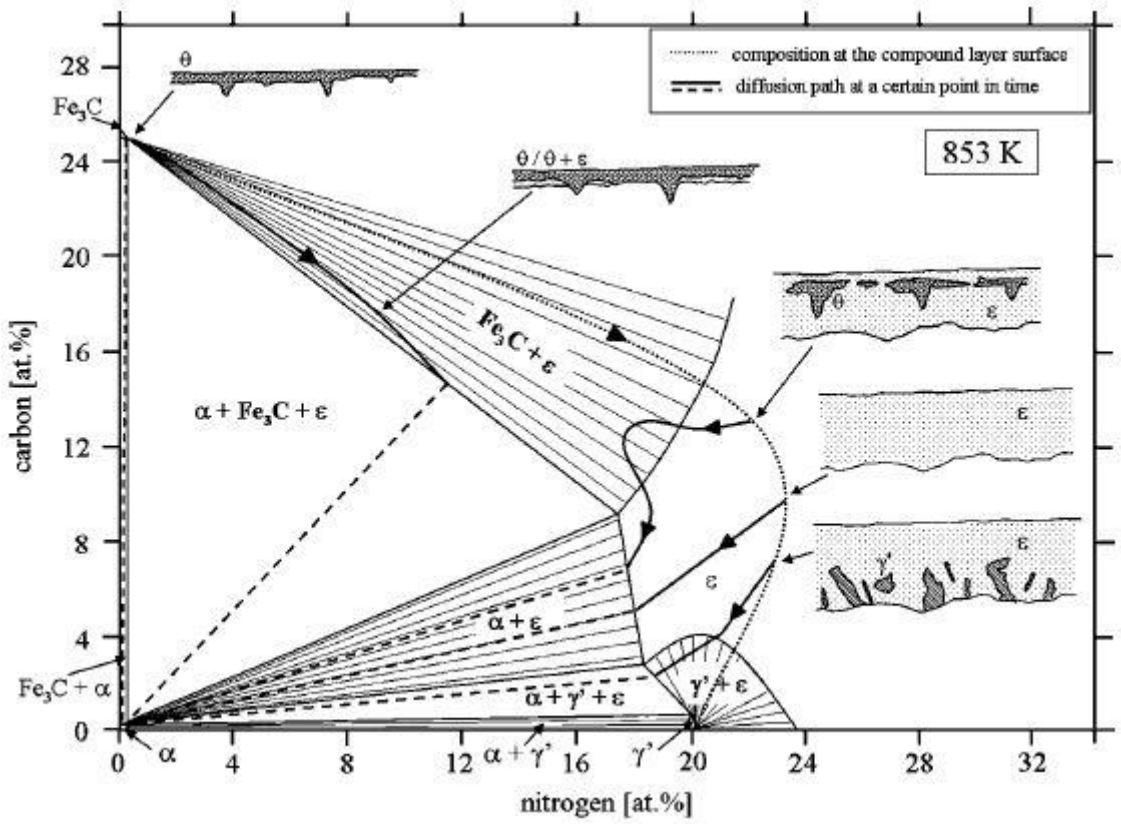

Figure 3.4 Isothermal section of the Fe-C-N phase diagram at 580 °C [57]

In the diffusion layer nitrogen and carbon exist either in an interstitial solid solution in the ferritic phase or in alloy nitrides and carbides [52]. Depending on the initial structure and composition of the core material, the nitrogen in the diffusion layer is dissolved in the iron lattice and/or precipitated as very fine nitrides. With unalloyed steels, the nitrogen is dissolved in the iron lattice. Due to the diminishing solubility of nitrogen in iron during slow cooling, γ' nitrides are precipitated in the outer region of the diffusion layer. With alloyed steels which contain nitride forming elements, the formation of stable nitrides or carbonitrides takes place in the diffusion layer independent of the cooling speed [53].

The diffusion layer brings about an improvement of fatigue strength when compared to an untreated material. The improvement in fatigue properties is directly related to the depth of nitrogen diffusion. In alloy or tool steels, the diffusion layer is also capable of very high hardnesses, owing to the heavy dispersion of alloy nitrides which form when alloy carbides interact with inward diffusing nitrogen [58].

3.4 Properties of Nitrocarburized Surface

Nitrocarburizing is widely applied in manufacturing of machine components and tools, since improved surface hardness, fatique strength, corrosion and wear resistance at elevated temperatures are achieved at minimal distortion. Thus, the service life of a part is significantly extended [59].

3.4.1 Hardness

One of the main reasons for utilizing nitrocarburizing is that it produces a very hard surface layer [52]. The surface hardness obtainable by nitrocarburizing process is mainly influenced by the composition of the material. The higher the content of nitride forming alloying elements (Cr, Mo, Al, V, Mn, Ti, W) the greater the surface hardness [60]. And also compound layer hardness increases with increasing alloy content in the steel as shown in Figure 3.5 [32]. The hardness of the diffusion layer follows the concentration gradients of nitrogen and carbon [52].

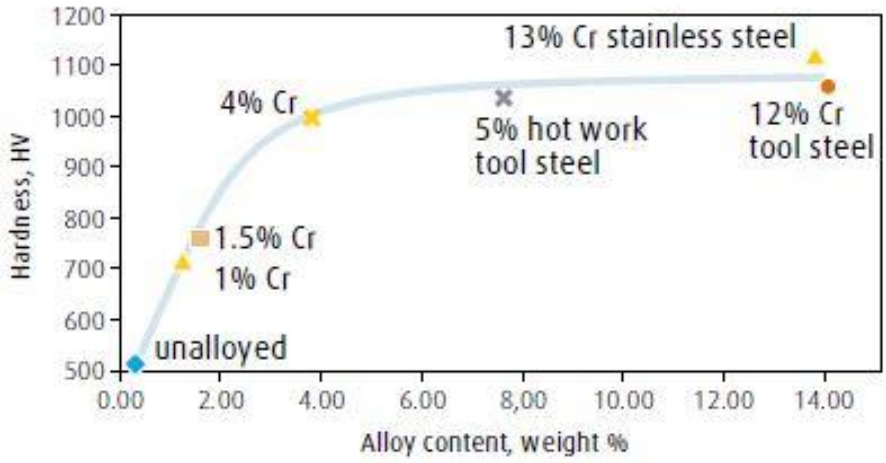

Figure 3.5 Approximate relation between hardness of the compound layer and alloying content (Sum of Cr+Mo+V+W) of the treated steel [32]

Microhardness profile of a steel after nitrocarburizing depends on its composition and the parameters of the process. The microhardness of the nitrocarburized layers is very high on the surface (compound layer). It gradually decreases through the diffusion layer and approaches the basic microhardness of the matrix in the unsaturated core [61].

3.4.2 Fatigue Strength

The nitrocarburizing is recognized as one of the most important thermochemical applications in enhancing the fatigue performance of machine components [62].

The fatigue strength of a nitrocarburized part is improved by compressive residual stresses created in the diffusion layer as a consequence of the heat treatment [52]. There is also a state of compressive stress in the compound layer if it consists of a γ'-phase, whereas tensile surface stress has been predicted but not clearly confirmed for ε-phase. The highest compressive stresses are obtained when nitrocarburizing is completed with a fast quench in water or oil [32].

3.4.3 Wear Resistance

The wear resistance of the nitrocarburized materials are increased by diffusion of C and N elements and growth of a compound layer of metallic carbides, nitrides [54].

The ability of the compound layer to resist wear is dependent on the type of wear system, specifically whether it is adhesive or abrasive wear. Adhesive wear occurs when two components are in relative motion in an essentially abrasive free environment. Under these conditions, the intrinsic physical characteristics of the compound layer, i.e. hardness and lubricity, notably improve the sliding and running behavior and consequently, increase the resistance to adhesive wear. The phase composition of the compound layer that demonstrates the best wear resistance consists predominantly of ε-phase with a very small amount of γ' prime phase.

Resistance to abrasive wear is dependent on the relative hardnesses of the abrading substance and of the compound layer. Increased hardness in the compound layer gives increased resistance to abrasive wear, in which abrasive particles such as sand wear a surface. Abrasive wear resistance is proportional to hardness and for nitrocarburized steels is therefore dependent on the type of steel used [7], [32].

3.4.4 Corrosion Resistance

The resistance against corrosion of ferritic workpieces is improved by the presence of the iron nitride based compound layer at the surface as produced by a nitrocarburizing treatment. Usually, such a compound layer is predominantly composed of the iron (carbo)nitrides ε-Fe_{2-3}(N,C) and y'-Fe_4(N,C) [63]. The ε-phase has better corrosion properties than the y'-phase because of its crystalline structure and higher nitrogen content. The quantity of ε-phase in the compound layer is the most important factor for improved corrosion resistance [52].

A further, immense improvement of the corrosion resistance of nitrocarburized workpieces is achieved by an oxidation treatment after the nitrocarburizing treatment [63]. The oxidation treatment of the nitrocarburized materials enhances the electrochemical properties due to the formation of oxide top layer [64].

3.5 Types of Nitrocarburizing

Nitrocarburizing is a subcritical heat treatment process, carried out by salt bath, gaseous or plasma techniques and involves the diffusion of carbon and nitrogen into the ferritic phase [50].

3.5.1 Gas Nitrocarburizing

Gas nitrocarburizing is the most commonly used in the industry today [52]. Gas nitrocarburizing involves the introduction of carbon and nitrogen into a steel at a specific temperature [6].

The nitrocarburizing process consists of three principal steps: heating, diffusion at the nitrocarburizing temperature and cooling.

The composition of the atmosphere is a very important parameter in gas nitrocarburizing and needs to be closely controlled. The atmosphere consists of nitrogen (N_2), ammonia (NH_3), carbon dioxide (CO_2) and hydrogen (H_2). Ammonia is used as source of nitrogen. Carbon dioxide decomposes into carbon monoxide which together with hydrogen is needed for the transfer of carbon to the steel surface. Sometimes carbon monoxide is used directly instead of carbon dioxide. Hydrogen is not always added separately as it forms from decomposition of ammonia. Nitrogen is used to control the percentage of the other gases and for purging the furnace before and after treatment as ammonia can form an explosive mixture with oxygen. The flow rates of different gases in each process step are plotted in Figure 3.6 [52]. Final cooling is carried out in gas or oil. The fast cooling in oil reduces the process time compared to when slow gas cooling is used [7], [32].

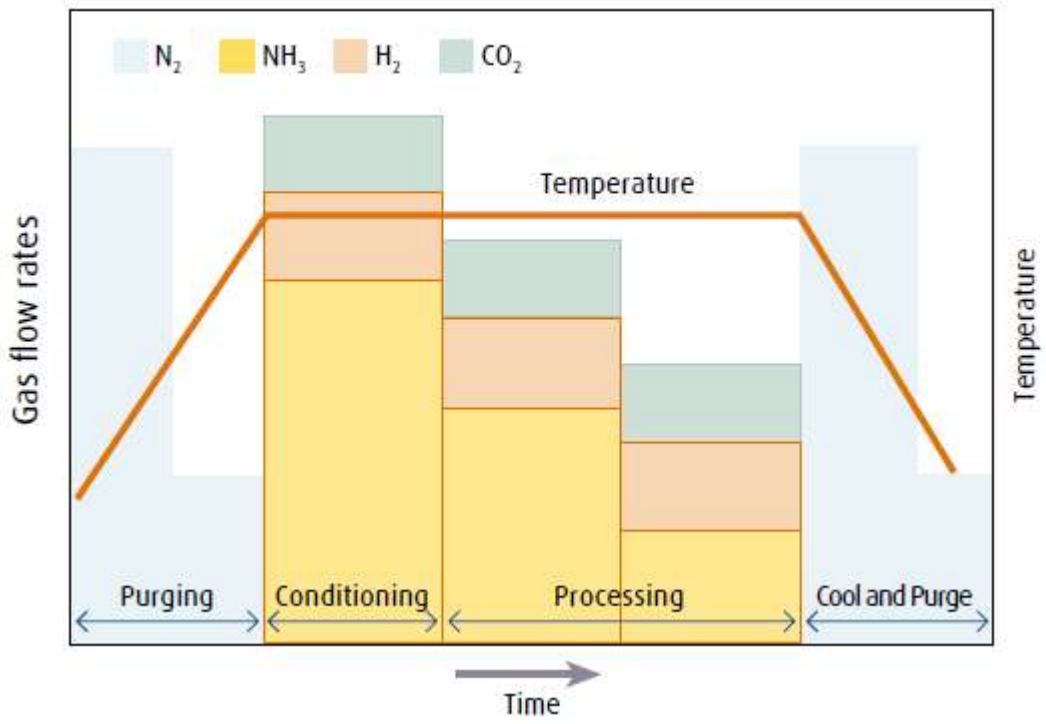

Figure 3.6 Nitrocarburizing steps and connected gas consumption [32]

In gas nitrocarburizing the transfer of nitrogen and carbon atoms can be divided into three steps:

I. Deposition onto the steel surface,

II. Diffusion in the compound layer and

III. Diffusion in the diffusion layer.

Ammonia is decomposed into hydrogen and nitrogen at the steel surface, making it possible for the surface to adsorb the nitrogen atoms. The reaction is described by Equation 3.1 [52].

$$2NH_3 \longrightarrow 2N + 3H_2 \quad (3.1)$$

If carbon dioxide is used as carbon source its decomposition takes place in two steps, described by Equation 3.2 and 3.3. First carbon dioxide reacts with hydrogen to form carbon monoxide and water. Thereafter carbon atoms are adsorbed by the steel surface when carbon monoxide reacts with hydrogen to form carbon and water [27], [52].

$$CO_2 + H_2 \longrightarrow CO + H_2O \quad (3.2)$$

$$CO + H_2 \longrightarrow C + H_2O \quad (3.3)$$

On the basis of reactions (Equation 3.1) and (Equation 3.3) the activities of adsorbed nitrogen, a_N, and carbon, a_C, can be defined at 1 bar pressure:

$$a_N = K_{3.1} \times K_N \qquad a_C = K_{3.3} \times K_N \quad (3.4)$$

$$K_N = \frac{P_{NH_3}}{P_{H_2}^{3/2}} \qquad K_C = \frac{P_{CO} P_{H_2}}{P_{H_2O}} \quad (3.5)$$

where $K_{3.1}$ and $K_{3.3}$ are the temperature dependent equilibrium constants of reactions (3.1) and (3.3), respectively, and K_N and K_C are nitriding potential and carburizing potential, respectively [56].

3.5.2 Salt Bath Nitrocarburizing

Salt bath or liquid nitrocarburizing was first established in the late 1940s when high cyanide nitrocarburizing salt baths were introduced [6]. Environmental considerations and the increased detoxification of cyanide containing effluents have led to the development of low cyanide nontoxic salt bath nitrocarburizing treatments [7].

Cyanates are the active nitrocarburizing constituent of both high cyanide and low cyanide nitrocarburizing baths. Reduction of the cyanide content permits markedly higher count concentrations in the low cyanide baths; this results in greatly increased nitriding activity. Unlike the reducing high cyanide baths, the nominal cyanate and carbonate composition of the low cyanide baths is oxidizing.

The baths are composed of predominately potassium salts with sodium salts. During nitrocarburizing, cyanates yield nitrogen to the steel and form carbonates. Cyanate concentration is maintained by the use of organic regenerators, which supply nitrogen to reform cyanates from carbonates [6]. Reactions that take place in the bath are as follows [65]:

$$4NCO^{-} \longrightarrow CO_3 + CO + 2N + 2CN \quad (3.6)$$

$$XFe + N \longrightarrow Fe_xN \quad (3.7)$$

$$2CN^{-} + O_2 \longrightarrow 2NCO^{-} \text{ (regeneration of } CN^{-}) \quad (3.8)$$

$$3CO_3 + \text{regenerator} \longrightarrow 6NCO^{-} + XH_2O \text{ (regeneration of } CO_3^{-}) \quad (3.9)$$

A reaction between the surface of the ferrous components and the salt melt takes place during the process. This causes the formation of atomic nitrogen, which diffuses into the steel surface, and the formation alkali carbonate in the melt. This carbonate is converted into active cyanate during regeneration of the bath [66].

Salt bath nitrocarburizing is well known under various trade names, including Sulfinuz, Sursulf, Tenifer, Tufftride, Melonite, Nutride [7].

3.5.3 Plasma Nitrocarburizing

Plasma nitrocarburizing is often described as an environmentally friendly process where gas consumption can be lowered compared to other nitrocarburizing techniques. It is widely applied to various materials such as carbon steels, alloy steels, tool steels, stainless steels, cast irons and sintered materials [54].

Plasma nitrocarburizing involves a plasma diffusion treatment in an atmosphere of nitrogen, hydrogen, and a carbon containing gas, usually methane or carbon dioxide.

In a vacuum, high voltage electrical energy is used to form plasma, in which nitrogen, hydrogen, and carbon positive ions are accelerated to impinge on the cathode. In the presence of electric field, the workpiece is maintained at a high negative DC voltage source of 250–850 V with respect to a grounded vessel (anode). Under the influence of the bias, the gases are dissociated, ionized, and accelerated toward the workpiece (cathode). The kinetic energy of ions is converted by the ion bombardment into thermal energy, which not only heats the workpiece but also implants ions directly and partly causes cathode sputtering. Thus, driving out electrons and elements such as iron, chromium, and oxygen from the workpiece surface. Some ions implant into sample surface, others cause the cathode sputtering [67].

Plasma nitrocarburizing process produces a uniform formation of iron nitride phase at the surface [6].

CHAPTER 4

EXPERIMENTAL PROCEDURE

4.1 Materials

DIN 1.2738 (Impax Supreme) premium pre-hardened plastic mould steel was the base material onto which surface modification is applied. The chemical composition was examined by Optical Emission Spectrometer (HILGER). The chemical composition (in wt. %) is shown in Table 4.1.

Table 4.1 Chemical composition of DIN 1.2738 (Impax Supreme) premium prehardened plastic mould steel

Elements	C	Si	Mn	Cr	Ni	Mo	S	Fe
Wt. %	0.334	0.234	1.35	1.92	0.913	0.229	0.017	Balance

The samples were cut into a size of 25x10x30 mm pieces by a wire erosion machine. The surfaces of the samples were mechanically grinded down to 1200 mesh SiC followed by polishing with 3 µm diamond suspension. The samples were ultrasonically cleaned in ethanol during 10 minutes.

4.2 Nitriding and Nitrocarburizing Processes

Gas nitriding, fluidized bed nitriding, plasma nitriding and nitrocarburizing processes were carried out in industrial facilities.

4.2.1 Gas Nitriding

Gas nitiriding (GN) of samples were carried out on QUANTUM[1] in vacuum furnaces. The furnace was flushed with nitrogen and the reaction temperature was established. Furnace residence time started when ammonia was introduced into the system. GN process was performed at 560 °C for 8 h with various gas mixtures of 94%NH_3 + 6%N_2O, 90%NH_3 + 5%N_2O + 5%N_2 and 89%NH_3 + 9%N_2 + 2%N_2O.

Figure 4.1 Image of the industrial vacuum furnace

4.2.2 Fluidized Bed Nitriding

Nitriding was carried out in a fluidized bed furnace, which uses particulate alumina as fluidized particles which flowed inside the chamber due to the flow of the nitriding gases. The nitriding gas composition was 40% NH_3 + 60% N_2.

[1] QUANTUM TAKIM SANAYİ ÜRÜNLERİ ÇELİK TİC.A.Ş.

Nitriding temperature used was 560 °C for treatment time of 8 h. After nitriding, the samples were cooled inside the furnace down to room temperature.

4.2.3 Plasma Nitriding

The samples were nitrided at "Istanbul Isıl Islem[1]" plant via plasma nitriding technique by using pulse plasma nitriding furnace. Nitriding time and temperature were selected according to commercial applications. Processes were carried out at temperatures of 520 °C for 8 h in a 500 Pa gas mixture of 25% N_2 + 75% H_2. After the nitriding process, the samples were slowly cooled to room temperature in a nitrogen atmosphere.

4.2.4 Nitrocarburizing

Gas nitrocarburizing process was carried out on ASSAB[2] in commercial furnace. The process was performed at 560 °C in 45% CO_2 + 29% NH_3 + 26% N_2 gas mixture for 8 h by vacuum furnace. After nitrocarburizing, the samples were cooled inside the furnace.

Table 4.2 Nitriding processes conditions

Nitriding Process	Gas Mixture	Temperature (°C)	Time (h)
Gas Nitriding (GN)	94%NH_3 + 6%N_2O, 90%NH_3 + 5%N_2O + 5%N_2 and 89%NH_3 + 9%N_2 + 2%N_2O	560	8
Fluidized Bed Nitriding (FBN)	60%N_2 + 40%NH_3	560	8
Plasma Nitriding (PN)	25%N_2 + 75%H_2	520	8
Nitrocarburizing (NC)	45%CO_2 + 29%NH_3 + 26%N_2	560	8

[1] İSTANBUL ISIL İŞLEM SAN. VE TİC.A.Ş.

[2] ASSAB ÇELİK VE ISIL İŞLEM A.Ş

4.3 Characterization Tests

Various techniques were used to characterize the microstructures and properties of the nitrided and untreated samples. Microstructure analysis was carried out using optical microscopy, X-ray diffraction (XRD) analysis was used for phase identification. The Vickers hardness test was used to measure the surface hardness for the samples. Cross section hardness profile measurements were conducted to determine the hardness profile in the nitrided parts. Besides, the thicknesses of the compound and diffusion layers were measured.

4.3.1 Microstructure

After preparation of the nitrided samples, microstructures were examined by optical microscope (Leica DM2500). Besides, the thicknesses of the compound and diffusion layers were measured by ImageJ (v1.37) software as a mean value of 15 measurements per sample.

4.3.2 XRD Analysis

X-Ray Diffraction (XRD) is a powerful technique that can produce crystallographic information about materials, through elastic scattering of X-Rays or diffraction, from within the sample. By comparing the diffraction spectra with a database containing the diffraction data from known materials, the sample structure can be identified [19]. Phase identification of the nitrided and untreated surfaces was performed using an X-ray differactometer (Cu Kα radiation, Bruker D8 Discover).

4.3.3 Hardness

After processing, surface hardness was measured using Emcotest Durascan Microhardness tester under load of 1 Kg for 15 s. (Figure 4.2). An average hardness value was based on five measurements obtained from representative positions on each sample.

Cross-sectional hardness profile measurements were conducted to determine the hardness profile in the nitrided parts.

The profiles were obtained by Emcotest Durascan Microhardness tester by applying 50 g load for 15s. To obtain statistically valid results, each sample was subjected to a series of 15 surface indentations before an average surface HV was obtained.

Figure 4.2 Emcotest Durascan Microhardness test device

4.4 Dry Sliding Wear Test

The wear tests were conducted under dry sliding wear testing conditions on a reciprocating wear tester at normal atmospheric conditions, by using PLINT TE 67/R tribometer. Prior to each test, samples and the counter materials were ultrasonically cleaned with propanol. The tests were performed against a counter material of an AISI 4140 steel (275 ± 12 $HV_{0.5}$) pin with 5 mm diameter. The tests were performed at room temperature, under a normal load of 100 N (initial contact pressure of 5.1 MPa), with the total stroke length of 10 mm (perpendicular to the sanding marks), the frequency of 1.5 Hz, and the total sliding distance of 400 m. A dry sliding wear test setup, can be seen in Figure 4.3. After tests, worn surfaces were characterized by FEI Nova 200 field emission gun scanning electron microscope (FEG-SEM) equipped with EDAX, energy dispersive X-ray spectroscopy (EDS). All worn surface images were taken as parallel to the sliding direction.

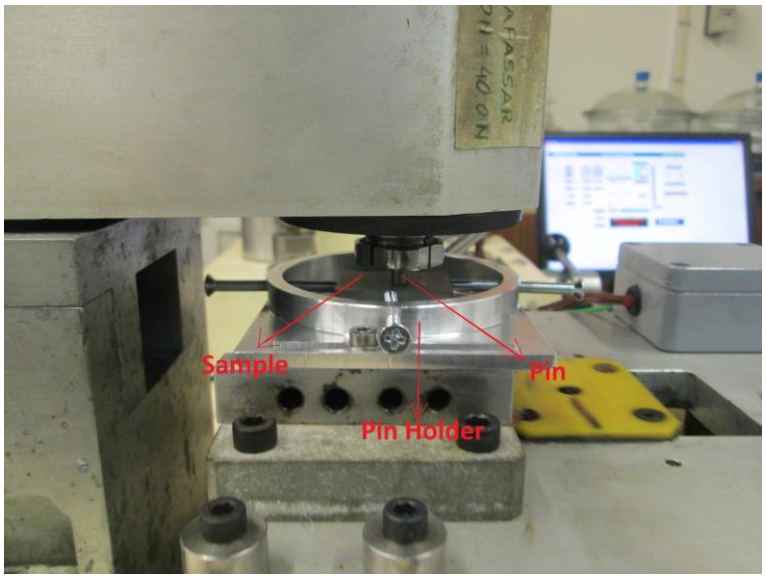

Figure 4.3 Dry sliding wear test setup

After wear tests, the volume loss values were determined by a geometric model where the length of the track was considered as 10 mm (i.e. the total stroke length) and each tip of the wear track was considered as a semicircle (Figure 4.4).

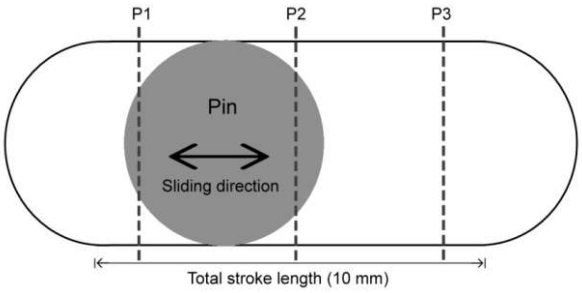

Figure 4.4 The estimated model used for calculating the wear loss volume. The lines P1, P2, and P3 indicates the 2D profile lines.

The width and the deepness of the wear tracks were measured by a contact profilometer (Mitutoyo Surftest SJ-500). For each wear track, three 2D profiles were obtained from the centre of the wear track (line P2 in Figure 4.4), and 3.5 mm away from the centre for both sides (lines P1 and P2 in Figure 4.4). For the calculation of wear loss volume, first, the wear loss area for each 2D profile was calculated with the following formula:

$$A_w = \sum_{i=0}^{n} 0.5(Y_i + Y_{i-1})(X_i - X_{i-1}) \tag{4.1}$$

where A_w is the wear loss area (mm^2), X is the width of each 2D profiles (mm), Y is the deepness (mm), and n is the number of counts. Then, average deepness was calculated with the following formula:

$$\bar{D} = \frac{\bar{A}_w}{\bar{W}} \tag{4.2}$$

where $\bar{D}$ is the average depth (mm), $\bar{A}_w$ is the average wear loss area of three 2D profiles for each wear track, $\bar{W}$ is the average width of each wear track. After calculating the wear loss area and average depth, the wear volume was calculated using the following formula:

$$\Delta V = \left[\pi \left(\frac{\bar{W}}{2}\right)^2 \bar{D}\right] + (\bar{A}_w \,.l) \tag{4.3}$$

where ΔV is the total volume loss for each wear track (mm^3) and l is the total stroke length (10 mm). Finally, the volume loss values were converted into specific wear rate with the following formula:

$$k = \frac{\Delta V}{NxS} \tag{4.6}$$

where k is the wear rate (mm^3/Nm) and N is the normal load (N) and S is the total sliding distance (m). All tests were repeated at least three times in order to have repeatability, and the wear rates were calculated from three tracks per condition.

4.5 Corrosion Test

Corrosion tests were performed at room temperature in an electrochemical cell containing 3.5 wt% NaCl solution. A PGZ 201 Potentiostat/Galvanostat (Radiometer Analytical, Copenhagen, Denmark) outfitted with analysis software the VoltaMaster 4 (Radiometer Analytical, Copenhagen, Denmark) was used to evaluate electrochemical behavior. The electrochemical cell consisted in a standard three electrode set up. The untreated and nitrided steel samples were used as the working electrode (WE) with an exposed area of 0.38 cm^2. As a counter electrode (CE) a Pt electrode was used while a saturated calomel electrode (SCE) was used as the reference electrode (RE).

Potentiodynamic polarization was performed after 60 min of immersion into the solution, in order to stabilize the surface at open circuit potential (OCP). The scan rate in potentiodynamic tests was 0.5 mV/s, starting at 0.25 V below the E_{ocp} moving in the anodic direction up to 0 V. At least three tests were carried out for each sample type for assessing the reproducibility.

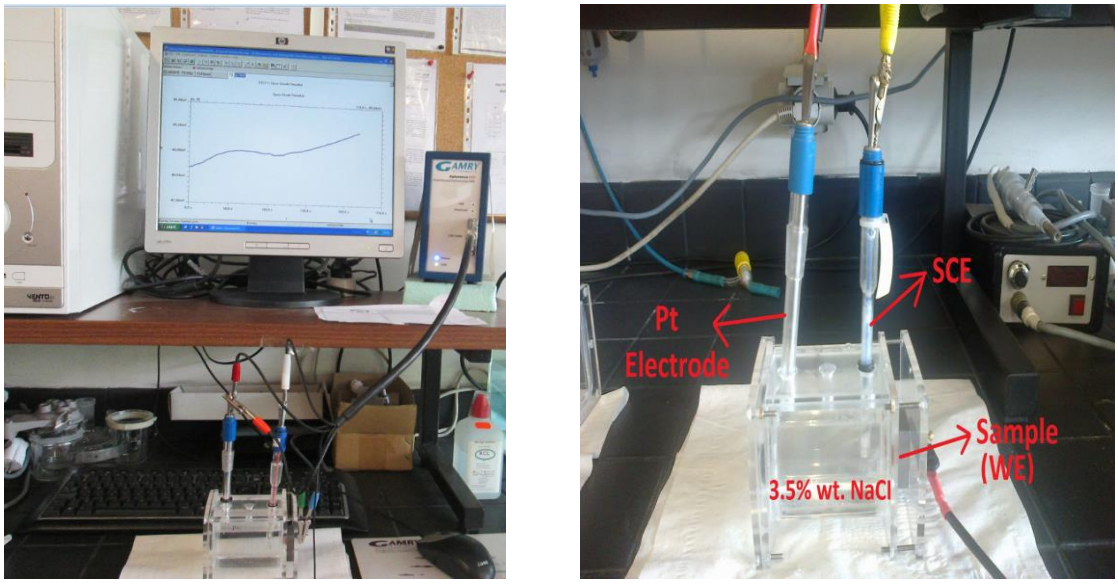

Figure 4.5 Schematic view of the corrosion test setup

4.6 Tribocorrosion Test

Before the tests the samples were ultrasonically cleaned in propanal for 10 minutes and then in distilled water for 10 minutes and finally dried. For tribocorrosion experiments, the untreated and nitrided steel test samples were fixed in an electrochemical cell. The cell was mounted on a pin-on-disc tribometer (CETR– UMT-2), surface facing upwards. In a three electrode setup, the untreated and nitrided test samples were used as the working electrode (WE), the counter electrode was a platinum electrode, and a saturated calomel electrode (SCE) was used as the reference electrode. The tribocorrosion tests were carried out in 3.5 wt% NaCl solution. An alumina ball (ø-10 mm, Goodfellow) was used as the counterbody, and was positioned on top of the test samples.

Tribocorrosion tests were carried out under reciprocating sliding at an applied normal load of 15 N. The displacement amplitude was 5 mm, and the sliding frequency was 1 Hz., the sliding time was 20 min. After testing, the sample was removed from the solution and ultrasonically cleaned in propanol and then in distilled water and finally dried. For each sample, the tests were repeated three times.

The tribocorrosion test system is given in Figure 4.6.

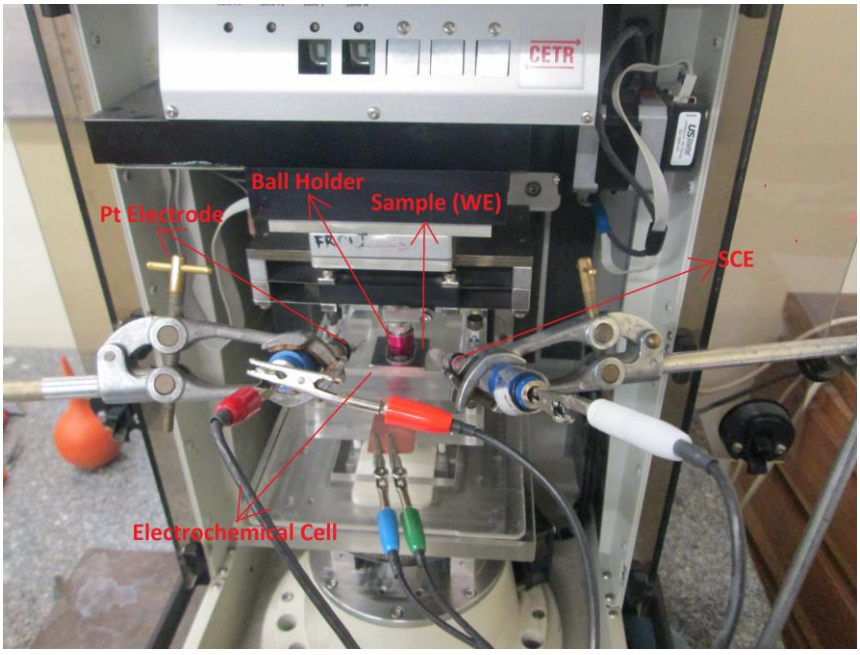

Figure 4.6 Tribocorrosion test setup

CHAPTER 5

RESULTS AND DISCUSSION

5.1 Characterization

The cross-sectional microstructures of the nitrided samples are given in Figure 5.1 per each treatment, presenting the compound layer, the diffusion layer, and the un-modified region.

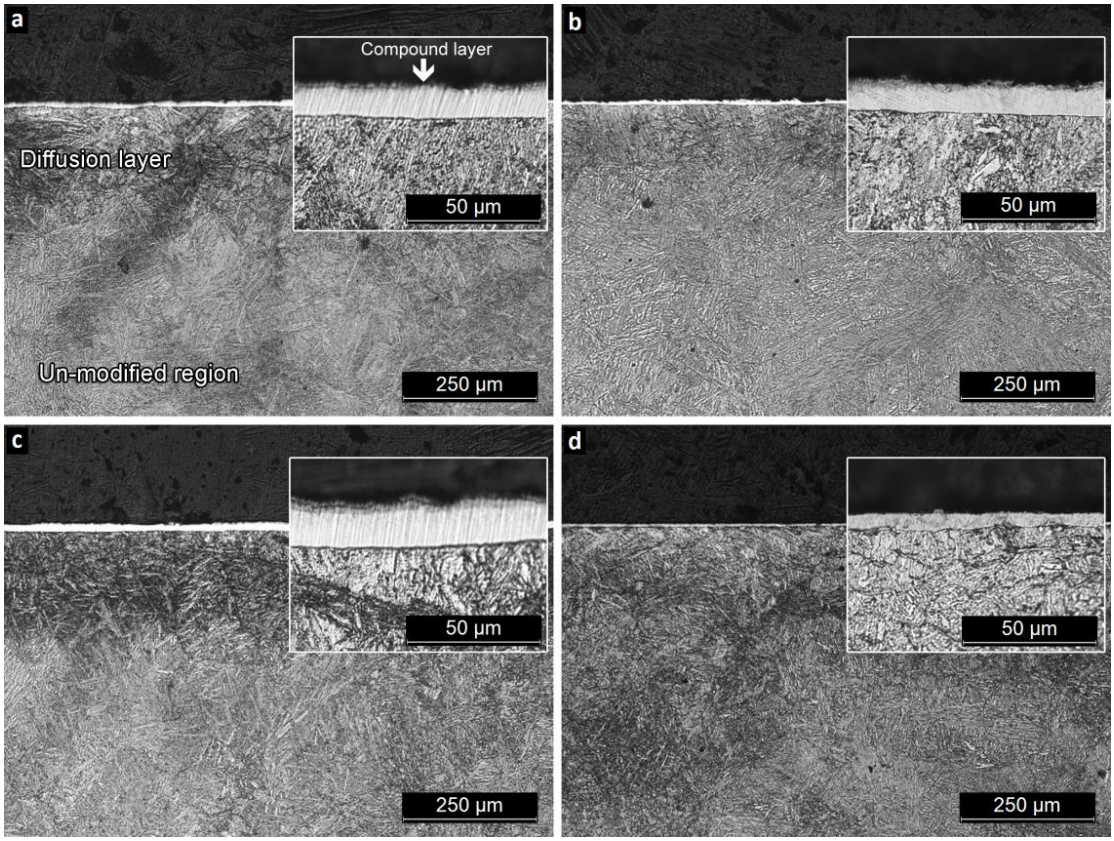

Figure 5.1 Cross-sectional OM images of the a) NC, b) GN, c) FBN, and d) PN samples

Different compound layer thicknesses were obtained from each treatment due to the dependence of the compound layer thickness to the type of the treatment and gas composition, as shown in Table 5.1 [68], [69]. The thickness of the compound layer varies between 5 and 12 µm. As can be seen on the results, PN presented much thinner compound layer as compared to the other treatments. It has been reported that PN gives a thinner compound layer due to effect of the material removal from the surface by cathode sputtering or due to the formation of the vapour deposited iron oxynitride layer which inhibits further nitriding [70].

Table 5.1 Compound layer thickness of the nitrided samples

Samples	**Compound Layer (µm)**
NC	11.55 ± 1.79
GN	9.27 ± 1.29
FBN	14.33 ± 1.32
PN	5.49 ± 1.39

The surface hardness of the untreated sample and the nitrided samples are given in Table 5.2. Even though the highest average hardness values were obtained for NC, when it considered within the range of the standard deviation, no clear difference was observed between NC, FBN, and PN. GN presented significantly lower surface hardness than the other treated samples, although, it was still approximately 3 times higher than the untreated steel.

Table 5.2 Surface hardness of the untreated sample and nitrided samples

Samples	**Surface Hardness (HV_1)**
UT	296 ± 8
NC	1037 ± 84
GN	838 ± 38
FBN	1010 ± 123
PN	980 ± 34

Measurement of the diffusion layer using image analysis tools is not as easy as the compound layer, thus, hardness profiles are considered as the most convenient technique to determine the case depth [16], [71]. The cross-sectional hardness profiles of the nitrided samples are given in Figure 5.2. The hardness decreases from surface to core, since the concentration of metal nitrides decreases towards core. As can be seen on the results, PN presented larger case depth as compared to the other samples. PN is reported as giving more effective and uniform case depth which has an important influence on the mechanical properties [4], [72].

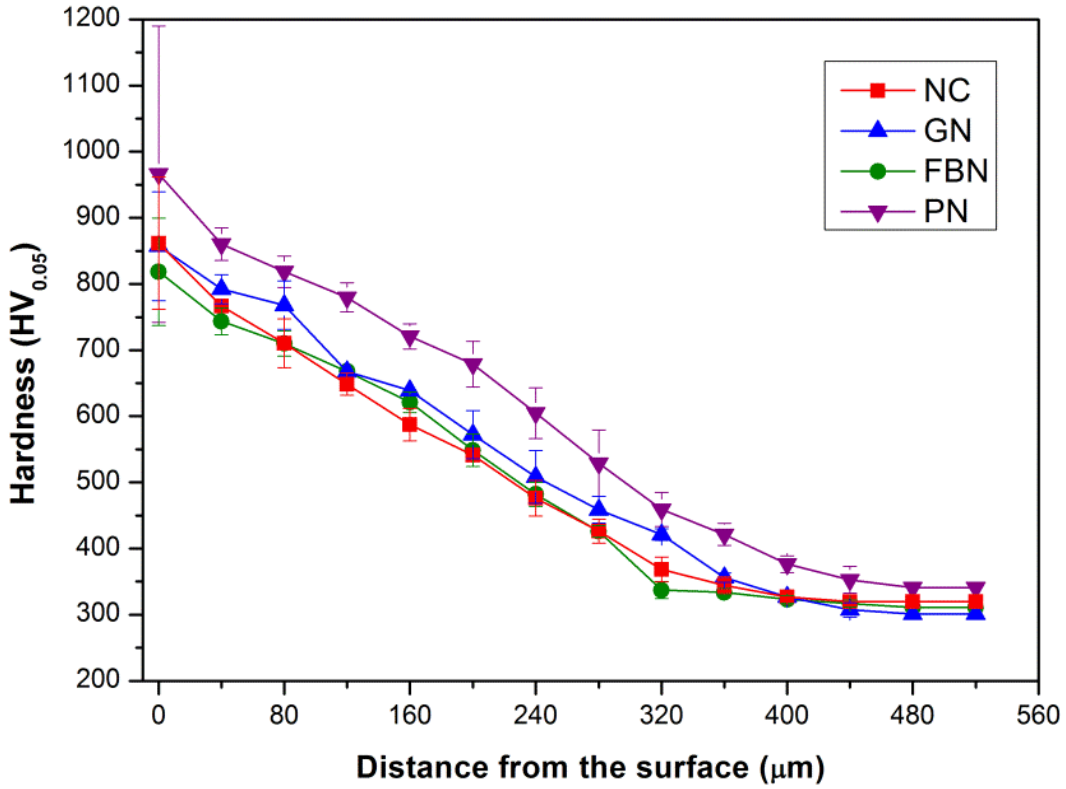

Figure 5.2 Cross-sectional hardness profiles of the nitrided samples

A comparison between XRD patterns of untreated and nitrided samples can be seen on Figure 5.3. Whereas α-ferrite was the only phase on the untreated steel, ε-nitride (ε-$Fe_{2-3}N$) and γ'-nitride (γ'-Fe_4N) phases were detected on all treated samples which have previously been reported by several authors as the main constituents of the compound layer after nitriding processes [72], [73]. Unlike other samples, FBN presented a considerable amount of Fe_2O_3 phase, which may be due to the residual air in the fluidized bed furnace during the process [74].

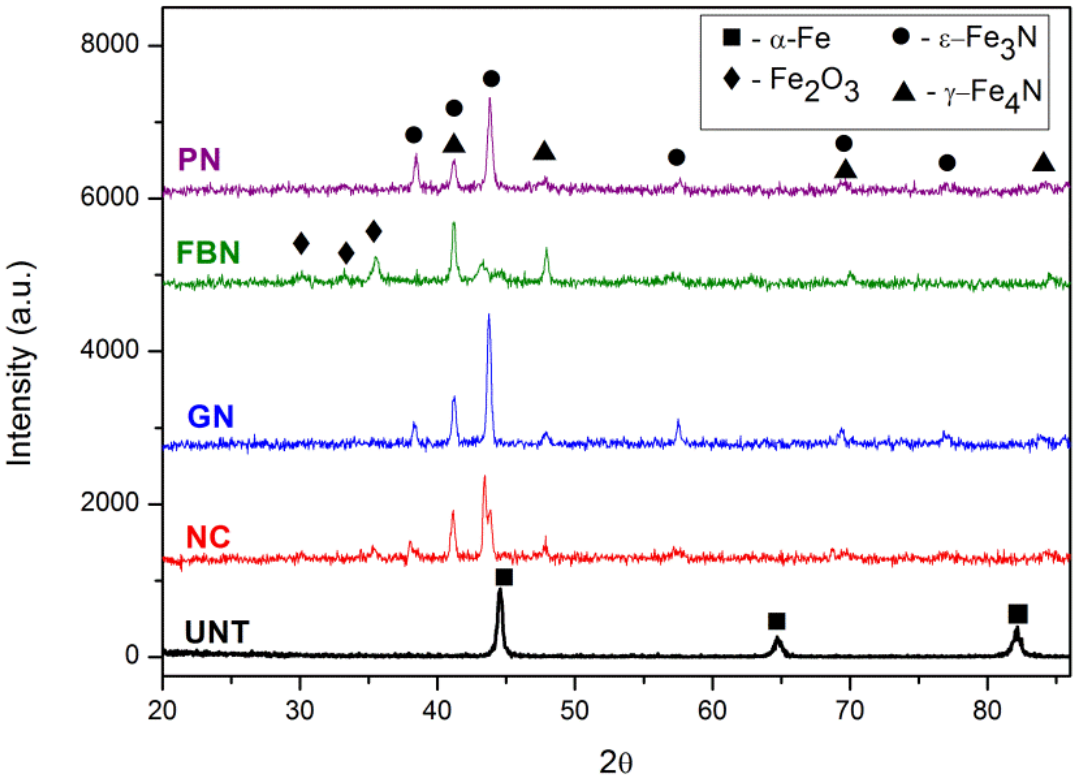

Figure 5.3 XRD spectra of untreated and nitrided samples

5.2 Dry Sliding Wear

The evolutions of the coefficient of friction (COF) during sliding time of untreated and nitrided samples are given in Figure 5.4. After a run-in period, which was very short on all cases except the untreated samples, all treated samples presented relatively stable and similar evolution whereas untreated sample presented a slight decrease of COF with time. The most distinguishable feature of the COF graphs occurs for the untreated surfaces that revealed high friction with large fluctuations during approximately first 45 m (23 min) of sliding.

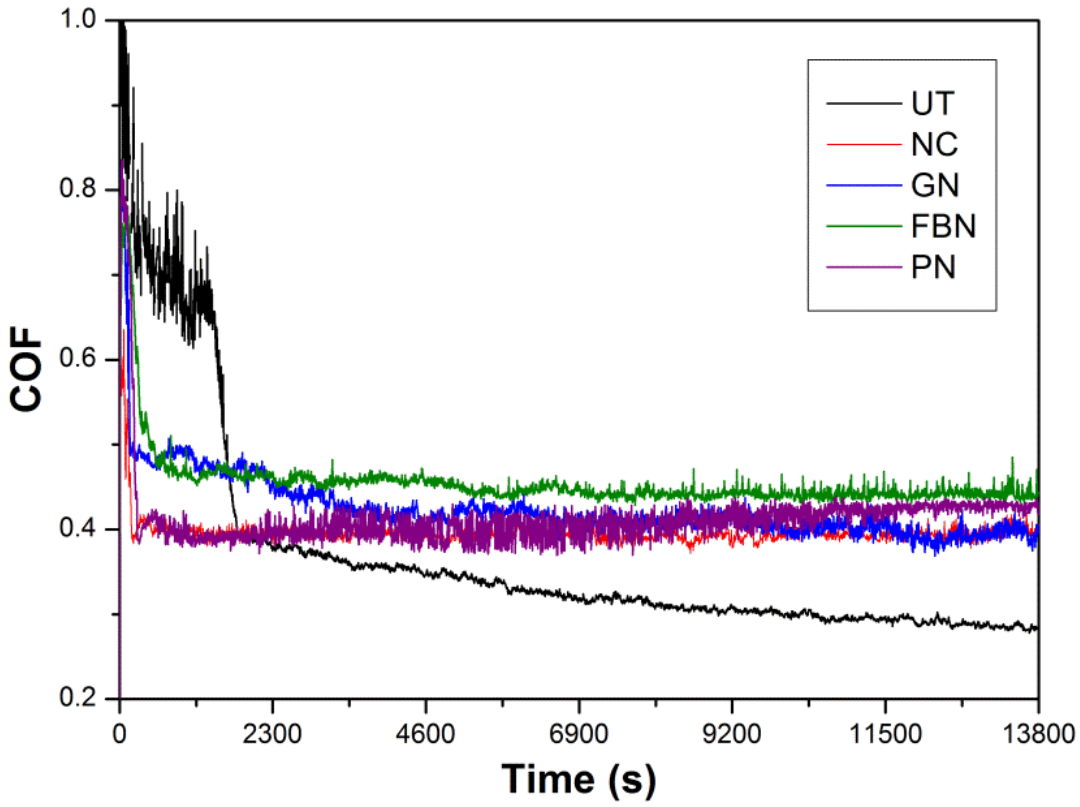

Figure 5.4 Evolution of the COF with sliding time for the untreated and nitrided samples

The wear mechanisms involved during sliding of untreated samples were determined by OM and SEM observations of the worn surfaces and the wear debris. For the untreated sample, due to its low surface hardness, it can be observed that the worn surface is deformed under the dry sliding wear condition. The optical wear track morphology image of the untreated sample is presented in Figure 5.5.

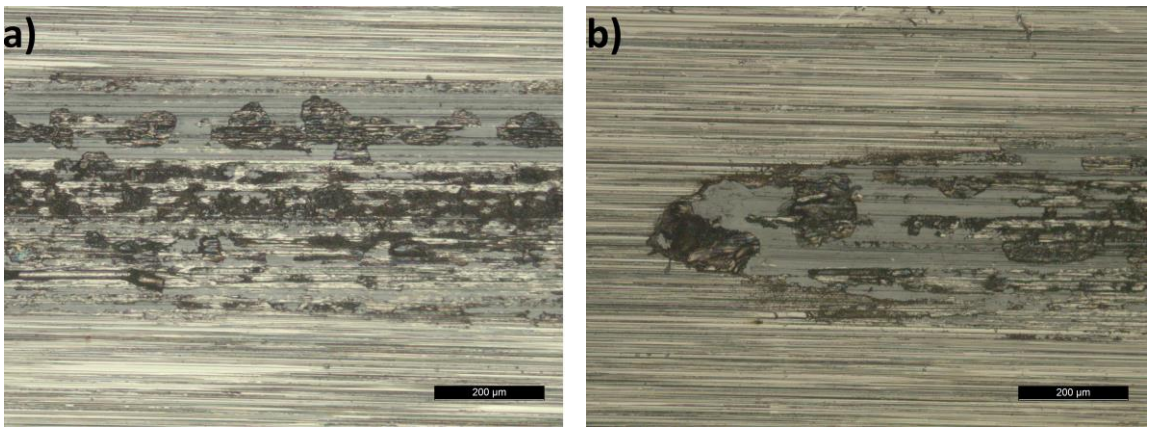

Figure 5.5 The optical wear track morphology image of the untreated sample at (a) middle of wear track and (b) edge of the wear track

Figure 5.6 represents the BSE and SE SEM images of the wear track of the untreated sample. Effect of the plastic deformation can be seen especially on the SE/SEM image (Figure 5.6 b). On the other hand, as can be seen on the BSE/SEM image, almost all wear track area was presented an oxidised surface after the tests (Figure 5.6 a).

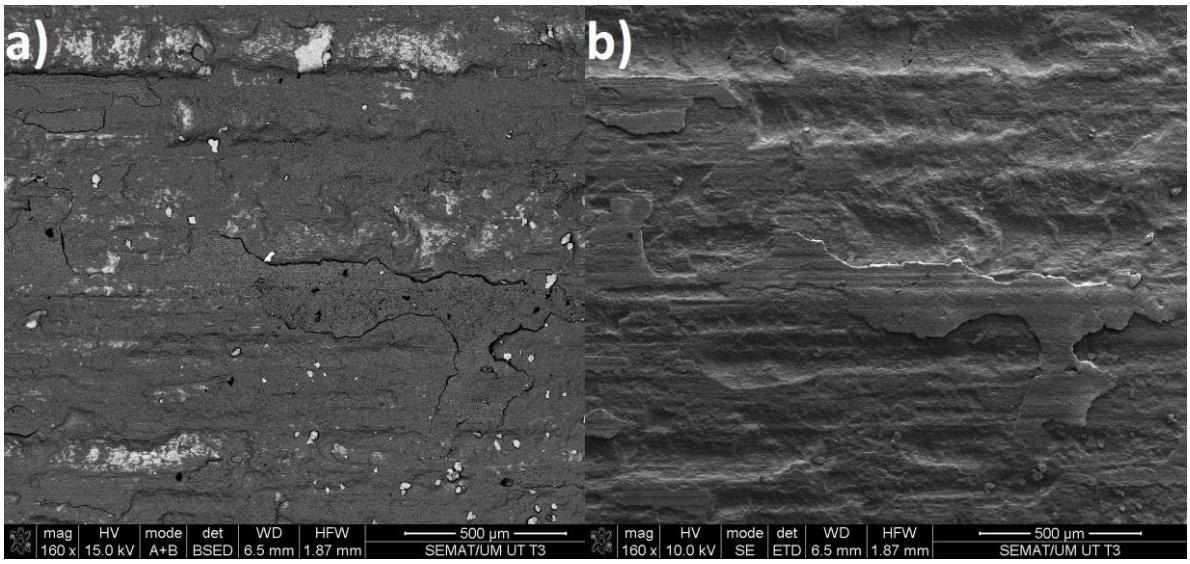

Figure 5.6 BSE/SE SEM image of the worn surface

Oxide particle is observed from the EDS, indicating that the oxidation wear also takes place during the sliding progress. An EDS analysis carried out in regions (Z1) and (Z2) in Figure 5.7 showed that the (Z1) areas have high oxygen content whereas lower amounts of oxygen was detected in the (Z2) areas.

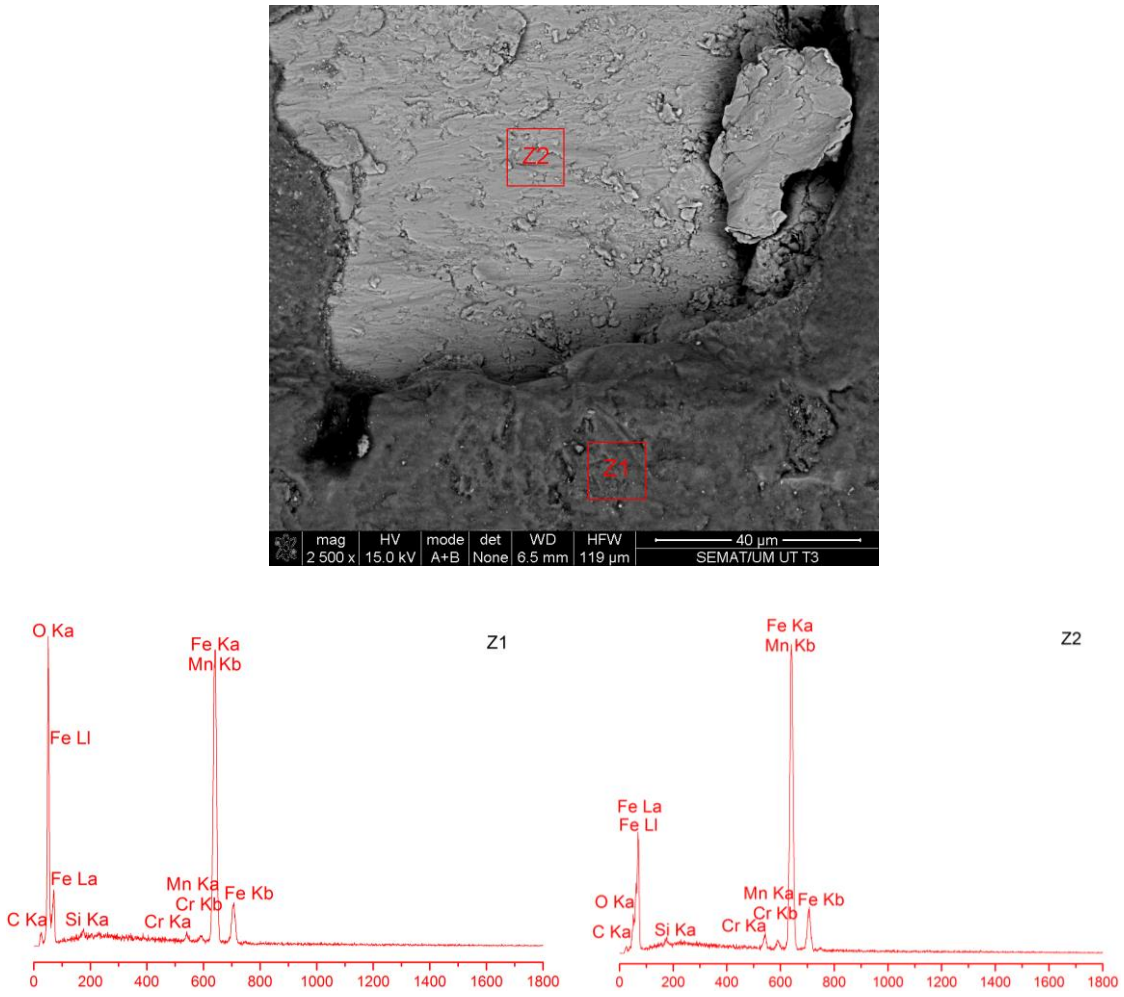

Figure 5.7 SEM image of the worn surface and matching EDS analysis for untreated sample

During the initial stage of the sliding for the untreated samples, plastic deformation may be occurred together with the adhesive wear, which resulted with superficial material detachment and therefore, debris creation [75], [76]. High friction with large oscillations on the COF values for the approximately the first 23 min of sliding may certainly be due to adhesion and could induce a stick-slip phenomena [77], [78], together with the additional contribution of the third body effect of the detached material, which may result in the grooves observed on the pin surface (Figure 5.8 a) [79]. The effect of the adhesive wear can also be seen on the plate-like metallic wear debris (Figure 5.8 b) which is a typical feature of the adhesive wear [80].

On the other hand, the wear debris may be adhered on the both sliding surfaces (Figure 5.6 and Figure 5.8 b) and they may be oxidised through the mechanical interactions together with the effect of the contact pressure and the frictional heat [81]. Thus, it is considered that the formation of the compact oxide layer or the mechanically mixed layer (MML) after the initial stage of the sliding led to a drop on the COF values [82], [83]. Moreover, since the oxide layer acts as a lubricant and minimize the metal/metal contact, it may be expected to obtain lower wear rates on that wear regime [70], [81]. Therefore, the main wear mechanism for the untreated samples may be suggested as a combination of adhesive and abrasive wear for the run-in period of the sliding (severe wear), and oxidative wear after the transition point (mild wear). The very fine wear particles observed in Figure 5.6b could have been generated by oxidative wear during this last period of the test.

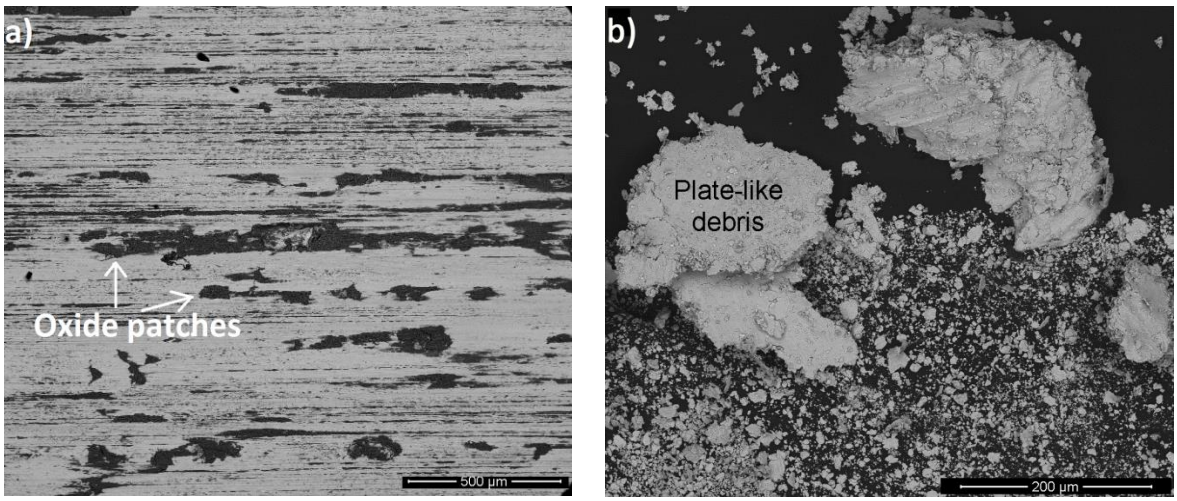

Figure 5.8 SEM image of the a) worn counter material surface b) wear debris for the UT sample

Figure 5.9-12 represents the BSE and SE SEM images of the wear tracks on each nitrided sample. All nitrided samples presented well-defined, but shallower wear tracks as compared to the untreated sample. It can be seen from the higher magnification SEM images that all nitrided samples presented similar worn surface features, namely oxide patches and relatively shallow abrasion grooves. However, FBN samples presented relatively deeper grooves and PN samples presented relatively smaller oxide patches as compared to the other nitrided samples.

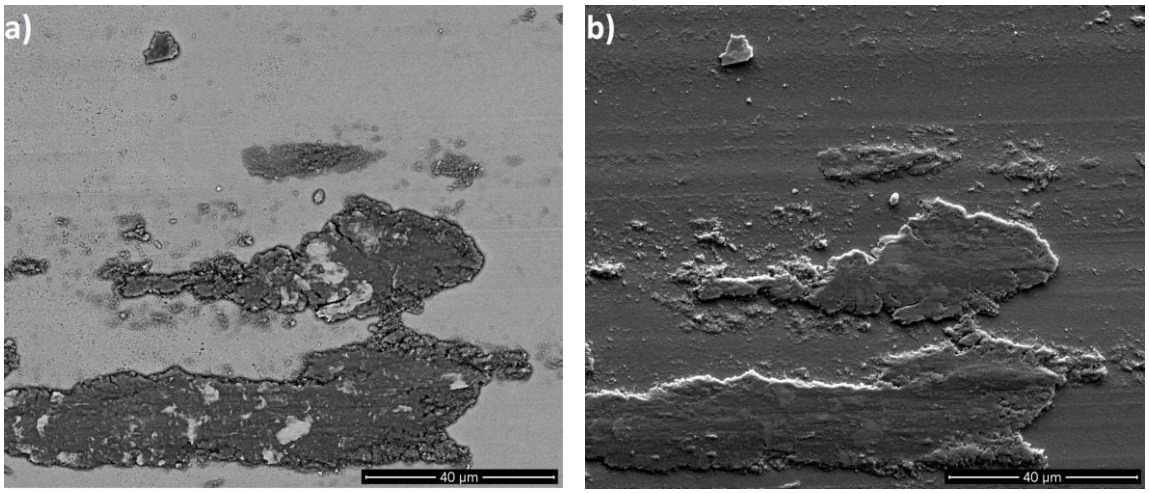

Figure 5.9 a) BSE b) SE SEM images of the worn surfaces for GN samples

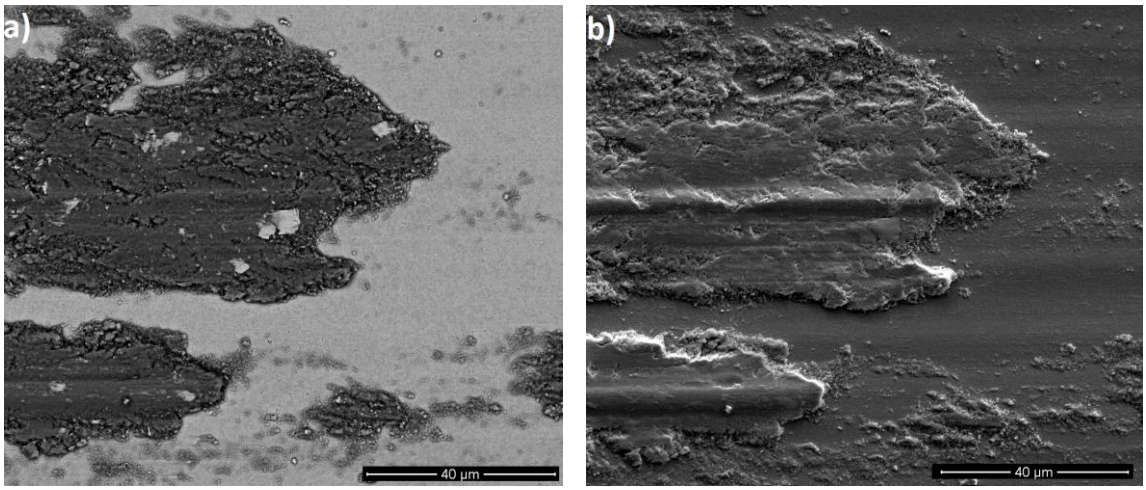

Figure 5.10 a) BSE b) SE SEM images of the worn surfaces for FBN samples

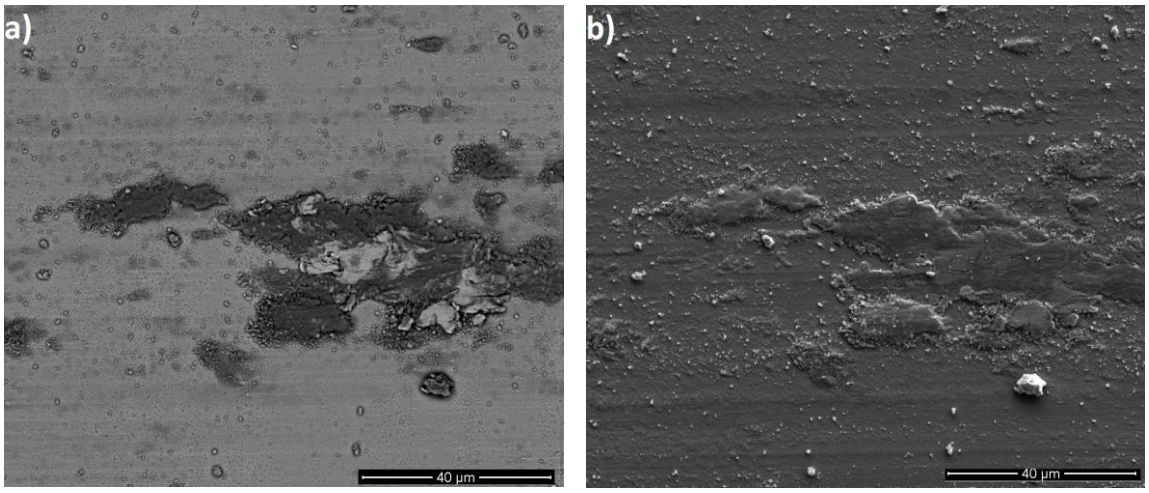

Figure 5.11 a) BSE b) SE SEM images of the worn surfaces for PN samples

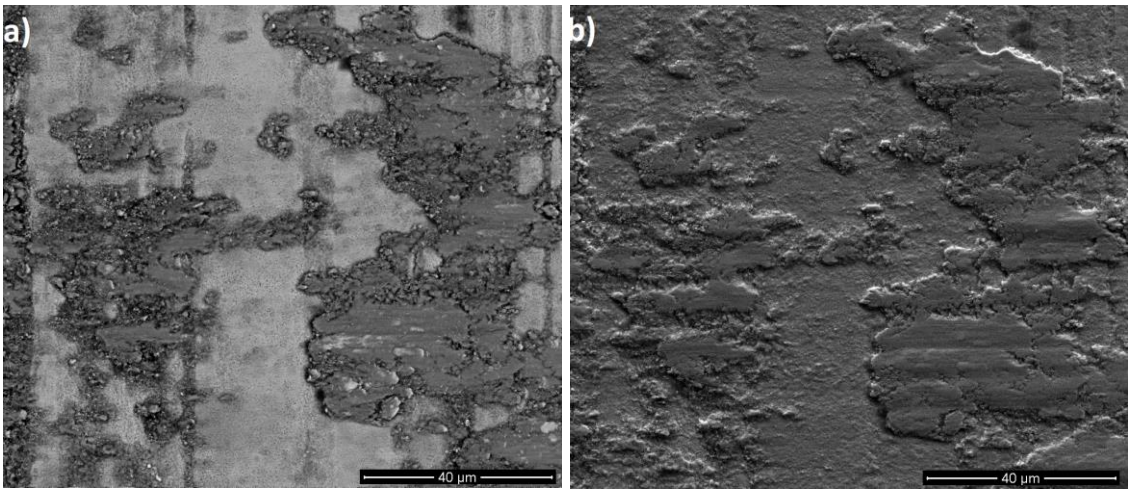

Figure 5.12 a) BSE b) SE SEM images of the worn surfaces for NC samples

As it stated above, all nitrided samples presented relatively higher but gradually decreased COF values in the run-in period (approx. first 2.5-5 min of sliding). This behaviour may be attributed to the adhesive and abrasive actions that were dominant in this period. At the very beginning of the sliding contact, plastic deformation and welding may occur between the sliding surfaces which points out the adhesive wear [84]. After that, the broken particles by welding may be entrapped between the sliding surfaces and as sliding proceeded, the energy dissipated by friction in the form of heat would be enough to oxidise these particles, meaning that they become harder and able of, creating grooves in the sliding surfaces (Figure 5.9-12) [84], [85].

During the sliding action the particles were constantly being ground and became thinner and were agglomerated in plateaus. Consequently, in the steady-state stage of the sliding, these debris may form the oxide patches by the effect of the contact pressure and temperature raise developed during the test [70], [77] justifying a low and stable friction.

Moreover, during sliding, nitrogen atoms of the worn surfaces may be replaced by oxygen which may result the oxidation of the nitrided worn surfaces [78]. Besides nitrided surfaces, pin surfaces also presented oxidised surfaces and oxide patches, however, the patches were much smaller as compared to those observed in the nitrided surfaces, or in the pins that worn against the untreated samples. On the other hand, the wear debris obtained from the nitrided samples presented fine oxidised morphology as compared to the ones obtained from the untreated sample. All nitrided samples presented relatively similar pin surfaces and wear debris morphology. Thus, from the COF evolution and microstructural investigations of the both sliding surfaces and wear debris, wear mechanism may be suggested as mainly combination of the adhesive and abrasive wear for the very short run-in period (severe wear), and mainly oxidative wear for the steady state (mild wear) for all nitrided samples.

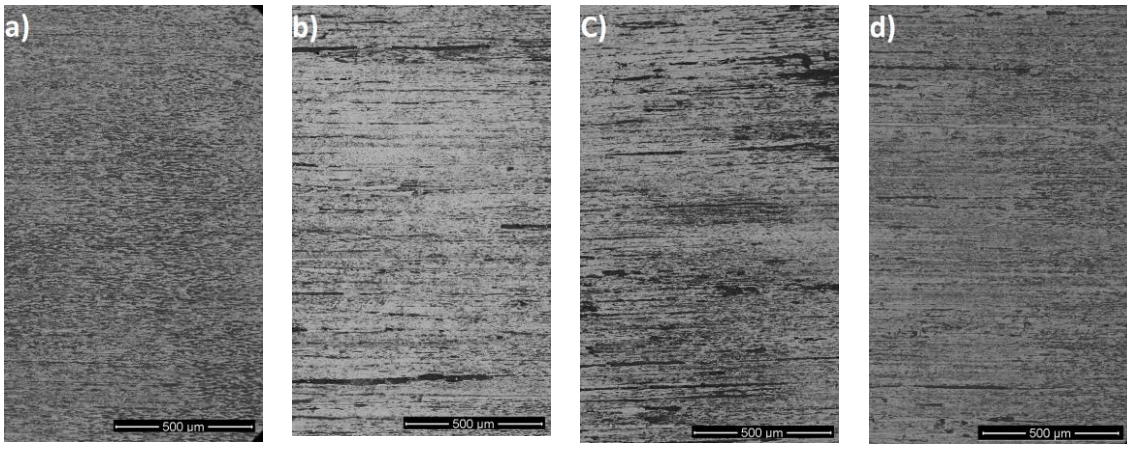

Figure 5.13 BSE SEM images of the worn surfaces of pin worn against nitrided a) NC, b) GN, c) FBN, and d) PN samples

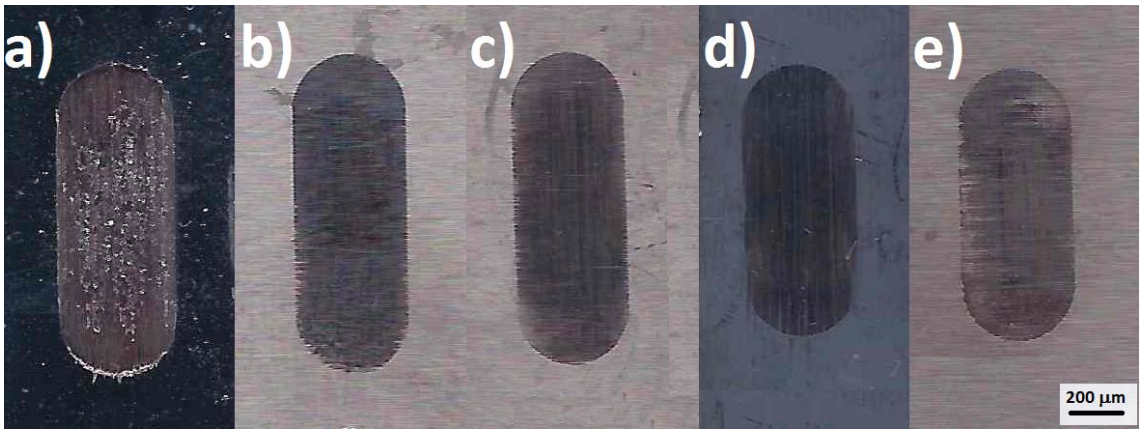

Figure 5.14 Macro images of the worn surfaces of pin worn against untreated and nitrided a) UT, b) NC, c) GN, d) FBN, and e) PN samples

The wear rate values after the reciprocal dry sliding test is presented in Figure 5.15. As can be seen nitrided samples presented more than 20 times lower wear rates than the untreated samples. Within the nitrided samples, when it considered within the range of the standard deviation, no significant difference was observed between the samples. However, as mean values, while NC and GN samples presented very similar values, FBN presented the highest wear rate and PN presented the lowest wear rate. It can be proven that the wear resistance of the steel significantly improved after the nitriding processes.

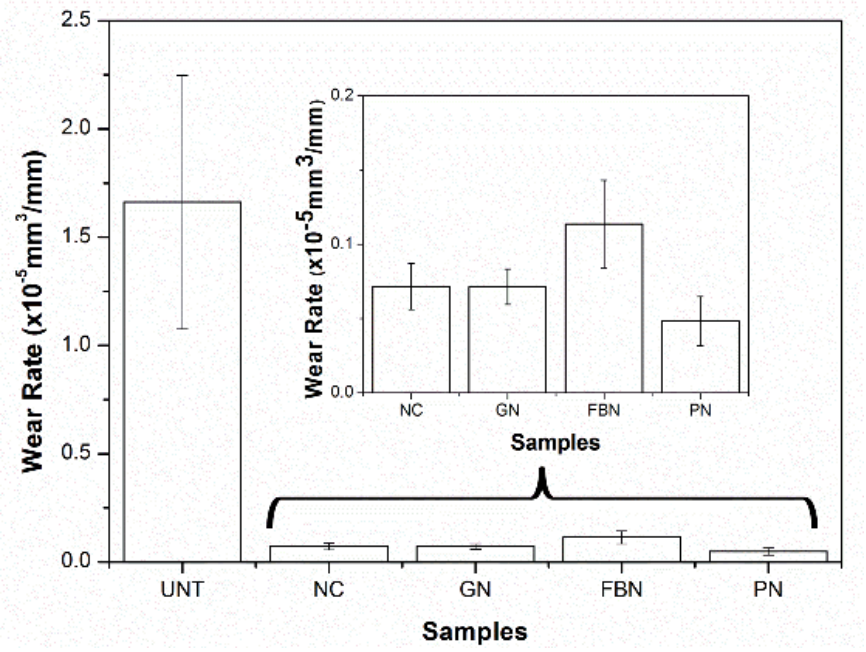

Figure 5.15 The wear rate derived from wear volume for all samples

5.3 Corrosion

The polarisation curves of the untreated and nitrided samples in 3.5% NaCl solution are given Figure 5.16 and corrosion current density (i_{corr}) and corrosion potential ($E_{(i=0)}$) of the samples were determined by Tafel slope extrapolation and listed in Table 5.3.

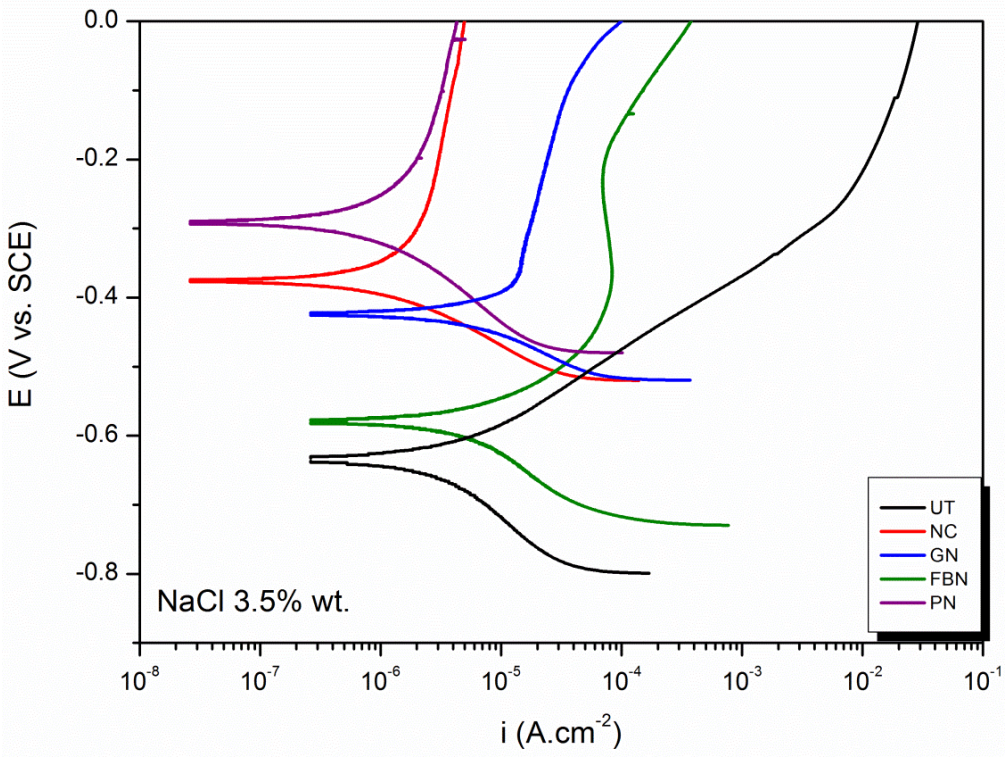

Figure 5.16 Potentiodynamic polarization curves of the untreated and nitrided samples

Table 5.3 Corrosion potential ($E_{(i=0)}$) and corrosion current density (i_{corr}) for all samples

Samples	$E_{(i=0)}$ (mV)	i_{corr} (μA.cm^{-2})
UT	-627 ± 8	1,82 ± 0,42
NC	-345 ± 24	0,70 ± 0,19
GN	-433 ± 60	2,86 ± 0,19
FBN	-586 ± 12	2,61 ± 0,07
PN	-320 ± 25	1,12 ± 0,26

The corrosion potential of untreated samples was obtained around −627 mV/SCE. On the other hand, the corrosion potential of the nitrided samples were shifted to more positive potential values than that of the untreated samples where the NC and PN samples presented the highest potential values. Regarding the corrosion current density (i_{corr}) the NC and PN samples presented lower values than the untreated samples.

It has been reported that the corrosion resistance improvement of the surface after nitriding or nitrocarburizing depends on the type of the nitride phase formed in the compound layer and the amount of ε nitride phase in the compound layer is the most important parameter for improving the corrosion resistance of the treated surface [4], [14], [15], [28], [86]. Furthermore, the corrosion resistance of the surface increases with increasing the amount of ε-phase in the compound layer. The formation of ε-phase is affected by the CO_2 gas, once that according with Fe-N-C phase diagram the solubility of carbon in ε-phase is much more than that in γ'-phase [15], [34]. It was observed from the XRD analysis (Figure 5.3) that both NC and PN are the samples presented the highest amount of ε nitride phase. In this way the lowest corrosion current density values of these samples may be explained by the amount of ε-phase. Although, the GN and FBN samples presented as well ε-phase, according to the XRD spectra γ'-phase was more dominant in the compound layer. It is known that the γ' nitride phase presents lower corrosion resistance than ε nitride phase, mainly due to its crystalline structure and lower nitrogen content [39]. Thus, the better corrosion resistance of the NC and PN samples may be explained by the presence of a ε nitride rich compound layer. Besides, it is known that the defects on the compound layer can decrease the corrosion resistance of the nitrided steels [16]. Therefore, relatively thicker porous layers on the GN and FBN samples may also influence the i_{corr} values.

The comparison of morphologies of the surfaces before (un-corroded surface) and after (corroded surface) the corrosion tests of samples are shown in Figure 5.17.

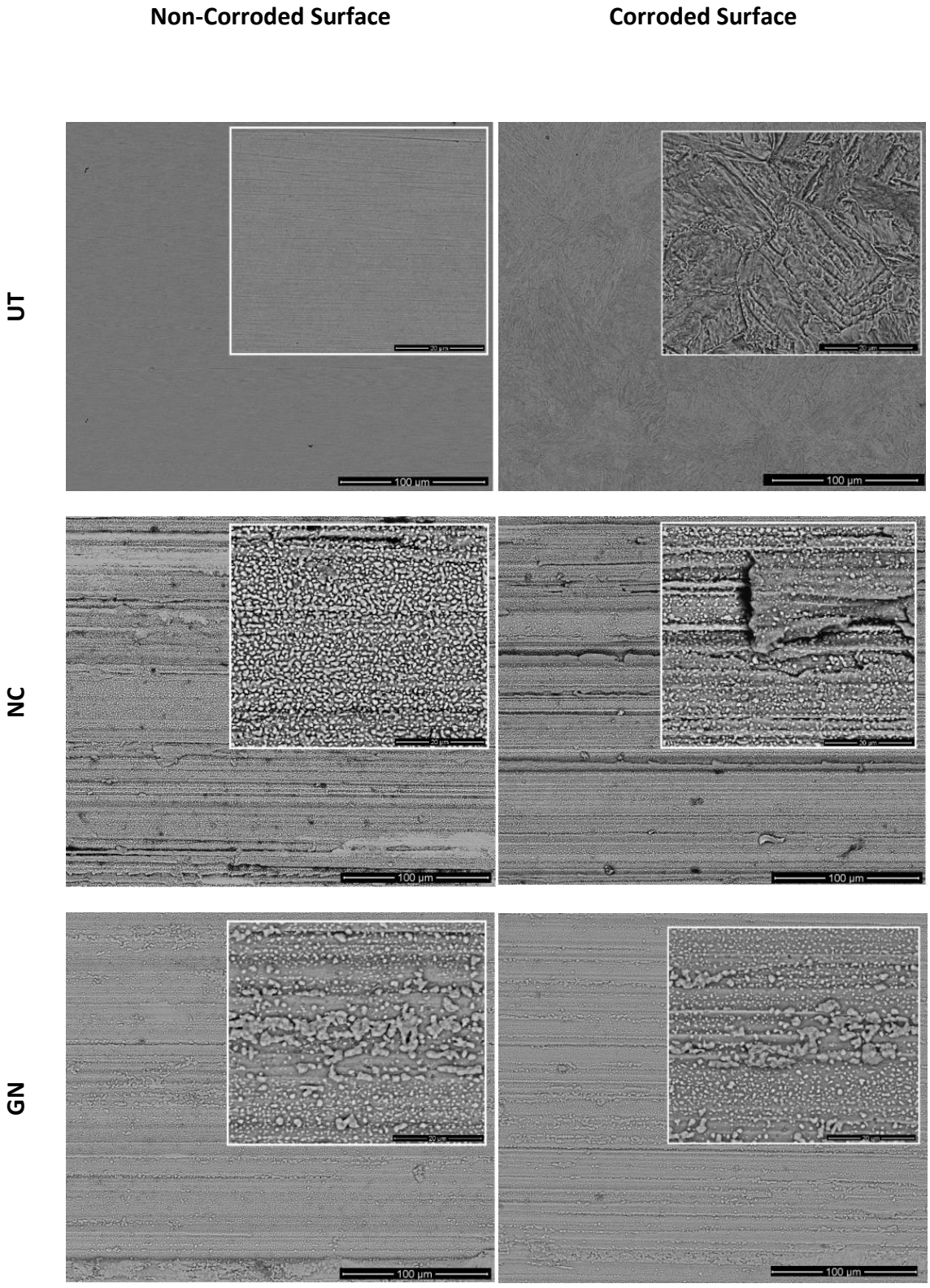

Figure 5.17 BSE/SEM images of the non-corroded and corroded surfaces of untreated and nitrided samples

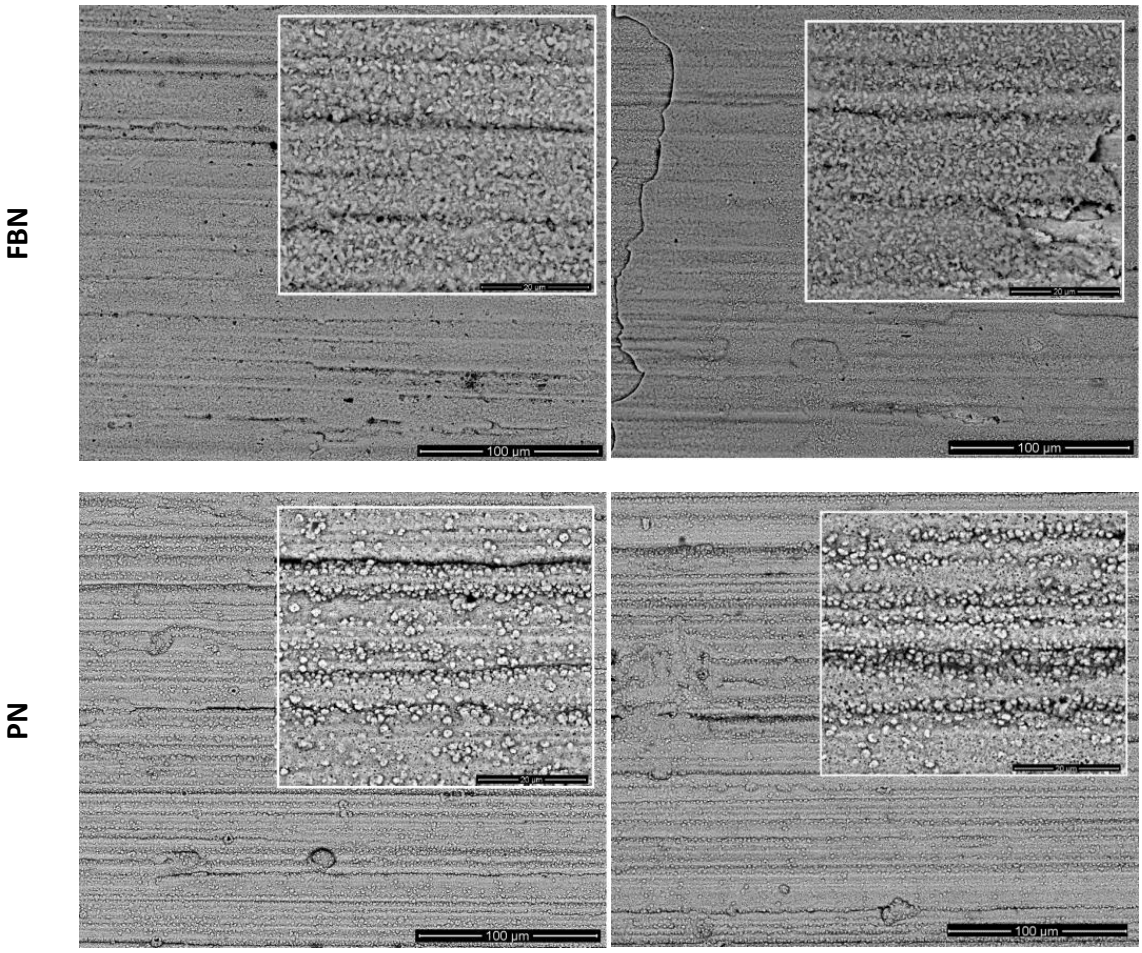

Figure 5.17 BSE/SEM images of the non-corroded and corroded surfaces of untreated and nitrided samples (cont'd)

The untreated samples after corrosion tests presented an obvious general and uniform corrosion. In contrast, the surface of nitrided samples was more resistant to general corrosion in comparison with the untreated samples. None of the nitrided samples showed significant differences on the surfaces after corrosion with exception of FBN samples. FBN samples presented the most non-homogenous compound layer, i.e., on the surface of the compound layer it was noticed a considerable amount of porosity. Even though, compound layer acts as a barrier to corrosion, a porous compound layer may lead to a corrosion attack that probably takes place on defects/pores in this layer [16].

5.4 Tribocorrosion

The evolution of OCP before, during and after sliding for the untreated and nitrided samples is given in Figure 5.18 together with evolution of COF during sliding. Before sliding, OCP values were stable for all samples. When sliding started, two different behaviour observed: OCP values of PN and NC decreased to more negative values whereas the values of UT, GN and FBN increased. After sliding, the potential values approached near the initial values except for the FBN sample where the values were kept on decreasing after sliding.

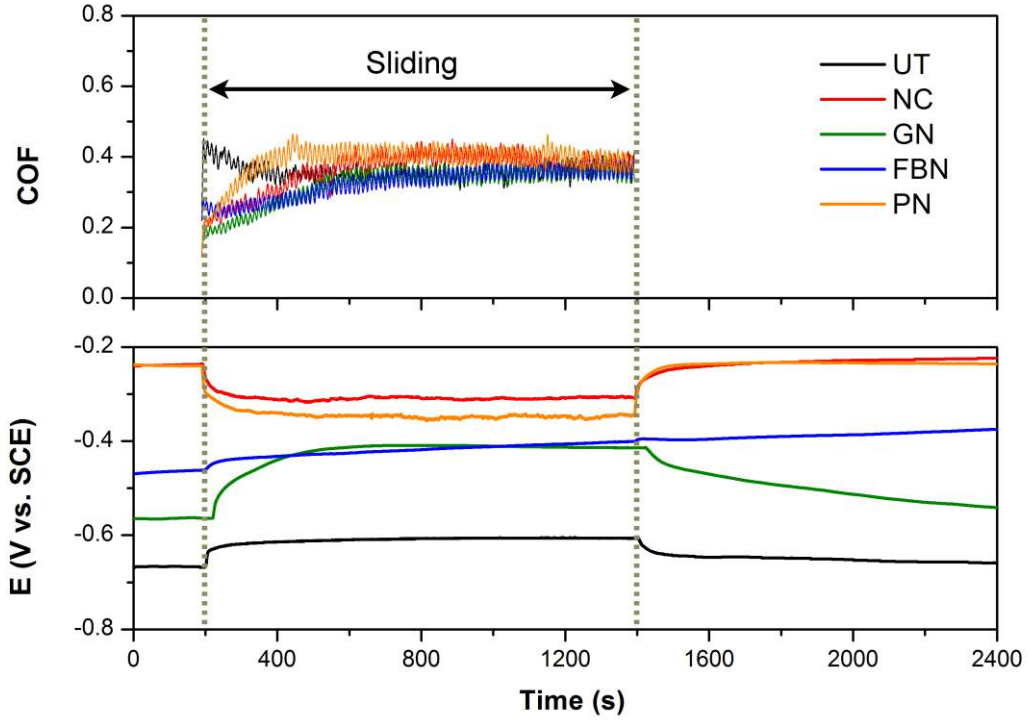

Figure 5.18 Evolution of COF and OCP in NaCl solution

On the evolution of OCP for the untreated sample, a sudden increase was observed on the onset of the sliding, followed by relatively stable values during sliding. After sliding, the values decreased rapidly near the initial values. On the other hand, COF values were decreased during approx. first 200 s then proceeded relatively stable till the end of the sliding. Slightly increased OCP values as COF values were decreasing can be attributed to the formation of the oxides and packing them to the surface by the counter material.

Oxide patches can be seen clearly on the SEM images of the worn surface (Figure 5.19). And also EDS analysis shown that the worn surface (Z2) contains higher concentration of oxygen as compared to the surroundings (Z4) (Figure 5.20). In addition to the oxide patches, grooves were observed on the worn surface. Thus, the main wear mechanism on the tribocorrosion of untreated sample can be as a combination of oxidative wear and abrasive wear. After sliding, OCP values were rapidly decreased near to the initial values and remained relatively stable till the end of the immersion time. Rapid decrease on the OCP values after sliding can be explained by the liberation of some oxide patches on the absence of the packing effect of the counter material.

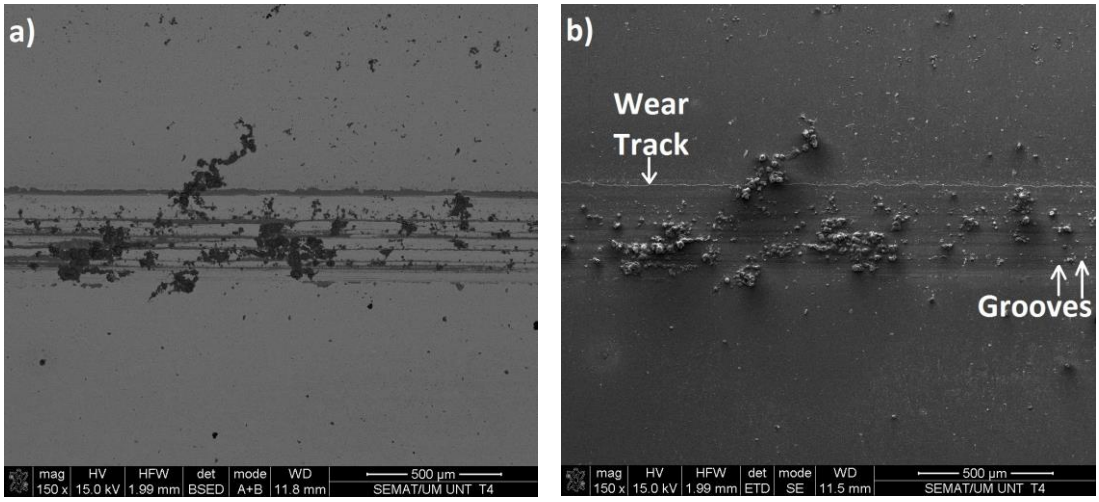

Figure 5.19 a) BSE b)SE images of the worn surfaces of untreated samples after tribocorrosion tests

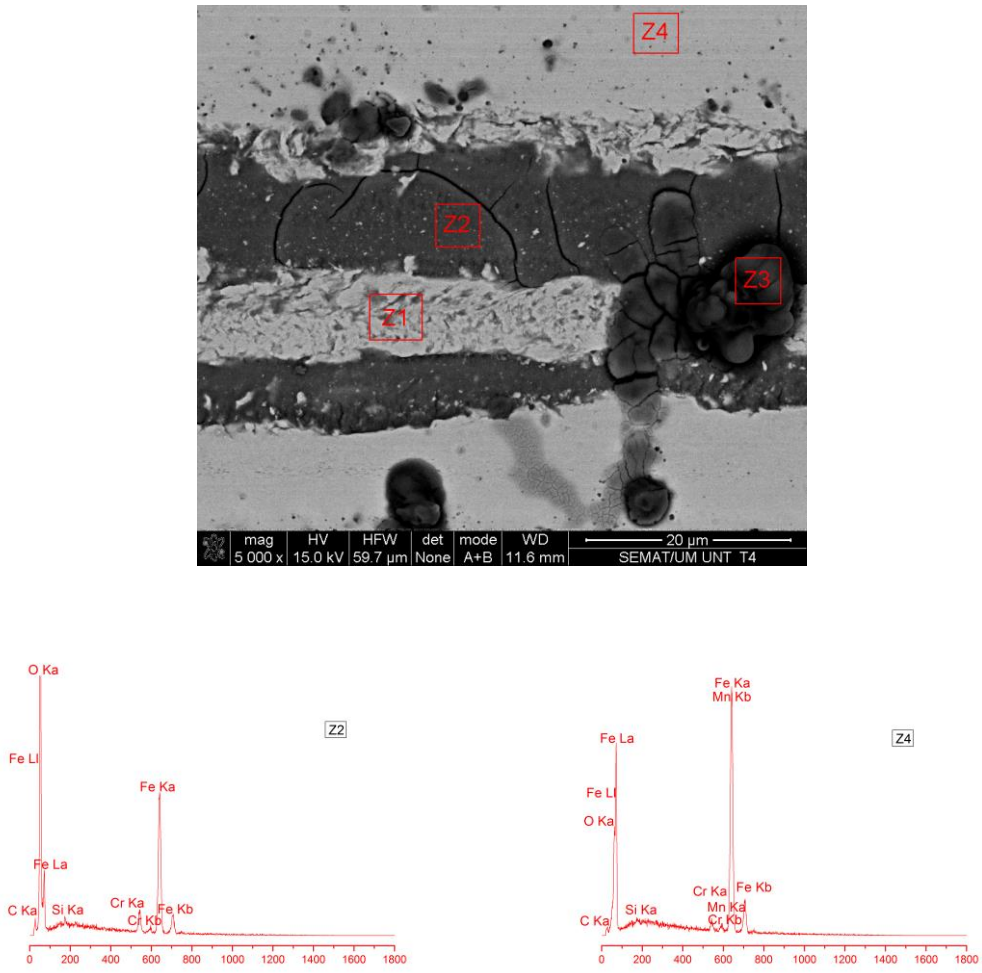

Figure 5.20 SEM image of the worn surface and matching EDS analysis for untreated sample

FBN and GN samples presented higher potential values under sliding as compared to the stabilization period. This behaviour may be attributed to the deeper outmost porous layer on these samples. During sliding, the wear debris can be accumulated on the pores and they may be compacted by the effect of the counter material. Though, the potential increase under sliding was higher on the GN sample as compared to the FBN. This may be explained by the difference on the thickness of the compound layer that was 14.33 ± 1.32 µm for FBN and 9.27 ± 1.29 µm for GN. Therefore, one may expect that it would be harder to damage the compound layer in order for electrolyte to reach through the diffusion layer on the FBN samples. After sliding, these two samples presented different behaviour. A potential drop was not observed for the FBN sample that can be considered as another proof of not having a significant damage on the compound layer.

However, after sliding the potential values for the GN sample decreased down to near the initial values that may be attributed to the liberation of the debris from the surface and pores on the absence of the packing effect of the counter material.

NC and PN samples, on the other hand, presented an evolution of OCP before, during and after sliding similar to a passive metal where a drop observed on the onset of the sliding due to the partial damage of the protective layer and a fast increase after sliding by the recovering of the protective layer [79], [87]. Although the potential values presented very similar values before and after sliding, the values during sliding were relatively lower on the PN sample indicating a relatively higher tendency to corrosion under sliding for the PN sample. This difference may be explained by the difference of the thickness of the compound layers that was 5.49 ± 1.39 µm for the PN sample and 11.55 ± 1.79 µm for the NC sample.

The COF values under sliding presented similar trends for the treated samples where a gradually increase was observed during approx. first 300 s of sliding and after that the values proceeded relatively stable till the end of the sliding. However, the increase on the values were relatively faster on the PN and NC samples, followed by slightly higher values during sliding. Nevertheless, in the end of the sliding, COF values were very similar in all samples. This difference on the evolution of COF values for the treated samples may also be attributed to the porous outmost layer where higher amount of porosity can facilitate the packing of the wear products on the surfaces thus reducing the third-body effect and therefore lowering the COF values for the GN and FBN samples.

Figure 5.21 presents the SEM images of the worn surfaces for each nitrided samples. Parallel abrasion grooves and oxide patches were visible on all worn surfaces. As a first approach to the comparison of the tribocorrosion behaviour of the nitrided and nitrocarburized steels, the focus was given on the first contact without totally removing the compound layer. Thus, due to the chosen tribological parameters, the machining marks were still visible on the wear tracks.

On the other hand, since the material removal after tribocorrosion tests were relatively lower, no methodological study was performed on quantification of the material loss after testing. Even though, it can be seen on the SEM images of the wear tracks that the PN sample presented the narrowest width as compared to the other samples. In order to have a better understanding the wear mechanism after tribocorrosion, further studies should be performed as testing with longer sliding times and analysing of the sub-surface of the worn surfaces and the mating surfaces.

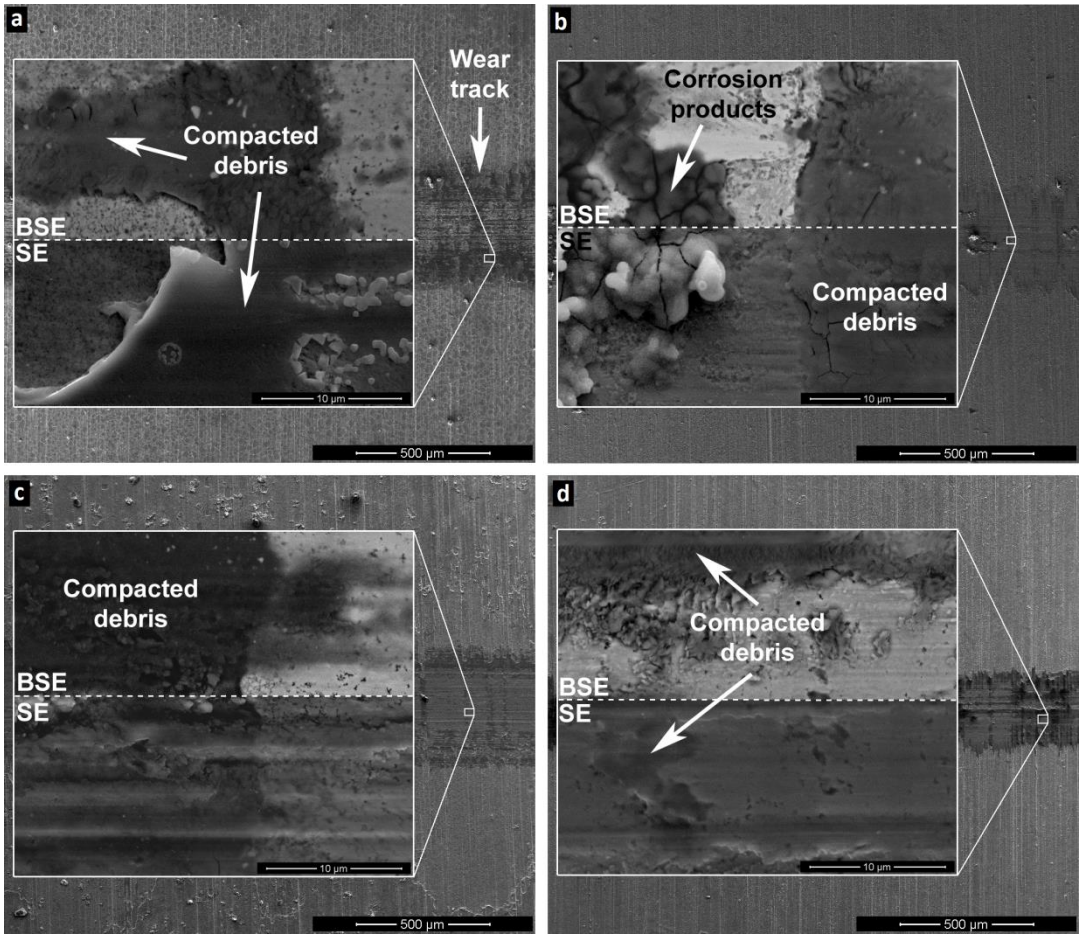

Figure 5.21 Worn surfaces of the nitrided samples after tribocorrosion tests a) NC, b) GN, c) FBN, and d) PN

CHAPTER 6

CONCLUSIONS

In this thesis, gas nitriding (GN), fluidized bed nitriding (FBN), plasma nitriding (PN) and nitrocarburizing (NC) methods were applied in industrial facilities on plastic mould steel, DIN 1.2738 (Impax Supreme), and the results were investigated by comparing the mechanical, chemical, tribological, electrochemical and triboelectrochemical properties.

Findings achieved from the experimental works can be summarized as follows

(1) While PN presented the thinnest compound layer and the largest case depth, when it considered within the range of the standard deviation, no clear difference was observed between the surface hardness of the nitrided samples.

(2) Nitriding/Nitrocarburizing effectively increased the surface hardness of the DIN 1.2738 (Impax Supreme) mould steel. The hardness analysis found out that the treated samples had higher hardness values than the untreated sample.

(3) After dry sliding wear tests, both untreated and nitrided samples presented mainly combination of adhesive and abrasive wear mechanism for the run-in period of the sliding and mainly oxidative wear mechanism for the steady state of the sliding. However, the run-in period was much shorter on the nitrided samples.

(4) Nitrided samples presented more than 20 times lower wear rates than the untreated samples.

Even though no significant difference was observed within the range of the standard deviation, NC and GN samples presented very similar values, FBN presented the highest wear rate and PN presented the lowest wear rate as mean values.

(5) The corrosion potential of the nitrided samples was shifted to more positive potentials values as compared to the untreated steel samples. The corrosion resistance improved after nitriding and nitrocarburizing treatments with respect to the untreated sample.

(6) The tribocorrosion resistance improved after nitriding and nitrocarburizing treatments with respect to the untreated sample. Nitriding type affected the wear and corrosion behavior of DIN 1.2738 (Impax Supreme) steels.

REFERENCES

[1] Martínez-Mateo, I., Carrión-Vilches, F.J., Sanes, J. and Bermúdez, M.D., (2011). "Surface Damage of Mold Steel and its Influence on Surface Roughness of Injection Molded Plastic Parts", Wear, 271:2512– 2516.

[2] Ozturk, O., Onmuş, O. and Williamson D.L., (2005). " Microstructural, Mechanical, and Corrosion Characterization of Plasma Nitrided Plastic Injection Mould Steel", Surface and Coatings Technology, 196: 341– 348.

[3] Tijani, Y.A., (2008). Modeling and Simulation of Thermochemical Heat Treatment Processes : A Phase Field Calculation of Nitriding in Steel, Dissertation, University of Bremen, Germany.

[4] Wen,D.C., (2009). "Plasma Nitriding of Plastic Mold Steel to Increase Wear and Corrosion Properties", Surface and Coatings Technology, 204:511-519.

[5] Hubbard, P., Partridge, J.G., Doyle, E.D., McCulloch, D.G., Taylor M.B. and Dowey, S.J., (2010). "Investigation of Nitrogen Mass Transfer within an Industrial Plasma Nitriding sSystem I: The Role of Surface Deposits", Surface and Coatings Technology, 204:1145–1150.

[6] ASM Handbook Committee., (1991). ASM Handbook 4, ASM International, Materials Park, Ohio.

[7] Pye, D., (2003). Practical Nitriding and Ferritic Nitrocarburizing, ASM International, Materials Park, Ohio.

[8] M. Berg, C.V. Budtz-Jørgensen, H. Reitz, K.O. Schweitz, J. Chevallier, P. Kringhøj, et al., On plasma nitriding of steels, Surf. Coatings Technol. 124 (2000) 25–31.

[9] Yang, M., (2012). Nitriding Fundamentals, Modeling and Process Optimization, Degree of Doctor, Worcester Polytechnic Institute, ABD.

[10] Wen,D.C., (2010). "Erosion and Wear Behavior of Nitrocarburized DC53 Tool Steel", Wear, 268:629–636.

[11] Pessin, M.A., Tier, M.D., Strohaecker, T.R., Bloyce, A., Sun, Y. and Bell, T., (2000). "The Effects of Plasma Nitriding Process Parameters on the Wear Characteristics of AISI M2 Tool Steel", Tribology Letters, 8:223–228.

[12] Akhtar, S.S., Arif, A.F.M. and Yilbas, B.S., (2009). “Evaluation of Gas Nitriding Process with in-process Variation of Nitriding Potential for AISI H13 Tool Steel”, The International Journal of Advanced Manufacturing Technology, 47:687–698.

[13] Al-Rubaie, K.S., Steinmeier, F. and Michael, P., (2000). “Two-body Abrasion of nNtrocarburised Steels for Hydraulic Cylinders” , Wear, 243:112–121.

[14] Basso, R.L.O., Candal, R.J., Figueroa, C.A., Wisnivesky, D. and Alvarez, F., (2009). “Influence of Microstructure on the Corrosion Behavior of Nitrocarburized AISI H13 Tool Steel Obtained by Pulsed DC Plasma” , Surface and Coatings Technology, 203:1293–1297.

[15] Fattah, M. and Mahboubi, F., (2010). “Comparison of ferritic and austenitic plasma nitriding and nitrocarburizing behavior of AISI 4140 low alloy steel” , Materials and Design, 31: 3915–3921.

[16] Novák, P., Vojtěch, D. and Šerák, J., (2006). “Wear and Corrosion Resistance of a Plasma-nitrided PM Tool Steel Alloyed with Niobium” , Surface and Coatings Technology, 200:5229-5236.

[17] Rosalbino, F., Scavino, G. and Mortarino, G., (2012). “Electrochemical Corrosion Behaviour of Innovative Mould Steels in a Chloride-containing Environment” , Materials and Corrosion, 63(2):105-110.

[18] Grill, A. and Itzhak, D., (1983). “Nitriding of AISI M2 Tool Steel in an Inductive R.F. Plasma” , Metallurgical and Protective Coatings 101:219-222.

[19] Hubbard, P., (2007). Characterisation of a Commercial Active Screen Plasma Nitriding System, Department of Applied Physics, RMIT University, Australia.

[20] Türk, A., Ok, O. and Bindal, C., (2005). “Structural Characterization of Fluidized Bed Nitrided Steels” , Vacuum 80: 332–342.

[21] Kooı, B. J., Somers, M. A. J. and Mittemeijer, E. J., (1996). “An Evaluation of the Fe-N Phase Diagram Considering Long-Range order of N Atoms in y' Fe_4N_{1-x} and ε-Fe_2N_{1-z}” , Metallurgical and Materials Transactions 27A: 1063-1071.

[22] Onmuş, O., (2003). Microstructural and Mechanical Characterization of Nitrogen Ion Implanted and Plasma Ion Nitrided Plastic Injection Mould Steel, Master Thesis, İzmir Institute of Technology, Materials Science and Engineering, Izmir.

[23] Dossett, J. and Totten, G.E., (2013). Steel Heat Treating Fundamentals and Processes, ASM Handbook, Volume 4A.

[24] Lantelme, F. and Groult, H., (2013). Molten Salts Chemistry: From Lab to Applications, First Edition, USA.

[25] Czerwinski, F., (2012). Heat Treatment - Conventional and Novel Applications, First published, InTech, Croatia.

[26] Meka, S.R., (2011). Nitriding of Iron-Based Binary and Ternary Alloys: Microstructural Development during Nitride Precipitation, Dissertation, Fakultät Chemie der Universität Stuttgart, Germany.

[27] Biró, A.S., (2013). “Trends of Nitriding Processes” , Production Processes and Systems, 6(1):57-66.

[28] Basso, R.L.O., Pastore, H.O., Schmidt, V., Baumvol, I.J.R., Abarca, S.A.C., Souza, F.S., Spinelli, A., Figueroa, C.A. and Giacomelli, C., (2010). ”Microstructure and corrosion behaviour of pulsed plasma-nitrided AISI H13 tool steel” , Corrosion Science, 52: 3133–3139.

[29] Hernandez, M., Staia, M.H. and Puchi-Cabrera, E.S., (2008). “Evaluation of Microstructure and Mechanical Properties of Nitrided Steels”, Surface and Coatings Technology, 202:1935-1943.

[30] Singh, G.P., Alphonsa, J., Barhai, P.K., Rayjada, P.A., Raole, P.M. and Mukherjee, S., (2006). “Effect of Surface Roughness on the Properties of the Layer Formed on AISI 304 Stainless Steel After Plasma Nitriding”, Surface and Coatings Technology, 200: 5807–5811.

[31] Totten, G.E., Funatani, K. and Xie L., (2004). Handbook of Metallurgical Process Design, The United States of America.

[32] Holm T., Furnace Atmospheres No. 3: Gas Nitriding and Nitrocarburising,

http://heattreatment.linde.com/international/web/lg/ht/like35lght.nsf/docbyalias/nav_apps_ntrdg, 17 Mart 2014.

[33] Sirin, S.Y., Sirin, K. and Kaluc, E., (2008). “Effect of the ion nitriding surface hardening process on fatigue behavior of AISI 4340 steel” , Materials Characterization, 59: 351-358.

[34] Sun, Y., Bell, T., (1991). “Plasma surface engineering of low alloy steel” , Materials Science and Engineering, A140:419-434.

[35] Castro, G., Fernandez-Vicente, A. and Cid, J., (2007). “Influence of the Nitriding Time in the Wear Behaviour of an AISI H13 Steel During a Crankshaft Forging Process” , Wear, 263:1375-1385.

[36] ASM Handbook Committee., (1992). Friction, Lubrication, and Wear Technology, ASM Handbook 18, ASM International, United States of America.

[37] Shih, H., (2012). Corrosion Resistance, First Edition, InTech.

[38] Michalski, J., Tacikowski, J., Wach, P., Lunarska, E. and Baum, H., (2005). “Formation of single-phase layer of γ’-nitride in controlled gas nitriding” , Chemicothermal Treatment, Metal Science and Heat Treatment, 47:35-38.

[39] Oliveira, S.D., Tschiptschin, A.P. and Pinedo, C.E., (2007). “Simultaneous plasma Nitriding and Ageing Treatments of Precipitation Hardenable Plastic Mould Steel” , Materials and Design 28:1714–1718.

[40] Weymer, P., (2008). “Close Process Control: Yields Nitriding Consistency, Repeatability” , Heat Treating Progress, (March/April):51-54.

[41] Darbellay, J., (2006), Gas Nitriding: An Industrial Perspective,

http://coursenotes.mcmaster.ca/701-702Seminars/2005-2006/701JeromeDarbellay March 2006.pdf, 22 Mart 2014.

[42] Lotze, T. H., Gas Nitriding,

http://www.supersystems.com/documentation/technical-papers/, 18 Aralık 2014.

[43] Subramanian, K., and Thameem Ansari, N., (2006). Surface Hardening of 316 ln Grade Austenitic Stainless Steel Using Gas Nitriding Process, A Project Report, Anna University, Mechanical Engineering,India.

[44] Renganathan, C. and Raghunath, V., (1994). "Fluidised Bed Heat Treatment - A Flexible Heat Treating Technology" , Workshop on Heat Treatment and Surface Engineering of Iron and Steels, 11-13 May 1994, Jamshedpur.

[45] Ikens, G.C., (1985), Fluidized Bed Furnaces Support Metal Surface Treatments,

http://www.dynablue.com/, 24 Mart 2014.

[46] Totten, G., (2007). Steel Heat Treatment: Metallurgy and Technologies, Second Edition, Taylor & Francis Group, The United States of America.

[47] Yousfi, M.A., (2011). Influence of Surface Roughness Lay and Surface Coatings on Galling During Hot Forming of Al-Si Coated High Strength Steel, Master Thesis, Luleå University of Technology, Advanced Materials Science and Engineering, Sweden.

[48] Basu, A., Majumdar, J.D., Alphonsa, J., Mukherjee, S. and Manna, I., (2008). "Corrosion resistance improvement of high carbon low alloy steel by plasma nitriding", Materials Letters, 62:3117–3120.

[49] Maalekian, M., (2007). The Effects of Alloying Elements on Steels (I), Christian Doppler Laboratory for Early Stages of Precipitation, Graz University of Technology, Institute for Materials Science and Welding, Austria.

[50] Davis, J.R., (2002). Surface Hardening of Steels: Understanding the Basics, First Printing, ASM International, Materials Park, United States of America.

[51] Du, H., Somers, M.A.J. and Agren, J., (2000). "Microstructural and Compositional Evolution of Compound Layers during Gaseous Nitrocarburizing", Metallurgical and Materials Transactions A, 31A:195–211.

[52] Flodström, I., (2012). Nitrocarburizing and High Temperature Nitriding of Steels in Bearing Applications, Master of Science Thesis, Chalmers University of Technology, Division of Surface and Microstructure Engineering, Sweden.

[53] Wahl, G. and Alwart, S., Improvement of Tribological Properties Through Nitrocarburizing

http://www.durferrit.com.br/downloads/18Improvement%20of%20tribological%20properties%20through nitrocarburizing.pdf, 19 Aralık 2014.

[54] Jaoul, C., Belmonte, T., Czerwiec, T. and David, N., (2006). "Nitrocarburizing Treatments Using Flowing Afterglow Processes", Applied Surface Science, 252: 8360–8366.

[55] Woehrle, T., Leineweber, A. and Mittemeijer, E.J., (2010). "Influence of the Chemical Potential of Carbon on the Microstructural and Compositional

Evolution of the Compound Layer Developing Upon Nitrocarburizing of α-iron", Journal of Heat Treatment and Materials, 65:243-248.

[56] Somers, M.A.J., Nitriding and Nitrocarburizing: Status and Future Challenges http://orbit.dtu.dk/files/57262608/Nitriding_and_Nitrocarburizing_Current_Status_and_Future_Challenges.pdf, 19 Aralık 2014.

[57] Dossett, J. and Totten, G.E., (2013). ASM Metals Handbook, Vol 4A, ASM International, Materials Park, Ohio.

[58] King, P.C., Reynoldson, R.W., Brownrigg, A. and Long, J.M., (2005). "Ferritic Nitrocarburising of Tool Steels", Surface Engineering, 21:86-98.

[59] Cajner, F., Landek, D. and Lisac, E.S., (2003). "Improvement of Properties of Steels Applying Salt Bath Nitrocarburizing With Post-oxidation" , Materiali in Tehnologije, 37:333-339.

[60] Boßlet, J., Tufftride®/QPQ®Process

http://www.durferrit.de/media/pdf/Tenifer QPQ eng.pdf, 19 Aralık 2014.

[61] Malinova, T., Malinov, S. and Pantev, N., (2001). "Simulation of Microhardness Profiles for Nitrocarburized Surface Layers by Artificial Neural Network" , Surface and Coatings Technology, 135:258-267.

[62] Zhang, J.W., Lu, L.T., Shiozawa, K., Zhou, W.N. and Zhang, W.H., (2011). "Effects of Nitrocarburizing on Fatigue Property of Medium Carbon Steel in Very High Cycle Regime" , Materials Science and Engineering A, 528: 7060–7067.

[63] Somers, M., (1989). Internal and External Nitriding and Nitrocarburizing of Iron and Iron-Based Alloys, Doctoral Thesis, Delft University of Technology, Netherlands.

[64] Lee, K.H., Nam, K.S., Shin, P.W., Lee, D.Y. and Song, Y.S., (2003). "Effect of Post-Oxidizing Time on Corrosion Properties of Plasma Nitrocarburized AISI 1020 Steel" , Materials Letters, 57: 2060–2065.

[65] Rajan, T.V., Sharma, C.P. and Sharma, A., (2011). Heat Treatment: Principles and Techniques, Second Edition, PHI Learning Private Limited, Haryana.

[66] Niku-Lari, A., (1987). Advances in Surface Treatments: Technology-Applications-Effects, Volume 5, First Edition, Pergamon Press, Oxford.

[67] Chang, C.N. and Chen, F.S., (2003). "Wear Resistance Evaluation of Plasma Nitrocarburized AISI 316L Stainless Steel" , Materials Chemistry and Physics, 82:281-287.

[68] Sirin, S.Y. and Kaluc, E., (2012). " Structural Surface Characterization of Ion Nitrided AISI 4340 Steel" , Materials and Design, 36:741–747.

[69] Alsaran, A., Karakan, M. and Celik, A., (2002). " The Investigation of Mechanical Properties of Ion Nitrided AISI 5140 Low Alloy Steel" , Materials Characterization, 48:323–327.

[70] Kato, H., Eyre, T.S. and Ralph, B., (1994). “Sliding Wear Characteristics of Nitrided Steels” , Surface Engineering, 10:65–74.

[71] Ashrafizadeh, F., (2003). “Influence of Plasma and Gas Nitriding on Fatigue Resistance of Plain Carbon (Ck45) Steel, Surface and Coatings Technology, 173-174:1196–1200.

[72] Mirjani, M., Shafyei, A. and Ashrafizadeh, F., (2009). “Plasma and Gaseous Nitrocarburizing of C60W Steel for Tribological Applications”, Vacuum, 83:1043–1048.

[73] Qiang, Y.H., Ge, S.R. and Xue, Q.J., (1999). “Microstructure and Tribological Behaviour of Nitrocarburizing-Quenching Duplex Treated Steel” , Tribology International, 32:131–136.

[74] Haruman, E., Sun, Y., Malik, H., Sutjipto, A.G.E., Mridha, S. and Widi, K., (2006). “Low Temperature Fluidized Bed Nitriding of Austenitic Stainless Steel” , Solid State Phenomena, 118:125–130.

[75] Li, G., Wang, J., Li, C., Peng, Q., Gao, J. and Shen, B., (2008). “Microstructure and Dry-sliding Wear Properties of DC Plasma Nitrided 17-4 PH Stainless Steel” , Nuclear Instruments and Methods in Physics Research B, 266:1964–1970.

[76] Vardavoulias, M., Jeandin, M., Velasco, F. and Torralba, J.M., (1996). “Dry Sliding Wear Mechanism for P/M Austenitic Stainless Steels and Their Composites Containing Al_2O_3 and Y_2O_3 Particles” , Tribology Internatiortal,29:499–506.

[77] Psyllaki, P., Kefalonikas, G., Pantazopoulos, G., Antoniou, S. and Sideris, J., (2002). “Microstructure and Tribological Behaviour of Liquid Nitrocarburised Tool Steels, Surface and Coatings Technology, 162:67–78.

[78] Corengia, P., Walther, F., Ybarra, G., Sommadossi, S., Corbari, R. and Broitman, E., (2006). “Friction and Rolling–Sliding Wear of DC-Pulsed Plasma Nitrided AISI 410 Martensitic Stainless Steel” , Wear, 260:479–485.

[79] Doni, Z., Alves, A.C., Toptan, F., Gomes, J.R., Ramalho, A., Buciumeanu, M., Palaghian, L. and Silva, F.S., (2013). “Dry Sliding and Tribocorrosion Behaviour of Hot Pressed CoCrMo Biomedical Alloy as Compared with the Cast CoCrMo and Ti6Al4V Alloys” , Materials and Design, 52:47–57.

[80] Sun, Y. and Bell, T., (1998). “Sliding Wear Characteristics of Low Temperature Plasma Nitrided 316 Austenitic Stainless Steel” , Wear, 218:34–42.

[81] Tuckart, W., Gregorio, M. and Iurman, L., (2010). “Sliding Wear of Plasma Nitrided AISI 405 Ferritic Stainless Steel” , Surface Engineering, 26:185–190.

[82] Baets, P., Kalacska, G., Strijckmans, K., Van de Velde, F. and Van Peteghem, A.P., (1998). “Experimental Study by Means of Thin Layer Activation of the Humidity Influence on the Fretting Wear of Steel Surfaces” , Wear, 216:131–137.

[83] Semenov, V.I., Shuster, L.S., Huang, S.-J. and Lin, P.-C., (2011). “Tribological Behavior of Low Carbon Steel Depending on Treatment and Structural State” , Journal of Friction and Wear, 32:205–211.

[84] Chiu, L.H., Wu, C.H. and Chang, H., (2002). “Wear Behavior of Nitrocarburized JIS SKD61 Tool Steel” , Wear, 253:778–786.

[85] Karamış, M.B., (1991). “Tribological Behaviour of Plasma Nitrided 722M24 Under Dry Sliding Conditions” , Wear, 147:385–399.

[86] Wen,D.C., (2009). “Microstructure and Corrosion Resistance of the Layers Formed on the Surface of Precipitation Hardenable Plastic Mold Steel by Plasma Nitriding” , Applied Surface Science, 256:797–804.

[87] Fernandes, A.C., Vaz, F., Ariza, E., Rocha, L.A., Ribeiro, A.R.L., Vieira, A.C., Rivière, J.P. and Pichon, L., (2006). “Tribocorrosion Behaviour of Plasma Nitrided and Plasma Nitrided+Oxidised Ti6Al4V Alloy” , Surface and Coatings Technology, 200:6218–6224.

CURRICULUM VITAE

PERSONAL INFORMATION

Name Surname : Esil BOZTEPE

Date of Birth and Place : 08. 01. 1985 / ESKİŞEHİR

Foreign Languages : English, Portuguese

E-mail : boztepeesil@hotmail.com

EDUCATION

Degree	Department	University	Date of Graduation
Master	Metallurgy and Materials Engineering	Yildiz Technical University	2015
Undergraduate	Metallurgy and Materials Engineering	Sakarya University	2008
High School	Sciences	Milli Piyango Anatolian High School	2003